

Validation of the SU2 Flow Solver

for Classical Non Ideal Compressible Fluid
Dynamics

Liam Bills

Validation of the SU2 Flow Solver for Classical Non Ideal Compressible Fluid Dynamics

by

Liam Bills

to obtain the degree of Master of Science
at the Delft University of Technology,
to be defended publicly on 13 July 2020 at 09:45.

Student number: 4788818
Project duration: September 2, 2019 – June 15, 2020
Thesis committee: Professor P. Colonna, TU Delft, Chair
Assistant Prof. R. Dwight, TU Delft, Examiner
Assistant Prof. M. Pini, TU Delft, Responsible supervisor
A. J. Head, TU Delft, Daily Supervisor

This thesis is confidential and cannot be made public until 1 July 2023.

An electronic version of this thesis is available at <http://repository.tudelft.nl/>.

Abstract

The validation of SU2 for modelling classical non-ideal compressible fluid dynamics will advance the research into efficient ORC turbomachinery design. This study determines the validity of the two-dimensional flow solver for predicting the isentropic expansion of Siloxane MM through a converging-diverging nozzle using compressible Euler equations, adiabatic flow, and the Peng-Robinson equation of state. Two flows with an inlet stagnation temperature of 525K were considered: an expansion from 18.4 bar to 2.1 bar, and an expansion from 11.1 bar to 1.3 bar. Mach number along the centreline and static pressure along the nozzle surface were used as the direct system response quantities used in the analysis. Experimental data and uncertainty came from the ORCHID, model input uncertainty was quantified using stochastic collocation, and the numerical uncertainty was calculated using the Richardson extrapolation. The conclusions were based on a hybrid of the ASME V&V 20 [4] and Real Space [54] validation metrics, with a novel Engineering Response Quantity analysis based on determining the effects of system uncertainty on performance parameters. The studied SU2 model provide valid predictions for Mach number, and invalid predictions for static pressure. The largest error is in the kernel region, where $E_{\text{Mach}} = 0.111$ and $E_{\text{pressure}} = 112$ kPa. Mach number has a maximum simulation uncertainty of 2% at the transition to the reflex region. Pressure has a maximum uncertainty of 3% at the throat. In the context of turbomachinery the simulation uncertainties translate to ± 0.001 and ± 0.02 on a loss coefficient calculated across a theoretical normal shock, for Mach and pressure respectively. Considering ± 0.01 as significant for a loss coefficient the Mach uncertainty is negligible. Input uncertainty is the largest component of the pressure uncertainty, while experimental uncertainty is dominant for Mach. The input parameters which provide the highest contribution to the uncertainty are critical pressure and temperature. The developed infrastructure can be used for expanding the validation of SU2 to different flow cases.

Title image: Visualisation of density gradients in a supersonic diverging nozzle with the working fluid of Siloxane MM. The bottom half is a schlieren image taken of an experiment while the upper half is a shadowgraph created using the data from an SU2 simulation of identical flow conditions. The lines seen are called expansion waves which result when a flow is expanding faster than the speed of sound and propagate at an angle proportional to the Mach number of the flow.

Preface

I love flying. I love power. These simple feelings sparked my interest in aerospace engineering many years ago. To this day, whenever I sit in an aircraft I feel my smile growing from ear to ear as the engines change from idle to full power. Whether it is a private, commercial, or military aircraft, at the beginning of a flight I can not help but think of the engineering miracle I am about to experience. Unfortunately, I have growing guilt every time I fly. The climate effects from the noise and emissions from the aerospace sector can not be ignored as it grows every year. My love has thus transformed into a specific goal: contributing to the development of technology which will reduce the fuel consumption and emissions of commercial aircraft. This is why I decided to continue my education with a masters degree from TU Delft.

For the past seven years, starting in my Bachelors degree, and continuing through my short time in industry into my masters degree, I have committed myself to learn about the principles of thermodynamics, fluid dynamics, structural mechanics, material science, and electronics. All fields which give me a stronger understanding of how aircraft work, and a stronger appreciation for the aerospace industry. This has culminated in my final year where I have worked on one small project which has the potential to change way commercial aircraft are built. Working with a knowledgeable and passionate team I have hopefully been able to progress the development of a tool which will be used to change the propulsion technology used in a multitude of power and propulsion systems. I truly care about the environmental challenges facing the aerospace community, and I hope my work can be used in a small way to assist moving the industry towards a sustainable future.

While I expect the reader to have a basic level of knowledge in thermodynamics, fluid dynamics, statistics, and validation theory, I recognize that the intersectionality of these fields is not often discussed. Other than those in the research field of flow solver validation I acknowledge that the reader will have less background knowledge in one or many of these fields. I have thus tried to provide a comprehensive introduction to allow all readers with an exposure to engineering principles the opportunity to understand and appreciate the work done. There may be sections which seem fundamental, but they are there to ensure this research is accessible. The body of the thesis, however, will move quickly into the subject matter at depth and assume the introduction was adequate for background information. To understand the fundamental thermodynamics and fluid mechanics any textbook should be sufficient as a reference such as “Fluid Mechanics” by White [67], or “Thermodynamics: Fundamentals and Engineering Applications” by Reynolds and Colonna [50]. The advanced reader can consider the text on modern compressible flow by Anderson [7]. Since the applications of my work are focused on sCO₂ systems, and the interested reader can go to Brun et al. [10] for more details.

For those interested in more work on SU₂ validation I would guide them to the works by Head [34], and Spinelli et al. [61]. Flow solver validation is well described by Eça et al. [24]; Cinnella et al. [13, 14] and Congedo [20] are the best resources for uncertainty quantification; and Coleman and Steele [15], Oberkampf and Roy [45], provide the base theory of experimental validation. The work of these authors far exceeds my own and I would encourage any future students to use them as a basis for building on my research.

*Liam Bills
Delft, June 2020*

“I want to build a plane”

Acknowledgements

Before presenting my work I must acknowledge my supporting team at the TU Delft aerospace faculty. I would like to thank Professor Piero Colonna, whose vision and determination has directed my research. The passion and interest you have in the field of ORC technology has kept me focused and hopeful about the future of aerospace. You have also built a team at TU Delft which has been incredible to be a part of. I would also like to express my gratitude to Assistant Professor Matteo Pini, my supervisor who has provided me with trust and support which I deeply appreciate. You have helped me overcome problems which would have taken me months to do alone. My daily supervisor, Ir. Adam Head, has given me all the guidance and support I needed and more. He has been a resource for me in more than just my research, and allowed me to produce the best work I am capable of. It has been an honour to be your student. My gratitude also goes to Dr. Carlo De Servi, Dr. Teus van der Stelt, and Ir. Nitish Anand. Each of you have either reviewed my work or given suggestions to overcome a challenge. Your support is appreciated and I hope my work can be of use to you in the near future. I must then thank Dr. Lucia Azzini, who took hours from her vacation to assist me with a problem. Also thanks to Assistant Prof. Richard Dwight for agreeing to be a part of my reviewing committee, even during the vacation period. Next to my research colleague, Fabio Beltrame MSc, who despite not knowing him 9 months ago, has turned into a good friend of mine. I was impressed from day one with your work ethic and ability to work with me in a team to achieve more than what we would have done as individuals. The entire turbomachinery group of the FPP department in the aerospace faculty of TU Delft has been a pleasure to work with. The best of luck to all of you in your future endeavours.

Finally thank you to my friends and family, in particular my parents. All of my success is based on your love and support. Without you I would not have made it to where I am today.

Contents

Preface	v
Acknowledgements	vii
List of Figures	xiii
List of Tables	xxi
Glossary	xxiii
1 Introduction	1
1.1 Motivation	1
1.2 Knowledge Gap	2
1.3 Objective	3
1.3.1 Research Questions	3
1.3.2 Deliverables.	3
1.4 Scope	4
1.5 Overview	4
2 Background of Classical NICFD	5
2.1 Organic Fluids	5
2.2 Quantification of Non-ideal Behaviour	7
2.2.1 Compressibility factor	7
2.2.2 Isothermal Compressibility	8
2.2.3 Polytropic Exponent	8
2.2.4 Fundamental Derivative of Gas Dynamics	8
2.2.5 Definition of Classical NICFD	8
2.3 Mathematical Representation of NICFD.	10
2.3.1 Flow Conservation Equations	10
2.3.2 Simplifications of Flow Equations	10
2.3.3 SU2 Framework	11
2.4 Thermo-physical Models	11
2.4.1 Equations of State	12
2.4.2 Fluid Properties.	13
2.4.3 Departure Functions	13
2.4.4 Transport sub-models	14
2.5 Compressible Flow Phenomena.	14
2.5.1 Expansion Waves	15
2.5.2 Shock Waves	15
2.5.3 Jump Conditions	16
2.6 CFD Validation	16
2.6.1 Validation Hierarchy	17
2.6.2 Validation Metrics.	17
2.7 Forward Propagation of Uncertainty in CFD Solvers	19
2.7.1 UQ of Siloxane MM Supersonic Expansion Model	20
2.7.2 UQ Studies on Thermodynamic models for Real Gases	21
2.8 Experiments in Non-Ideal Compressible Fluid Dynamics	21
2.8.1 SU2 Accuracy Assessment	22
2.8.2 SU2 Validation Framework.	23
2.9 Validity of SU2 for NICFD	24

3	Design of a Validation Study for NICFD	25
3.1	Validation Study Framework	25
3.1.1	Flow Case: High Speed Isentropic Expansion	27
3.1.2	Direct Response Quantities	28
3.1.3	Engineering Response Quantities	29
3.2	Nozzle Test Section Experiments	30
3.2.1	Converging Diverging Nozzle Profile	31
3.2.2	Test Case Operating Conditions	31
3.2.3	Data Processing	32
3.3	SU2 Model Definition	33
3.3.1	Assumptions	33
3.3.2	Spatial Discretisation	34
3.3.3	Thermodynamic Model	35
3.3.4	SU2 Configuration	37
3.4	Discussion on the SU2 Configuration	39
3.4.1	Thermodynamic Model	39
3.4.2	Viscous Effects	39
4	Uncertainty Quantification of the SU2 Flow Solver	41
4.1	Quantifying Model Uncertainty	41
4.1.1	Applied Numerical Infrastructure	42
4.1.2	Infrastructure Verification	42
4.2	Model Uncertainties for Non-Ideal Compressible Flow	43
4.2.1	Discretization Uncertainty	43
4.2.2	Forward Propagated Input Uncertainty	45
4.2.3	Total Uncertainty of the DRQ	48
4.3	Engineering Significance of System Response Uncertainties	49
4.3.1	Mass Flow Uncertainty	49
4.3.2	Loss Coefficient Calculation	50
4.3.3	Loss Coefficient Sensitivity Analysis	51
4.3.4	Loss Coefficient Uncertainty	52
4.3.5	DRQ to ERQ Uncertainty Maps	53
4.4	Discussion on SU2 uncertainty quantification	55
4.4.1	Tools and Methods	55
4.4.2	Magnitude and Sensitivity	56
4.4.3	System Responses	57
5	Validation of SU2 for NICFD Simulations	59
5.1	Engineering Uncertainty Threshold	59
5.2	Results of DRQ Validation	61
5.2.1	Test Case PR.027-NT.001	61
5.2.2	Test Case PR.025-NT.001	63
5.2.3	Mass Flow	64
5.3	Discussion of SU2 Validation	66
5.3.1	Methodology	66
5.3.2	Converging-Diverging Nozzle Flow	67
5.3.3	Metrics	67
5.3.4	Hypothesised Source of Error	68
6	Conclusion	69
6.1	Research Answers	69
6.2	Recommendations	71
6.3	Future Work	72
A	Proof of Assumptions	75
A.1	Adiabatic Flow	75
A.2	One Dimensional Mass flow	76

B Ideal Specific Heat Uncertainty Quantification	77
C Residuals	79
D Remaining Results	81
D.1 Uncertainty Quantification PR.025-NT.001	81
D.2 Uncertainty Quantification PR.027-NT.001	87
D.3 Validation	90
E Detailed UQ Code Structure	93
F List of Equipment	97
G Configuration Files	99
H Tips for Converging NICFD SU2 Simulations	103
Bibliography	105

List of Figures

2.1	Diagrams of common compounds used in Rankine cycles to illustrate the molecular complexity of organic fluids. a) Chemical structure of the organic compound MM, $C_6H_{18}OSi_2$. Note that CH_3 and H_3C are the same organic compound (methyl) but silicon always bonds with carbon, thus for clarity the 'C' is placed closest to the 'Si'. b) Chemical structure of water, H_2O , which is not organic.	6
2.2	Generic simplified T - s diagram showing the different phases of a fluid. Isobars are drawn in grey dashed lines with pressure increasing from bottom right to top left. The critical temperature and pressure are constants for a fluid and are identified with a black dotted line and black dashed line respectively. The intersection of these values indicates the critical point, around which the fluid must be considered non-ideal. In real physics the transition between phases are also less clearly pronounced as in this diagram.	6
2.3	Variation of compressibility factor as a function of pressure along constant temperature lines. The temperature and pressure are written in reduced form; non-dimensionalised with respect to the critical values. This figure is produced using air as a representative fluid but has the same trends as dense organic gas.	7
2.4	$T - s$ Diagrams of Siloxane MM illustrating the region of non-ideality near the critical point where ORC turbomachines operate. a) The surface contour is the isothermal compressibility β_T with superimposed constant pressure lines and constant compressibility factor Z lines. b) The surface contour is the compressibility factor Z with superimposed constant polytropic exponent γ_{pv} lines, and fundamental derivative Γ lines.	9
2.5	Generic simplified p - h diagram showing the processes from state A to state B. States W,X,Y, and Z are all potential intermediate states in the process which will have only one possible enthalpy rise.	14
2.6	Schematics of steady shock waves in compressible flow. In these cases the flow is adiabatic and inviscid, starting from supersonic flow on the left, $V_1 > a$, and resulting in subsonic flow on the right, $V_2 < a$ a) Normal Shock wave b) Oblique Shock wave with normal and tangential components of the flow velocity with respect to the shock.	15
2.7	$\beta - \theta - M$ diagram for Siloxane MM modelled with the ideal gas law. The angle of a shock, β , is directly related to the flow turning angle, θ , of a flow for a given Mach number assuming a constant specific heat ratio of 1.02605. There are two possible solutions for the shock angle: one is related to the weak shock, and one is related to the strong shock. Both shocks are possible, but the weak is more likely due to the principles of energy conservation. If the flow turning angle is larger than the maximum point on the given Mach curve, then the shock detaches from the surface.	16
2.8	Graphical representations of the ASME V&V 20 metric comparing the validation uncertainty with the comparison error between the mean simulation response and the mean experimental response. a) Valid case where the validation uncertainty is larger than the comparison error. b) Invalid case where the comparison error is larger than the validation uncertainty.	18

2.9	Graphical representations of the four validity cases defined by the real-space metric. The experimental and simulation mean values are kept separate with the relation between the uncertainty bars characterising the level of validity for the model. a) Valid case where the simulation uncertainty contains the experimental uncertainty, representing that the simulation contains all possible reality; Referred to as zero-order validity. b) Dubious validity where the simulation uncertainty is less than the experimental uncertainty. IN this case the simulation only captures a portion of possible reality, indicating that experiment must be improved. c) Dubious validity where the uncertainty bars overlap, but do not contain each other. Here the simulation only captures a portion of reality, indicating that the error is significant. d) Invalid case where there is no overlap between uncertainty bands.	19
3.1	Flow chart of the developed validation procedure for this thesis. The procedure is broken into four phases, expressed by different colours in the diagram. The items with a white star in the top right corner are covered in this thesis, while the light colours are either completed by other researchers or omitted for simplicity.	26
3.2	Simplified breakdown of Turbomachine system used in an organic Rankine cycle to unit model cases for validation. The highlighted route is the validation case study of SU2 in relation to the end objective of optimising turbomachinery designs. This study focuses on the thermodynamic submodels of SU2 which can be applied to NICFD flows within turbomachines. This hierarchy is adapted from American Institute of Aeronautics and Astronautics (AIAA) [3].	28
3.3	Expansion section of a converging-diverging nozzle designed for Siloxane MM as the working fluid with Mach 2.1 at the outlet. The Mach number increases at different rates in the diverging nozzle, resulting in three regions of the flow. In the kernel region the Mach number is lower at the centreline and larger at the wall. In the reflex region the mach number at the wall lower and it increases towards the centre of the flow. The uniform flow region has constant Mach number and constant properties, this is where the flow is fully expanded. Figure taken from Head [34].	29
3.4	Two dimensional cross section of the ORCHID nozzle profile. The inlet on the left is the plane of reference from where all dimensional measurements are taken. Pressure tap locations are also indicated on the nozzle walls. The nozzle geometry is superimposed on plots of flow conditions for the remainder of this thesis as a reference. Taken from Head [34].	31
3.5	T - s diagram of Siloxane MM with process runs 25 and 27 of the ORCHID nozzle test section identified with isentropic lines. The isobaric lines are provided for the two experiments, with γ_{pv} contours and Γ contour lines also identified. Both expansions have a pressure ratio of nine and take place within the non-ideal dense gas region. The critical point is given as a reference.	32
3.6	Schlieren image of Siloxane MM in the diverging part of the nozzle from PR25 taken from the ORCHID processed by the Beltrame [9] tool. The nozzle profile, centreline, and throat are given to the software which superimposes the reference geometry on the raw image in yellow, purple, and dotted red, respectively. The expansion waves can be seen in the raw image, with the tool identified angles superimposed with green lines. The image has been flipped to agree with the positive flow direction convention of left to right. Taken from Head [34].	33
3.7	Discretised ORCHID half nozzles for the SU2 flow solver. The top mesh is has 10000 unstructured elements with uniform size. This can be used for Euler simulations. The bottom mesh is a hybrid of structured and unstructured cells designed for RANS simulations. The unstructured component is in the free stream and the structured mesh is on the nozzle wall to capture the boundary layer development. There are nearly 15000 elements total in the hybrid mesh.	34

- 3.8 Grid convergence study showing the change in SU2 system responses between different mesh resolutions of the ORCHID nozzle. The error values are plotted as a function of number of cells in the grid, showing the trend of grid independence. The error represents the average difference between the finest mesh solution (110000 elements) and the mesh solution with the number of elements listed on the x-axis. It is calculated by taking the square of the difference between the DRQ of the given mesh and the finest mesh at every discrete point along the centreline, then taking the average of the squared differences and calculating the square root. This root sum of squares procedure gives an average error for the system response. The value is non-dimensionalised by dividing by the average value of the variable for the given simulation, and multiplied by 100%. For one variable there is one value of RMS error for each grid. Each variable can then be plotted on the same graph. Seven meshes were examined and compared against the finest mesh for five system variables. 35
- 3.9 Comparison of two-dimensional SU2 simulations for the supersonic expansion of Siloxane MM through a converging-diverging nozzle with inlet temperature of 252°C. The top half of each contour plot is an Euler simulation with the Peng-Robinson equations implemented as the EoS. The bottom half of each contour plot is a RANS simulation with the iPRSV EoS implemented. The meshes are as illustrated in Figure 3.7. **a)** Pressure distribution calculated for PR.027-NT001. Units are bar absolute. **b)** Mach distribution calculated for case PR.025-NT.001. 36
- 3.10 Comparison of the different thermodynamic state equations which can be used to close the Euler equations in SU2. Four Euler simulations of Siloxane MM, each with a different EoS, are plotted for the two variables of interest along the ORCHID nozzle test section. The results are compared against a RANS simulation using the iPRSV EoS and against experimental data points. The pressure data is from PR.027-NT.001, and the Mach data is from PR.025-NT.001. The Peng-Robinson, fluidprop SW equation, iPRSV, and ideal gas models are compared with error calculated with respect to the experimental value. **a)** The absolute static pressure along the nozzle surface. **b)** The error of the simulation static pressure with respect to the experimental values along the nozzle surface. **c)** The Mach number along the nozzle centreline. The position is non-dimensionalised with respect to the throat height. **d)** The error of the simulation Mach number with respect to the experimental values along the nozzle centreline. The position is non-dimensionalised with respect to the throat height. 38
- 3.11 Comparison of the temperature along the centreline of the nozzle calculated using different thermodynamic state equations which can be used to close the Euler equations in SU2. Four Euler simulations of Siloxane MM, each with a different EoS, are compared against a RANS simulation using the iPRSV EoS. The ideal gas law is off by nearly 80K at the outlet, while the Peng-Robinson EoS also deviates from the accurate models due to the polytropic constant γ approximation. 40
- 4.1 Applied framework to implement a sparse grid stochastic collocation UQ for SU2. The code, implemented in Linux, accepts PDFs of SU2 model inputs and evaluates the uncertainties of the DRQ along with the Sobol indices for the given configuration of SU2. 43
- 4.2 Total expanded numerical uncertainty of direct system responses calculated on a 10000 element mesh in SU2 using the Richardson Extrapolation method of Eça and Hoekstra [22]. The flow is a converging-diverging nozzle with Siloxane MM as the working fluid. The inlet flow is at Mach 0.2 and the outlet is Mach 2, with an expansion ratio of approximately nine. The uncertainty is calculated at discrete points along the nozzle and connected with linear sections for clarity. The nozzle profile is superimposed to illustrate the relative position of the uncertainty values along the nozzle. **a)** Pressure along the nozzle surface for PR.027-NT.001. **b)** Mach number along the centreline of the nozzle for PR.025-NT.001 **c)** Oblique shock wave angle uncertainty for different flow turning angles created by a wedge at the nozzle outlet. The shock angles are solved using the jump conditions across a steady shock for non-ideal gas dynamics. 44

4.3	Kernel transition for PR.027-NT.001 illustrated by a white line overlaying the contour plot of the Mach number. The Mach number has a change in gradient at 70 mm along the nozzle centreline, and 5.5 mm along the nozzle surface which represents the transition from kernel region to reflex region.	45
4.4	Sobol indices representing the relative influence of uncertain input parameters on the system responses of a converging-diverging nozzle with Siloxane MM as the working fluid modelled in SU2 assuming two-dimensional flow using the compressible Euler equations. The inlet flow conditions are at Mach 0.2 and the outlet is Mach 2, with an expansion ratio of approximately nine. a) The effect on the uncertainty of pressure of PR.027-NT.001 calculated along the nozzle surface using the Peng-Robinson EoS. b) The effect on the uncertainty of Mach number of PR.025-NT.001 evaluated along the centreline using the Peng-Robinson EoS. c) The effect on the uncertainty of the oblique shock angle calculated at the outlet of the nozzle for PR.025-NT.001 using the iPRSV EoS.	46
4.5	Expanded input uncertainties for the system responses of a converging-diverging nozzle with Siloxane MM as the working fluid modelled in SU2 assuming two-dimensional flow using the compressible Euler equations. The inlet flow at Mach 0.2 and the outlet is Mach 2, with an expansion ratio of approximately nine. The nozzle profile is superimposed for reference. a) The Mach number uncertainty calculated along the nozzle centreline for PR.025-NT.001 evaluated using the Peng-Robinson EoS. The results from three different UQ studies are superimposed to illustrate the independence of the results from the UQ method and EoS selected. b) The pressure uncertainty calculated along the nozzle surface for PR.027-NT.001 evaluated using the Peng-Robinson EoS. c) The uncertainty of the oblique shock angle calculated at the outlet of the nozzle for PR.025-NT.001 using the iPRSV EoS.	47
4.6	Total expanded uncertainties for the system responses of a converging-diverging nozzle with Siloxane MM as the working fluid. The inlet flow at Mach 0.2 and the outlet is Mach 2, with an expansion ratio of approximately nine. The proportion of the uncertainty due to the numerical, input, and experimental uncertainties is highlighted in blue, red, and yellow, respectively. The nozzle profile is superimposed for reference. a) The pressure uncertainty calculated along the nozzle surface for PR.027-NT001. The simulation components of the uncertainty are evaluated using the Peng-Robinson EoS. b) The Mach number uncertainty calculated along the nozzle centreline for PR.025-NT-001. The simulation components of the uncertainty are evaluated using the Peng-Robinson EoS. Only the diverging section of the nozzle is presented.	48
4.7	Sobol indices representing the relative influence of uncertain input parameters on the mass flow at teh throat of a converging-diverging nozzle with Siloxane MM as the working fluid modelled in SU2 using the Peng Robinson EoS. a) PR.025-NT001 with an inlet pressure of 18 bar. b) PR.027-NT001 with an inlet pressure of 11 bar.	50
4.8	Locations of pressure taps along the ORCHID test section nozzle profile superimposed on the contour plot of the Mach number from PR.025-NT.001. Theoretical steady normal shocks are placed at each of the indicated x positions, and the loss across them is calculated using the conditions corresponding to the centreline as the conditions before the shock. Black lines are analysed in detail in Sec. 4.3.4.	50
4.9	Applied framework to evaluate the loss coefficient across a normal shock. The code accepts the conditions before a shock and evaluates the entropy rise across the shock before no-dimensionalising the value.	51
4.10	Sobol indices representing the relative influence of uncertain input parameters on the loss coefficient calculated across a non-ideal steady normal shock with Siloxane MM as the working fluid using an iterative shock solving method and the iPRSV EoS. The sensitivities are calculated for a shock occurring with inlet conditions of Mach 2, pressure at 1.9 bar and temperature of 477 K.	52

- 4.11 Loss Coefficient across a non-ideal normal shock located in different positions of a converging-diverging nozzle with Siloxane MM as the working fluid. **a)** The loss coefficient value and expanded uncertainty as a function of the Mach number before the shock. **b)** Variation of Sobol indices representing the relative influence of uncertain input parameters on the loss coefficient uncertainty. The nozzle is superimposed for reference. 53
- 4.12 Relation of a flow parameter uncertainty to the loss coefficient uncertainty calculated across a non-ideal steady normal shock located in a converging-diverging nozzle with Siloxane MM as the working fluid. The shock is calculated using an iterative numerical procedure summarised in section 2.5, and using the iPRSV EoS. The flow conditions from the SU2 model of the ORCHID nozzle are presented with black stars. **a)** Map of pressure uncertainty to loss coefficient uncertainty. PR.027-NT001 results are superimposed as black stars. **b)** The same as a), but in absolute uncertainty instead of percent. **c)** Map of Mach uncertainty to loss coefficient uncertainty. PR.025-NT001 results are superimposed as black stars. 54
- 5.1 Validation uncertainty diagram. The sources of uncertainty in a validation campaign are identified and related to the forms of uncertainty relevant to validation metrics. The experimental sources of uncertainty are coloured in red while the simulations sources of uncertainty are highlighted in blue. The diagram illustrates the focus of the validator in producing the uncertainty bands and comparing the results of simulation and experiment for a given system response quantity, while the focus of an engineer is to determine the value of a design or performance metric, called ERQ, to a given level of accuracy. The ERQ uncertainty can be converted to an SRQ uncertainty using a UQ, thus defining an upper limit of precision called U_{sig} 60
- 5.2 Validation plots of static pressure for a converging-diverging nozzle modelled in SU2 using the compressible Euler equations and the Peng-Robinson EoS. The test case is described in Sec. 3.2 and the model definition summarised in Sec 3.3. The mean simulation results along the nozzle surface are compared against the mean ORCHID PR.027-NT.001 pressure tap data. **a)** Absolute static pressure as a function of nozzle position. **b)** Absolute static pressure with respect to the SU2 model mean simulation value as a function of nozzle location. This is a version of the real space metric. **c)** Absolute static pressure as a function of polytopic exponent γ_{pv} . **d)** ASME V&V 20 validation metric plot of absolute static pressure as a function of nozzle position. 62
- 5.3 Validation plots of Mach number for a converging-diverging nozzle modelled in SU2 using the compressible Euler equations and the Peng-Robinson EoS. The test case is described in Sec. 3.2 and the model definition summarised in Sec 3.3. The mean simulation results along the nozzle centreline are compared against the mean ORCHID PR.025-NT.001 schlieren data. **a)** Mach number as a function of nozzle position non-dimensionalised with respect to the throat height. **b)** Mach number with respect to the SU2 model mean simulation value as a function of nozzle location non-dimensionalised with respect to the throat height. This is a version of the real space metric. **c)** Mach number as a function of polytopic exponent γ_{pv} . **d)** ASME V&V 20 validation metric plot of Mach number as a function of nozzle position non-dimensionalised with respect to the throat height. 64
- 5.4 Validation plots of mass flow through a converging-diverging nozzle modelled in SU2 using the compressible Euler equations and the Peng-Robinson EoS. The test case is described in Sec. 3.2 and the model definition summarised in Sec 3.3. The mean simulation mass flow at the nozzle throat when operating at a given inlet pressure are compared against the mean measured ORCHID mass flow on the liquid side of the nozzle at the same inlet pressure. **a)** Absolute value of the mass flow with the design value for reference. **b)** Mass flow with respect to the SU2 model mean simulation value. This is a version of the real space metric. **c)** ASME V&V 20 validation metric plot of mass flow. 65

5.5	Comparison of two simulations with experimental results of the Mach number along the centreline of a converging-diverging nozzle modelled in SU2 using the compressible Euler equations and the Peng-Robinson EoS. The test case is described in Sec. 3.2 and the model definition summarised in Sec 3.3. The two models use the same nozzle profile as the experiment, but have different throat areas. The model of a nozzle with a 6.66 mm throat is in blue dashed lines, while the model with a 8 mm throat is in solid red. The nozzle profile is superimposed in black to provide a reference.	68
A.1	X-momentum in the ORCHID nozzle for PR25. RANS simulation using the iPRSV Eos. centreline values are compared against the average and the integrated value for the inlet, throat, and outlet.	76
B.1	image of the C_p^{ig} sensitivity to its coefficients. An example of the Sobol Index	77
C.1	Residuals for the convergence of a PR.025-NT.001 compressible Euler flow case in SU2 run using the Peng-Robinson Equation of State. The simulation starts from the first order converged solution and is run second order.	79
C.2	Residuals for the convergence of a PR.027-NT.001 compressible RANS flow case in SU2 run using the iPRSV Equation of State. The simulation starts from the first order converged solution and is run second order.	80
D.1	PR.025-NT.001 Centreline: UQ Results for Pressure. a) Sobol Indeces using Peng Robinson EoS. b) Sobol Indeces using iPRSV EoS. c) Response with uncertainty bars using Peng Robinson EoS. d) Plot of U_{in} vs location. The reference value is the LHS mean.	81
D.2	PR.025-NT.001 Centreline: UQ Results for Density. a) Sobol Indeces using Peng Robinson EoS. b) Sobol Indeces using iPRSV EoS. c) Response with uncertainty bars using Peng Robinson EoS. d) Plot of U_{in} vs location. The reference value is the LHS mean.	82
D.3	PR.025-NT.001 Centreline: UQ Results for Velocity. a) Sobol Indeces using Peng Robinson EoS. b) Sobol Indeces using iPRSV EoS. c) Response with uncertainty bars using Peng Robinson EoS. d) Plot of U_{in} vs location. The reference value is the LHS mean.	83
D.4	PR.025-NT.001 Centreline: UQ Results for Temperature. a) Sobol Indeces using Peng Robinson EoS. b) Sobol Indeces using iPRSV EoS. c) Response with uncertainty bars using Peng Robinson EoS. d) Plot of U_{in} vs location. The reference value is the LHS mean.	84
D.5	PR.025-NT.001 Centreline: UQ Results for μ . a) Sobol Indeces using Peng Robinson EoS. b) Sobol Indeces using iPRSV EoS. c) Response with uncertainty bars using Peng Robinson EoS. d) Plot of U_{in} vs location. The reference value is the LHS mean.	85
D.6	PR.025-NT.001 Centreline: UQ Results for γ_{pv} . a) Sobol Indeces using Peng Robinson EoS. b) Response with uncertainty bars using Peng Robinson EoS. c) Plot of U_{in} vs location.	86
D.7	PR.027-NT.001 Nozzle Profile: UQ Results for Temperature. a) Sobol Indeces using Peng Robinson EoS. b) Response with uncertainty bars using Peng Robinson EoS. c) Plot of U_{in} vs location.	87
D.8	PR.027-NT.001 Nozzle Profile: UQ Results for Density. a) Sobol Indeces using Peng Robinson EoS. b) Response with uncertainty bars using Peng Robinson EoS. c) Plot of U_{in} vs location.	88
D.9	PR.027-NT.001 Nozzle Profile: UQ Results for γ_{pv} . a) Sobol Indeces using Peng Robinson EoS. b) Response with uncertainty bars using Peng Robinson EoS. c) Plot of U_{in} vs location.	89

D.10	Validation plots of Mach number for a converging-diverging nozzle modelled in SU2 using the compressible Euler equations and the Peng-Robinson EoS. The test case is described in Sec. 3.2 and the model definition summarised in Sec 3.3. The mean simulation results along the nozzle centreline are compared against the mean ORCHID PR.025-NT.002 schlieren data. a) Mach number as a function of nozzle position non-dimensionalised with respect to the throat height. b) Mach number with respect to the SU2 model mean simulation value as a function of nozzle location non-dimensionalised with respect to the throat height. This is a version of the real space metric. c) Mach number as a function of polytopic exponent γ_{pv} . d) ASME V&V 20 validation metric plot of Mach number as a function of nozzle position non-dimensionalised with respect to the throat height.	90
D.11	PR.025-NT.001: Comparison of the measured μ angle along the centreline of the nozzle test section and the SU2 simulated value. a) Absolute Value of μ vs nozzle position. b) μ with respect to the SU2 model mean simulation value as a function of nozzle location non-dimensionalised with respect to the throat height. This is a version of the real space metric. c) Absolute Value of μ as a function of polytopic exponent γ_{pv} . d) ASME V&V 20 validation metric plot of μ as a function of nozzle position.	91
D.12	PR.025-NT.002: Comparison of the measured μ angle along the centreline of the nozzle test section and the SU2 simulated value. a) Absolute Value of μ vs nozzle position. b) μ with respect to the SU2 model mean simulation value as a function of nozzle location non-dimensionalised with respect to the throat height. This is a version of the real space metric. c) Absolute Value of μ as a function of polytopic exponent γ_{pv} . d) ASME V&V 20 validation metric plot of μ as a function of nozzle position.	92
E.1	Flow chart of ' NumericalUncertainty.m '. The numerical uncertainty calculations which integrates the SU2 solutions with the Richardson extrapolation. The executable code from Refresco is in red, while the MatLab scripts are in blue. The solutions from each grid must be complete before the code is used.	94
E.2	Top level of the UQ infrastructure. The Dakota input file must be configured, then when Dakota is run the python scripts are called automatically. Dakota selects the inputs for the simulation and provides them to the ORCHID nozzle analysis.	94
E.3	Mid-level UQ infrastructure: ' ORCHIDNozzle_UQ.py '. The script is run on every evaluation of the SU2 solution. The Python script is called by Dakota to run SU2 and post-process the results. A unique solution for the ORCHID nozzle simulation is produced for the set of input variables passed into the code by Dakota. The script can be run independently for a single run and analysis of the nozzle model.	95
E.4	Bottom level UQ infrastructure: ' postprocess.m '. The post-processing framework for shock solving and data storage of the SU2 solution. This code can be run independently to extract the SRQ of interest from an SU2 solution file and present them in a txt file and figures. Producing figures is not done on every loop of a UQ, but can be done for analysis of a single SU2 solution.	95

List of Tables

2.1	Classifications of gas dynamics as a function of the fundamental derivative. In ideal flow the speed of sound increases with the density, while non-ideal flow has decreasing speed of sound with increasing density. The special cases of $\Gamma = 0$ and $\Gamma = 1$ are theoretical and do not happen in practice.	9
3.1	The two experiments considered in the validation study.	31
3.2	Configuration settings for the boundary conditions of the ORCHID nozzle mesh.	35
3.3	Fluid Parameters of Siloxane MM	37
4.1	Uncertainty quantification studies conducted to verify the UQ framework for SU2 NICFD forward propagated input uncertainty quantification. The studied were all done on a model of the ORCHID nozzle test section using PR.025-NT.001 as the reference flow condition.	42
4.2	Uncertainties of inputs used for the SU2 model of the ORCHID nozzle test section using the Peng-Robinson Eos.	45
4.3	Mass flow calculated at the throat of a converging-diverging nozzle with Siloxane MM as the working fluid modelled in SU2 using the Peng Robinson EoS.	49
4.4	Input uncertainties used to calculate the loss coefficient due to entropy rise across an imaginary shock located at the outlet of a converging-diverging nozzle with Siloxane MM as the working fluid. The first six uncertainty distributions for flow parameters are normal, the remaining thermodynamic parameters have uniform uncertainties.	52
B.1	Comparison of the VBD and SC sobol index results	78
B.2	Comparison of LHS and SC uncertainty calculation results	78
E.1	Input uncertainties used for the PR.025-NT.001 iPRSV UQ.	96

Glossary

Acronyms

AIAA	American Institute For Aeronautics And Astronautics. 25
ASME	American Society Of Mechanical Engineers. 17
CFD	Computational Fluid Dynamics. 5, 25, 41
CREA	Compressible-fluid Dynamics For Renewable Energy Applications. 24
DRQ	Direct Response Quantities. 27, 28, 41
EOS	Equation Of State. 4, 11, 33, 35, 41, 97
ERQ	Engineering Response Quantities. 27, 29, 49, 59, 69
GUM	Guide To The Expression Of Uncertainty In Measurement. 17, 41
IPRSV	Improved Peng-Robinson EoS Modified By Stryjek And Vera. 12, 33, 97
JANNAF	Joint Army Navy NASA And Air Force. 19
LHS	Latin Hypercube Sampling. 19, 42
MAH	Martin-Hou. 21
MM	Hexamethyldisiloxane. 4, 5, 29, 69, 97
NICFD	Non-ideal Compressible Fluid Dynamics. 1, 5, 27, 41, 69, 97
NS	Navier-Stokes. 10, 39, 41
ORC	Organic Rankine Cycle. 2, 5, 27, 42, 69
ORCHID	Organic Rankine Cycle Hybrid Integrated Device. 4, 21, 30, 32
PDE	Partial Differential Equations. 2
PDF	Probability Distribution Function. 20
PP	Power And Propulsion. 1, 24
PR	Process Run. 31, 41
PRSV	Peng-Robinson EoS Modified By Stryjek And Vera. 12, 37
RANS	Reynolds-Averaged Navier-Stokes. 10, 35
RKS	Redlich-Kwong-Soave. 21
SC	Stochastic Collocation. 19, 42
SRQ	System Response Quantities. 16, 25
SU2	SU2 Multiphysics Simulation And Design Software. 2, 5, 69
SW	Span-Wagner. 13, 33, 35, 97
TROVA	Test-Rig For Organic VApours. 21
T-S	Temperature Entropy. 6, 39
TUD	Technical University Of Delft. 2, 24, 97
UMG2	Unstructured Mesh Generator 2 Dimensional. 34
UQ	Uncertainty Quantification. 3, 19, 41
VBD	Variance Based Decomposition. 20, 42
VV	Verification And Validation. 17

Notation

Area	A	[m ²].	30
Conservative variable vector	B	[-].	11
Speed of sound	c	[m/s].	8
Isochoric heat capacity	C_v	[kJ /kg.K].	8
Isobaric heat capacity	C_p	[kJ /kg.K].	8, 13, 46,
			96
Diameter	D	[mm].	31
Internal energy	e	[kJ/kg].	13
Comparison error	E	[kJ/kg].	17, 27
Fluxes	F	[-].	11

Body force	f	[N].	10
Enthalpy	h	[kJ/kg].	13
Identity matrix	I	[-].	11
Thermal conductivity	k	[-].	14
Mass flow	\dot{m}	[-].	30
Molecular mass	MW	[kg/mol].	5
Mach number	M	[-].	4, 14
Pressure	p	[Pa].	4, 7
Heat conduction	q	[-].	14
Source term	Q	[-].	11
Universal gas constant	R	[J /K.mol].	7
Entropy	s	[J/kg.K].	13
Temperature	T	[C].	7
Specific volume	v	[m ³ /kg].	7
Velocity component	u	[m/s].	14
Velocity	\vec{U}	[m/s].	10
Uncertainty	U	[-].	27
Compressibility factor	Z	[-].	7
Shock wave angle	β	[deg].	4, 15
Isothermal compressibility	β_T	[-].	8
Ideal specific heat ratio	γ	[-].	8
Polytropic exponent	γ_{PV}	[-].	8
Thermodynamic constant	κ	[-].	12
Fundamental derivative	Γ	[-].	8
Flow turning angle	θ	[deg].	15
Ideal specific heat coefficients	η	[-].	13
Shear stress	τ	[kg/(m s ²)].	14
Density	ρ	[kg/m ³].	7
Expansion angle	μ	[deg].	15
Viscosity	μ^v	[kg/(m s)].	14
Acentric factor	ω	[-].	5, 12
Loss coefficient	ζ	[-].	30

Subscripts

Critical	cr	12	Experimental	D	41
Directional index	i	10	Engineering	eng	60
Directional index 2	j	10	Forward propagated input	in	41
Stagnation	o	30	Numerical	num	41
Throat	th	30	Significant	sig	60
Type A	A	41	Simulation	S	41
Type B	B	41	Validation	val	18

Introduction

Demand for Power and Propulsion (PP) technology is growing annually, however the efficiency gains in the past decade for traditional PP systems are negligible when compared to the previous century. The increased demand, without significant improvement to fuel efficiency or decrease of emissions, is a major contributing factor to the global environmental crisis. The lack of innovation is partially due to the high costs and risks of developing new power systems concepts. To overcome the limits of current PP technology the focus of research must be directed towards developing novel designs to harness new energy sources in an affordable way, or to harness energy which was thought to be inaccessible. This can be done by targetting a fundamental principle of thermodynamics: in order to extract power there must be heat input to the system *and heat output* to the environment. Even if the system itself is fully insulated, waste heat must be produced in every PP system. For example, exhaust from a gas turbine can be between 370°C and 540°C and could be used to produce an extra 2 MW of electrical energy for a system designed to only produce 10 MW. Poerner and Rimpel [49] provides a list of other examples where waste heat could be efficiently recovered. As such, novel systems to recover energy from waste heat are being designed for use in combination with existing technology. While this is a simple concept, these new system designs require innovation in the engineering hardware of thermodynamics: heat exchangers, designed to transfer as much heat as possible from one fluid to another; and turbomachinery, designed to extract or add energy from a fluid flow. The validation of the SU2 flow solver for non-ideal compressible fluid dynamics (NICFD) would enable rapid and low cost development of turbomachinery for these novel thermodynamic systems.

1.1. Motivation

Turbomachinery combines the fundamental engineering fields of thermodynamics and fluid mechanics for the purpose of energy conversion. Those who study turbomachinery are focused on designing more efficient machines which can extract or add energy, in the form of work, from a fluid flow. The machines, such as turbines, compressors, and pumps, are components used in larger PP systems where energy is converted from a heat source into useful work. While the first thoughts of turbomachines may be regarding Brayton cycle energy conversion, for example gas turbines used in aircraft propulsion or electric power generation, the study of turbomachinery is also critical for its use in Rankine cycle power plants.

The Rankine cycle is a closed loop method for converting thermal energy into usable mechanical or electrical energy. This is done through pumping or condensing a fluid through a heat source and then extracting energy from the heated fluid through a turbine. The work extracted from the turbine is used to drive the pump or compressor, and the excess energy can be used to drive a mechanical device or a motor to create electricity. After the turbine, the fluid then goes through a condenser or cooler where the residual heat is emitted. The fluid continues through the loop, being heated and cooled continuously, acting as the conduit for energy transfer. This method is currently used in coal and nuclear power plants with water as the working fluid.

Most Rankine cycles have used steam since water is easily available and a chemically simple compound, however in theory the Rankine cycle can be used with any working fluid. Each fluid has unique

properties which lead to different optimal operating temperatures of the cycle, and thus the choice of fluid directly affects the efficiency of the cycle. If the thermal energy source is relatively small and at a high temperature, such as the waste heat of traditional energy production methods listed in the opening paragraph, the selection of a fluid formed by complex molecules in a superheated cycle is the optimal configuration. This is the basis for one proposed novel development in PP, to use organic fluids in a novel Rankine cycle to efficiently recover waste heat energy. Any fluid with carbon atoms which have covalent bonds in chain like structures are considered organic, and these fluids often have complicated molecules capable of storing large amounts of energy. Using an organic fluid in a Rankine cycle is called an organic Rankine cycle (ORC) and has become a focus of energy production research.

The ORC has a size advantage compared to a standard Rankine cycle with the same heat input, and operates at conditions well suited for renewable energy systems, or extracting energy from the waste heat of large scale energy production methods. e.g. the ORC can be used in combination with already existing Brayton and Rankine cycle power and propulsion systems to extract power from the waste heat. This novel concept of combined cycle power systems using organic working fluids is one step towards overcoming the limits of current PP systems.

Research in turbomachinery now includes the design of turbo-expanders for applications in ORC power generation. The challenge arises from the fluids used, such as siloxanes, which are dense organic vapours and do not behave ideally at the cycle design conditions. At these temperatures and pressures the fluids becomes highly compressible and fall in the realm of NICFD. NICFD is classified by flow in which the speed of sound decreases if the pressure and density increase. This is the opposite trend experienced by air and steam, and is representative of the complex interaction between molecules experienced by an organic fluid subjected to high pressure and temperature. ORC power conversion has large potential but, because of the non-ideal thermodynamic and gas dynamic behaviour, traditional turbines designed for air or steam are not efficient. New turbines must be designed for ORC applications, but to do so the design tools must provide a reliable representation of the real physics.

Historically, the development of turbines and compressors was done through building prototypes and testing the designs. Now, after 70 years of turbomachinery performance being recorded, a database of performance characteristics for different blade shapes and spacing allows efficient machinery for water and air to be designed with empirical data. However for ORC machines there is no historical data to use as a basis, and the cost in time and monetary value to build a database of experiments comprehensive enough to use as a design basis is too large. As such, the engineering community has turned to software tools for modelling new designs for these complex flow conditions. Using software to simulate a new machine and assess its theoretical performance before building and testing allows for the design process to have a significantly lower cost.

The primary design tool used by researchers at the Technical University of Delft (TUD), Stanford University, Imperial College London, and Politecnico di Milano for NICFD turbomachinery is SU2 multiphysics simulation and design software (SU2). SU2 is a software suite designed by Economon et al. [25] to solve multiphysics Partial Differential Equations (PDE) problems and PDE constrained optimisation problems. In particular, SU2 is designed for solving fluid dynamic problems, and equipped with an adjoint design optimisation tool. The unique construction of the SU2 software makes it well suited for the design of turbomachinery. Yet, for a simulation tool to be trusted in design or analysis it must be verified and validated. Verification ensures that the mathematical model devised has been implemented correctly in the flow solver, while validation ensures that the model is representative of reality.

To predict the gas dynamic behaviour of non-ideal internal flows Pini et al. [47] have updated SU2, verified it analytically, and compared it against other solvers. Vitale et al. [66] then updated the optimisation tools to be used designing ORC turbines. Therefore the SU2 suite now provides the ability to simulate NICFD effects in internal flow applications, and design turbomachines for non-ideal flows seen in ORCs. However, to use the solver with confidence, it must be validated.

1.2. Knowledge Gap

Until 2015 the experimental ability to validate the SU2 solver was non-existent. The development of test facilities at TU Delft by Head et al. [33], and Politecnico di Milano by Spinelli et al. [58] have allowed for classical non-ideal compressible flows to be observed under controlled conditions. While Gori et al. [30] have produced experimental data, and compared it with results from the solver, the validation of SU2

for NICFD has not been achieved to a standard which was set by Eça et al. [23, 24] for computational flow solvers. Oberkampf and Roy [45] explain that a complete validation exercise requires producing experimental data to compare with model outputs, and quantifying all the uncertainties in the solver and the experiment. Once the experimental data is obtained the validation metrics require careful computation of the solver uncertainties, and therefore require uncertainty quantification (UQ). UQ is the area of study in computer science and statistics use to identify the uncertainty of a solver output based on uncertain parameters used in the model construction.

Now, despite all the requirements of validation being available, they have not yet been put together for a full validation of SU2. What remains is a comparison of results produced by an NICFD model made in SU2 with experimental data from an experimental facility. The uncertainties arising from instrumentation, random fluctuations and disturbances in the experiments, numerical discretisation of the model, and uncertain model inputs must then all be quantified. There must also be an interpretation of the resultant accuracy of SU2 for the purposes of turbomachinery design. This is a gap in academic knowledge on the validation of SU2 for classical NICFD. The SU2 solver needs to be validated before additional confidence can be put in the design exercises for advanced ORC turbines. This research project begins filling that gap.

1.3. Objective

The objective is to determine if the SU2 flow solver can accurately predict the gas dynamic behaviour of a dense organic vapour during a high speed non-ideal expansion. This can be done by building an infrastructure for assessing the predictive capability of the solver; quantifying the uncertainties in the simulation arising from input uncertainties for a dense organic vapour expansion; and assessing the accuracy of the flow solver against experiments over a range of compressibility. To use the SU2 solver for simulating flows in ORC technology and thus for refining ORC technology designs it must eventually be validated for all classical non-ideal compressible fluid flows. The specific research questions and deliverables of the thesis project are described in this section.

1.3.1. Research Questions

The main research question of this thesis is “Can the SU2 flow solver be validated to predict high speed non-ideal flows of dense organic vapours?” To get an answer to this query three sub-questions are posed:

1. **How accurately can the SU2 solver predict transonic to supersonic flows of non-ideal organic fluid?**
2. **What effect does forward propagation of model input uncertainties have on the probability distribution of the SU2 simulation results of dense organic flows?**
3. **What is the domain over which the SU2 solver can be applied when solving non-ideal dense organic vapour flows?**

The domain refers to a collection of unique flow conditions imposed on an organic fluid for which the flow solver may be used in solving an isentropic expansion. This could determine if the suitability is a function of non-ideality, temperature, or even flow geometry. The answer to the final research question would be a drawn region on a digram of fluid states where SU2 models with specific configuration can be used.

1.3.2. Deliverables

To answer the research questions three deliverables are needed:

- An infrastructure, including procedures and code, to assess the accuracy of the SU2 flow solver with clearly defined metrics;
- an uncertainty breakdown of an SU2 NICFD simulation, with total uncertainty translated to engineering values significant to performance and design; and,
- a validation assessment of the SU2 solver for predicting gas dynamic behaviour in a non-ideal expansion using defined validation metrics.

1.4. Scope

This project will assess SU2 using already acquired and processed experimental data. Experiments were conducted in 2019 by Head [34], thus the validation campaign only considers SU2 modelling the experimental case: “the high speed non ideal gas expansion of hexamethyldisiloxane (MM) through the organic Rankine cycle hybrid integrated device (ORCHID) nozzle test section at design conditions”. The focus is to quantify the software uncertainty due to the input parameters, and calculate the final validation metrics. The metrics will be calculated for two independent parameters: once with the Mach number, M , along the centre line of the nozzle, and once with static pressures, p , along the profile of the nozzle.

The validation will not include extrapolation of data, or assessment of the flow solver beyond the experimental flow conditions. Only validation of conditions for which there is exact experimental data will be conducted. All possible uncertainties in the simulation are considered, including the total pressure ratio at the inlet, total temperature ratio at the inlet, and the closure coefficients of the equation of state (EoS). Additional quantities, such as shock wave angles β produced by a wedge in the flow, will be assessed for uncertainty in SU2 but not validated against experiments. Details on the experimental aspects can be seen in Beltrame [9], and Head [34].

1.5. Overview

The theoretical background of the research and a literature review of related research from the past twenty years are presented in Chap. 2. Chapter 3 will describe the validation framework, physical design, and numerical construction of the validation study. Chapter 4 contains the uncertainty quantification, and Chap. 5 presents the results of the validation study in conventional metrics, along side a newly proposed engineering metric. The research question answers and suggestions for future work are in Chap. 6.

2

Background of Classical NICFD

The study of organic fluids in high velocity flows, as seen in organic rankine cycle (ORC) turbomachines, is covered in the discipline of classical non-ideal compressible fluid dynamics (NICFD); a unique flow regime characterised by complex thermodynamic and fluid dynamic relations. In a thermodynamic context a fluid is considered an ideal gas when intermolecular forces are negligible. This happens either at low pressures or high temperatures, when the spacing between molecules is large enough that they have no effect on each other. A fluid is also considered incompressible unless the fluid is a gas travelling at a velocity larger than Mach 0.3. High velocity gas flows have significant changes in density throughout the flow field; the study of these flows is known as gas dynamics [67]. Ideal gas dynamics is flow in which the speed of sound increases if the pressure and density increase. For flows in ORC turbomachines neither assumption of ideality is valid, and non-ideal compressible fluid dynamics must be considered. This subset of fluid dynamics and is researched with experimentation and computational fluid dynamics (CFD) models.

In this chapter the distinction of classical NICFD within the study of fluid dynamics will be further explained, along with the significance of the classification with regards to compressible flow phenomena, thermo-physical sub-models, and the equations implemented in CFD. The fundamental theory is followed by a summary of the most recent research into modelling NICFD phenomena and recreating NICFD conditions with experiments. Literature is reviewed which can directly be applied to the validation of the SU2 flow solver for classical NICFD of dense organic fluids such as Siloxanes. This includes the state of the art validation and uncertainty quantification techniques which are applied to a CFD solver for use in NICFD turbomachinery applications. The background focuses on the overlap in the research fields of 'CFD flow solver validation' and 'NICFD flow' to determine how to assess the credibility of the SU2 flow solver for modelling classical NICFD of dense organic fluid.

2.1. Organic Fluids

The distinction between fluids is defined by the unique combination of elements creating their molecules. While the assembled elements prescribe the mass of a given chemical composition, the structure of these elements is what defines the remaining properties of that substance. For example, any fluid with carbon atoms which have covalent bonds is considered organic. Due to the inclusion of carbon in chain like structures, organic fluids often have a large molecular mass and complex molecular structure. Figure 2.1 shows the difference in relative molecular complexity between an organic fluid, hexamethyldisiloxane (Siloxane MM), and water, which could both be used in Rankine cycles.

Figure 2.1a shows that an organic fluid, such as MM has a complicated structure which strays from a simple spherical shape. The magnitude which the shape deviates from having spherical symmetry about a centre point is captured by the acentric factor. It was introduced by Pitzer et al. [48] in 1955 as a way to capture the connection between molecular complexity and deviation from simple thermodynamic models. Models would typically be based on experimental data which used small molecules that had close to spherical geometries. Pitzer noted that when these models were applied to complex fluids the behaviour would deviate, so the acentric factor was devised as a correction factor to match the model with experimental data for all fluids. In addition to the large acentric factors, organic fluids also have

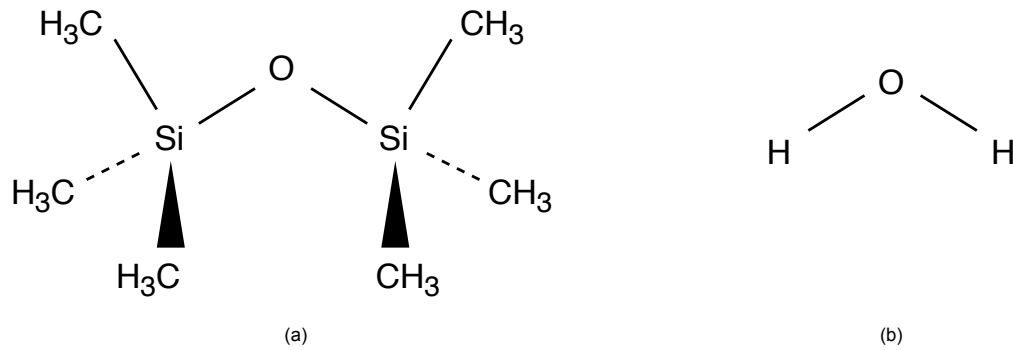


Figure 2.1: Diagrams of common compounds used in Rankine cycles to illustrate the molecular complexity of organic fluids. **a)** Chemical structure of the organic compound MM, $C_6H_{18}OSi_2$. Note that CH_3 and H_3C are the same organic compound (methyl) but silicon always bonds with carbon, thus for clarity the 'C' is placed closest to the 'Si'. **b)** Chemical structure of water, H_2O , which is not organic.

a large number of chemical bonds, which effects the fluids ability to store and transmit energy. This indicates that organic fluids have behaviour different from standard liquid and vapour flows when used in a thermodynamic system.

In addition to the molecular structure, fluid behaviour is also related to the phase of the flow. This is made more complicated by the transition between phases, such as evaporation, where some energy is used to alter the fluid phase instead of being stored in the particles themselves. This is called two phase flow and is outside the scope of this thesis. In ORC turbomachines the fluid state is near the intersection between the gas, liquid, and two-phase regions, called the critical point. The critical point and phases of a generic fluid are illustrated in Fig. 2.2 with a *temperature entropy* (T - s) diagram. It is a simplified map of fluid states for a generic compound with constant pressure lines, known as isobaric lines, superimposed.

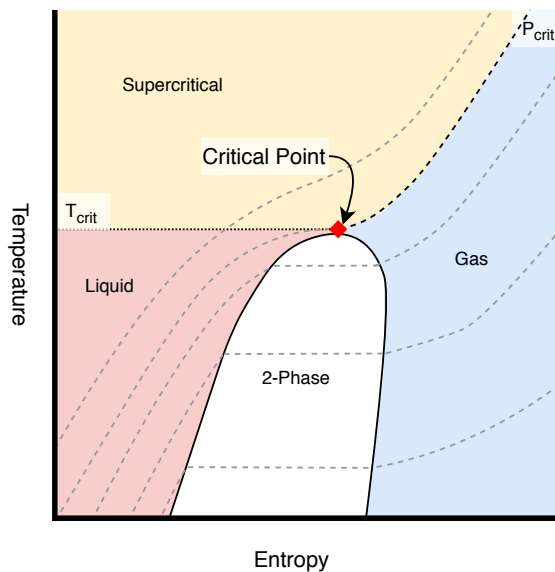


Figure 2.2: Generic simplified T - s diagram showing the different phases of a fluid. Isobars are drawn in grey dashed lines with pressure increasing from bottom right to top left. The critical temperature and pressure are constants for a fluid and are identified with a black dotted line and black dashed line respectively. The intersection of these values indicates the critical point, around which the fluid must be considered non-ideal. In real physics the transition between phases are also less clearly pronounced as in this diagram.

Note on Fig. 2.2 that with temperature and pressure combinations above the critical point the fluid is in the supercritical region. This is good in a thermodynamic sense, since there is no energy lost to

phase change. Supercritical fluids can be considered as very dense gas, but have characteristics that can not be captured by ideal gas models which neglect intermolecular forces. These characteristics are described as *non-ideal* and become more pronounced as you get closer to the critical point. Non-ideal behaviour can also be noticed in high pressure gas flows or high temperature liquids. When the molecules are closely packed in a dense gas the intermolecular forces can not be ignored and the molecular complexity can have an impact.

2.2. Quantification of Non-ideal Behaviour

The severity of non-ideality in a flow can be quantified by several non-dimensional parameters. By characterising the flow it is possible to make informed decision on the models and sub-models to implement in representing the flow. Popular characterisations of non-ideality are the compressibility factor, the isothermal compressibility, the pressure-volume polytropic exponent, and the fundamental derivative of gas dynamics. Each of these parameters can be used to quantify the domain of an ideal fluid, but are constructed differently and may relate to either thermal or gas dynamics ideality. This section will describe each parameter and provide the limits which define the region of NICFD.

2.2.1. Compressibility factor

The compressibility factor considers the relation between basic thermodynamic parameters and is defined as,

$$Z = \frac{pv}{RT} \quad (2.1)$$

where R is the universal gas constant divided by molecular mass, p is the pressure, T is the temperature, and v is the specific volume, defined as the inverse of density, $v = \rho^{-1}$. The variation of Z for air is illustrated in Fig. 2.3.

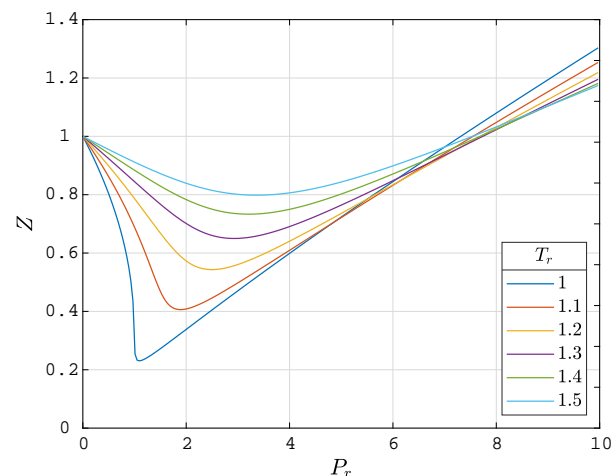


Figure 2.3: Variation of compressibility factor as a function of pressure along constant temperature lines. The temperature and pressure are written in reduced form; non-dimensionalised with respect to the critical values. This figure is produced using air as a representative fluid but has the same trends as dense organic gas.

At $Z = 1$ the fluid is considered an ideal gas where intermolecular forces are not affecting the fluid behaviour. In engineering practice values between 0.95 and 1.05 are considered close enough to ideal for the assumption to hold. When values are less than one the fluid is considered non-ideal, as the density of the fluid has increased beyond what would be expected given the pressure and temperature if the intermolecular forces are neglected. The value of Z can also be larger than one in the case of hypersonic flow, this is a result of dissociation or ionisation of molecules, however this is not a consideration of dense organic fluids used in turbomachinery.

The compressibility factor is an easy parameter to assess and provides a quick assessment of deviation from ideality, however it is not a term which can be used for many other analyses regarding flow performance. It only states if the ideal assumption is valid, and can not be used as a definition of compressibility.

2.2.2. Isothermal Compressibility

Compressibility by definition relates the change in volume of a given mass with a change in pressure [8]. To make the definition useful the value of compressibility must be made holding one parameter constant. For example the isothermal compressibility, determined at constant temperature is,

$$\beta_T = -\frac{1}{v} \left(\frac{\delta v}{\delta p} \right)_T. \quad (2.2)$$

Isothermal compressibility can be related to the compressibility factor by,

$$\beta_T = \frac{1}{p} + \frac{1}{Z} \left(\frac{\delta Z}{\delta p} \right)_T. \quad (2.3)$$

In an ideal case $\beta_T = \frac{1}{p}$ and the percent change in pressure is equal to the percent change in density. In non-ideal cases any changes in pressure to the system will have a non proportional change in density.

2.2.3. Polytropic Exponent

While a measurement of compressibility is convenient for representing complexity in a flow, it can not be used to directly evaluate the performance of a machine in non-ideal conditions. This must be done with the polytropic exponent.

Consider an isentropic process with no entropy generation, this is represented as a vertical line on the T - s diagram and is the most efficient method of adding or extracting work from a flow. Any such process can be represented mathematically with the polytropic equation $pv^\gamma = constant$, which can be used to represent any quasi-equilibrium process. Each isentrope is represented by a different constant value and in an ideal case the exponent is the ideal specific heat ratio, $\gamma = C_p/C_v$. C_v is the heat capacity of the fluid at constant volume, and C_p is the heat capacity of the fluid at constant pressure. In a real case $pv^{\gamma_{pv}} = const$ is used as the relation and the exponent is called more generically the polytropic exponent. Let

$$\gamma_{pv} = -\frac{v}{p} \left(\frac{\delta p}{\delta v} \right)_s. \quad (2.4)$$

The term can be used instead of the original γ for turbomachinery applications and internal flows to model polytropic or isentropic processes in any real gas flow. The relation between γ_{pv} and γ is

$$\gamma_{pv} = \frac{\gamma}{\beta_T p} \quad (2.5)$$

which in an ideal case simplifies to $\gamma_{pv} = \gamma$. The polytropic exponent not only conveys a deviation from ideal behaviour, but can be used to asses machine performance in a flow [43].

2.2.4. Fundamental Derivative of Gas Dynamics

The final parameter used to characterise non-ideal flow is the fundamental derivative of gas dynamics [63]. It is linked to the speed of sound, c , and is also used to classify all compressible gas flows. The fundamental derivative,

$$\Gamma = 1 + \frac{\rho}{c} \left(\frac{\delta c}{\delta \rho} \right)_s, \quad (2.6)$$

can be written as a function of γ_{pv} ,

$$\Gamma = \frac{1}{2} \left[\gamma_{pv} + 1 - \frac{v}{\gamma_{pv}} \left(\frac{\delta \gamma_{pv}}{\delta v} \right) \right]. \quad (2.7)$$

In an ideal case the fundamental derivative becomes a constant evaluated as $\Gamma = \frac{\gamma+1}{2}$.

2.2.5. Definition of Classical NICFD

Classical NICFD is defined as one subset of gas dynamics using the fundamental derivative. The classification of gas dynamics can be found in Tab. 2.1

$\Gamma > 1$	$\left(\frac{\delta c}{\delta \rho}\right)_s > 0$	Classical Ideal Behaviour
$0 < \Gamma < 1$	$\left(\frac{\delta c}{\delta \rho}\right)_s < 0$	Classical Non-Ideal Behaviour
$\Gamma < 0$	$\left(\frac{\delta c}{\delta \rho}\right)_s < 0$	Non-Classical Behaviour

Table 2.1: Classifications of gas dynamics as a function of the fundamental derivative. In ideal flow the speed of sound increases with the density, while non-ideal flow has decreasing speed of sound with increasing density. The special cases of $\Gamma = 0$ and $\Gamma = 1$ are theoretical and do not happen in practice.

The fundamental derivative of gas dynamics classifies flow into classical ideal, classical non-ideal, and non-classical flow regimes. Non-classical behaviour is outside the scope of this work, and not typically found in nature. However the Γ function gives a clear distinction between ideal and non-ideal flow. In an ideal flow, where $\Gamma > 1$, the speed of sound is positively correlated to the changes in density, and thus the changes in pressure. As the molecules get closer together and pressure increases so does the speed of sound. In non-ideal flow cases, where $\Gamma < 1$, the speed of sound will decrease if the pressure and density increase. At $\Gamma = 1$ the speed of sound theoretically does not vary with pressure.

Looking at the four parameters which are presented to characterise non-ideality one can see that they are functions of each other from Eq 2.3, 2.5, and 2.7. The differences arise in their applicability; for example Z can quantify the thermodynamic non-ideality, while Γ defines the gas dynamic non-ideality, and γ_{pv} represents the difference in physics of a real gas vs an ideal gas in a turbomachine. Figure 2.4 contains T - s diagrams of Siloxane MM showing contours of the compressibility factor, the isothermal compressibility, the pressure-volume polytropic exponent, and the fundamental derivative of gas dynamics.

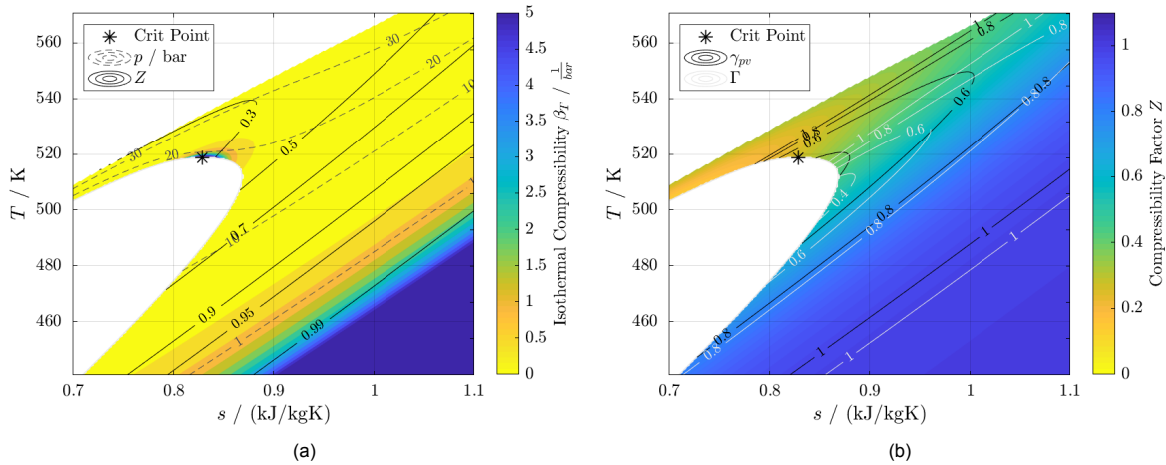


Figure 2.4: $T - s$ Diagrams of Siloxane MM illustrating the region of non-ideality near the critical point where ORC turbomachines operate. **a)** The surface contour is the isothermal compressibility β_T with superimposed constant pressure lines and constant compressibility factor Z lines. **b)** The surface contour is the compressibility factor Z with superimposed constant polytropic exponent γ_{pv} lines, and fundamental derivative Γ lines.

The contour plots both demonstrate the region of ideal gas is consistently identified by all of the parameters. In the ideal region of Fig. 2.4a β_T is the exact inverse of the pressure, and the values of Z are above 0.99. In the ideal region of Fig. 2.4b γ_{pv} and values of Γ are above one. The ideal relation

of β_T and pressure continues until near the critical point, where the compressibility suddenly rises at a rate much larger than the pressure gradient. This is different from the non-dimensional parameters which gradually decrease in ideality, and thus the isothermal compressibility should not be used as a measurement of ideality.

The transition into non-ideality is similar for the non-dimensional parameters Z , γ_{pv} , and Γ , however the compressibility factor continues to decrease beyond where the defined region of NICFD from Γ is valid. This is representative of how the value of Z can be misleading when taken as the only parameter describing a fluid state. When Z goes much below one there may be an assumption of gas-dynamic non-ideality in addition to the thermal non-ideality, when in fact the only assumption which can be made about the flow is that intermolecular forces are relevant. Conversely non-ideal gas dynamic behaviour defined by Γ as an independent metric also identifies non-ideal thermodynamic behaviour. If the gas dynamics are non-ideal then the thermodynamics must be non-ideal, however if the thermodynamics are non-ideal there is no conclusion which can be made about the gas-dynamics.

γ_{pv} has similar trends to Γ , but has a small offset as seen in Fig. 2.4b. Both parameters can be useful, with Γ defining the region of NICFD, and γ_{pv} providing a value which can be used for turbomachinery analysis. Therefore the two parameters which best convey the magnitude of non ideal behaviour in the turbomachinery context are γ_{pv} and Γ .

The contour maps in Fig.2.4 illustrate that the region near the critical point is non-ideal by every metric. Since ORC turbomachines operate in this region there must be careful attention put to accurately modelling the fluids in this domain.

2.3. Mathematical Representation of NICFD

To fully capture any fluid dynamic system the flow must be modelled with CFD. The principle of CFD is to model the flow by dividing the region of interest into infinitesimally small cells, and use fundamental conservation equations to solve the state of the fluid in one cell given the state in a neighbouring cell. This can be done with different levels of fidelity, and different structural forms of equations depending on the required resolution and solving techniques. This section will introduce the conservation equations used in fluid dynamics and the two most common simplified forms. The form of the equations implemented in SU2 is presented in the final subsection.

2.3.1. Flow Conservation Equations

The laws of physics dictate that mass, energy, and momentum must be conserved in any system, unless acted on by external forces, work, and/or heat addition. In the context of a fluid flow these relations are referred to as the Navier-Stokes (NS) equations:

$$\frac{\delta \rho}{\delta t} + \nabla \cdot (\rho \vec{U}) = 0 \quad (2.8)$$

$$\frac{\delta(\rho u_j)}{\delta t} + \frac{\delta \rho u_i u_j}{\delta x_i} + \frac{\delta p}{\delta x_j} - \frac{\delta \tau_{ij}}{\delta x_i} - f_j = 0 \quad (2.9)$$

$$\frac{\delta(\rho e)}{\delta t} + \frac{\delta(u_i \rho e)}{\delta x_i} + \frac{\delta(u_i p)}{\delta x_i} - \frac{\delta u_i \tau_{ij}}{\delta x_i} + \frac{\delta q_i}{\delta x_i} - u_i \rho f_i = 0 \quad (2.10)$$

where \vec{U} is the vector of flow velocities in the Cartesian coordinate system, f are all body forces such as gravity, and i and j are directional indices in the Cartesian coordinate system. Equation 2.8 describes the conservation of mass, Eqn. 2.9 describes the conservation of momentum, and Eqn. 2.10 describes the conservation of energy.

The NS equations are the basis for modelling NICFD. They include the effects of compressibility, and viscosity, and capture turbulent flow features.

2.3.2. Simplifications of Flow Equations

The NS equations are often simplified to the Reynolds-Averaged Navier-Stokes (RANS) equations to decrease computational time. Instead of solving the value of turbulent fluctuations at every location Reynolds proposed to take the averages of the fluctuations over time to capture the average flow. In the derivation of the RANS equations the averages of most terms can be considered either zero, or a constant mean value. The full derivation is outside the scope of this thesis, however it leaves a term

called the Reynolds stress tensor which in two dimensional space is the average of velocity fluctuations in one direction multiplied by the average of velocity fluctuations in the perpendicular direction. This term does not simplify to zero, and therefore must be solved.

The Reynolds stress tensor can be represented with empirical approximations called turbulence models. These models make assumptions regarding the relation between turbulence quantities and use estimated constants to complete the relations. For example the $k - \epsilon$ model assumes a relation between the turbulent kinetic energy, k , and the turbulence dissipation rate, ϵ .

In the simplest case, where viscosity is neglected completely, the equations become the Euler equations. The τ_{ij} term is omitted from the flow conservation equations and there are no turbulent fluctuations captured. While the RANS equations in combination with a turbulence model will capture effects of viscosity on the overall flow, if there is no turbulence the viscous forces are orders of magnitude lower than the other forces and the Euler relations will converge to the same solution.

To solve the simplified mathematical representations of non-ideal compressible flows appropriate spatial numerical schemes are needed. The RANS and Euler equations can be solved with numerical schemes generalized for complex thermodynamic models, such as those implemented in SU2.

2.3.3. SU2 Framework

SU2 has been configured to be able to simulate NICFD by Pini et al. [47] and for design optimisation by Vitale et al. [66]. In all versions of SU2 Economon et al. [25] has configured the flow solver to solve the NS Eqns. 2.8, 2.9, and 2.10 in the form of

$$\frac{\delta B}{\delta t} + \nabla \cdot F^c - \nabla \cdot (\mu^v F^v) - Q = 0 \quad (2.11)$$

where B is the conservative variable vector, F are fluxes, and Q is a vector of source terms. The conservative variables are:

$$B = \{\rho, \rho \vec{V}, \rho E\}^T \quad (2.12)$$

the convective fluxes are:

$$F^c = \begin{pmatrix} \rho \vec{V} \\ \rho \vec{V} \times \vec{V} + \bar{I} p \\ \rho E \vec{V} + p \vec{V} \end{pmatrix} \quad (2.13)$$

with I representing an identity matrix. The viscous fluxes from Eqn. 2.11 are represented as:

$$F^v = \begin{pmatrix} \cdot \\ \bar{\tau} \\ \bar{\tau} \cdot \vec{V} + C_p \nabla T \end{pmatrix} \quad (2.14)$$

The flow solver allows the user to select from a variety of simplifications and submodels, some of which are described in Sec. 2.4.

2.4. Thermo-physical Models

The Euler equations relate pressure, density, velocity, and energy of a fluid. Unfortunately it is impossible to solve all four variables given there are only three conservation equations, thus a fourth equation is required. This is the purpose for the introduction of thermodynamic models, which relate the state variables pressure, density, and temperature together. Without a thermodynamic relation to connect the state variables, modelling of flows would be impossible. The viscosity and other constants used in the RANS equations also vary with the state of the fluid. Therefore to use CFD an accurate equation of state (EoS) and property model must be selected for the particular purpose. For example ORC turbomachines operate in highly non-ideal conditions, so in order to predict the flow of organic fluids correctly non-ideal models and sub-models must be used.

While the molecular mass, acentric factor, critical pressure, and critical temperature are constant values of a fluid, the thermodynamic and physical properties vary. To accurately predict fluid characteristics at a given state condition the property variations can be defined by mathematical equations. These equations are broadly called thermo-physical models since they cover thermodynamic properties, physical properties, and the link between them. With fully established thermo-physical models, all

the properties of a group of fluid molecules can be identified based on only two known values, such as the pressure and temperature. This section introduces the core models which are used in SU2 which are applicable to NICFD conditions.

2.4.1. Equations of State

Relationships between the pressure, temperature, and density of a fluid is called an EoS. Any relation between the thermodynamic properties and physical traits, such as viscosity and conductivity, are called transport models in the context of CFD. The models range in complexity and accuracy, some based on empirical data, and others based on theory. While the majority of the models use instantaneous values, occasionally the derivatives of properties are used in the equations for more accuracy.

When the ideal gas assumption is made, the ideal gas law,

$$pv = RT \quad (2.15)$$

can be used as the EoS. It is derived from Eqn. 2.1 with $Z = 1$. This simple relation is never exactly correct, but gas flows approach the ideal conditions as they move away from the critical point.

As was discussed in Sec. 2.1, ORC turbomachines operate with non-ideal fluids. To provide a more accurate EoS Peng and Robinson [46] developed a cubic equations of state in 1976,

$$p = \frac{RT}{v - b} - \frac{a}{v^2 + 2bv - b^2}, \quad (2.16)$$

where,

$$a = \left(\frac{0.457235R^2T_{cr}^2}{p_{cr}} \right) \alpha \quad (2.17)$$

$$b = \left(\frac{0.077796RT_{cr}}{p_{cr}} \right). \quad (2.18)$$

This uses the α function proposed by Soave [57],

$$\alpha = \left[1 + \kappa \left(1 - \sqrt{\frac{T}{T_{cr}}} \right) \right]^2 \quad (2.19)$$

with,

$$\kappa(\omega) = 0.37464 + 1.54226\omega - 0.26992\omega^2. \quad (2.20)$$

Here ω represents the acentric factor, and cr indicates the critical values of the fluid. This equation was improved upon by Stryjek and Vera [62] who changed the function of κ to include the temperature ratio and a new κ_1 parameter. This is called the Peng-Robinson EoS modified by Stryjek and Vera (PRSV) and replaces Eqn. 2.20 with

$$\kappa = \kappa_0 + \kappa_1 \left(1 + \sqrt{\frac{T}{T_{cr}}} \right) \left(0.7 - \frac{T}{T_{cr}} \right) \quad (2.21)$$

and

$$\kappa_0 = 0.378893 + 1.4897153\omega - 0.17131848\omega^2 + 0.0196554\omega^3. \quad (2.22)$$

κ_1 is constant which is defined experimentally for each fluid.

Another improvement was made by van der Stelt et al. [65] in 2012 to correct for the discontinuity in fluid properties which occurred near the critical point. It is referred to as the improved Peng-Robinson EoS modified by Stryjek and Vera (iPRSV) and replace Eqn. 2.21 with

$$\kappa = \kappa_0 + \kappa_1 \left[\sqrt{\left(A - D \left(\frac{T}{T_{cr}} + B \right) \right)^2 + E + A - D \left(\frac{T}{T_{cr}} + B \right)} \right] \sqrt{\frac{T}{T_{cr}}} + C. \quad (2.23)$$

The A, B, C, D, and E terms are constants set at 1.1, 0.25, 0.2, 1.2, and 0.01 respectively. κ_0 is the same as in PRSV.

The latest EoS with applicability to the organic fluid MM uses a twelve parameter Span-Wagner (SW) functional form and was developed by Colonna et al. [17, 18]. It empirically fits the twelve parameter model on to experimental measurements of the thermodynamic properties of siloxanes. The equations are not shown here as they are outside the scope of this theory, but this model has been implemented in RefProp [44] and the academic community has accepted them as accurate.

2.4.2. Fluid Properties

To create a full thermodynamic model the EoS needs to be combined with a calorific equation of state. This accounts for the energy storage within the flow along with the effect of the energy on the state parameters. Recall that the heat content of a system is a combination of the internal energy e and the potential for work, quantified by enthalpy, $h = e + pv$. The enthalpy is also a direct function of the temperature, $h = C_p T$.

The isobaric heat capacity defines how much energy addition is required to raise the temperature of the compound. In simple fluids like air the values are near constant so they can be permanently set in equations used to solve flows. However, in an organic fluid the molecular complexity leads the characteristics to be susceptible to changes in temperature, thus thermodynamic properties, such as C_p , are not constant.

The specific heat at ideal conditions is can be modelled for a fluid using the polynomial

$$C_p^{ig} = \eta_1 + \eta_2 T + \eta_3 T^2 + \eta_4 T^3, \quad (2.24)$$

where the η parameters are constant coefficients unique to each fluid. The coefficients are determined experimentally.

Other work such as from Aly and Lee [2] show alternate more complicated forms of calorific state equations based on physics which are more reliable for extrapolation. However within the bounds of experimental data they offer similar accuracy. Details on the alternate $C_p^{ig} = f(T)$ are not discussed since the polynomial form is trusted. The ideal gas heat capacity at constant volume can be found using $R = C_p^{ig} - C_v^{ig}$.

2.4.3. Departure Functions

Using the ideal gas specific heat to calculate enthalpy is acceptable even in non-ideal cases due to enthalpy being an extensive thermodynamic property. In thermodynamics the value of an extensive property such as enthalpy and s is not useful, the change in value is what provides useful insights into the flow. The change in enthalpy is a measure of work or heat added or removed from the flow, while a change in entropy characterises irreversibilities in the process, which can be interpreted as losses. For extrinsic properties if the initial state and final state can be identified the process is irrelevant. Departure functions take advantage of this feature to allow ideal gas relations to be used even in non-ideal conditions. Consider Fig. 2.5 where a process is undertaken to move from state A to state B.

The process can take any path and will have the same change in enthalpy. The enthalpy change of process AWB, heating at constant pressure followed by expansion at constant temperature, is equivalent to process AXB, expanding first followed by heating. Therefore any imaginary path can be used to determine the enthalpy change of a real process. Process AYZB reduces the pressure to 0 where there is no intermolecular forces and the fluid becomes an ideal gas, heat is added to the ideal gas, and then pressure is reintroduced to account for the intermolecular forces. AY and ZB are described by the departure functions, and YZ is an ideal gas process. The departure functions are calculated as,

$$\frac{H^{ig} - H}{RT} = \int_V^\infty \left[T \left(\frac{\delta Z}{\delta T} \right)_V \right] \frac{dV}{V} + 1 - Z \quad (2.25)$$

for enthalpy, and

$$\frac{S^{ig} - S}{RT} = \int_V^\infty \left[T \left(\frac{\delta Z}{\delta T} \right)_V \right] \frac{dV}{V} - \int_V^\infty [1 - Z] \frac{dV}{V} + \ln Z \quad (2.26)$$

for entropy. Therefore the ideal specific heat can be used at each state to calculate the ideal enthalpy and entropy values, then Eqns. 2.25 and 2.26 can be used to correct them.

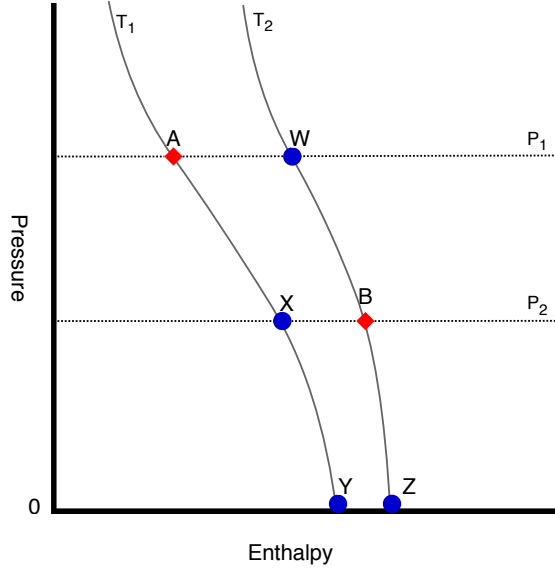


Figure 2.5: Generic simplified p - h diagram showing the processes from state A to state B. States W, X, Y, and Z are all potential intermediate states in the process which will have only one possible enthalpy rise.

2.4.4. Transport sub-models

The remaining fluid properties such as viscosity, μ^v , and thermal conductivity, k , can be calculated as functions of the already established thermodynamic flow parameters. Viscosity represents intermolecular collisions transporting momentum through a fluid, which connects the velocity gradients of a flow to the shear stress between particles. Thermal conduction is intermolecular collisions transporting energy through a fluid, which connects the temperature gradients of a flow to the heat transfer between particles. On an x - y Cartesian coordinate system the momentum relation is written as

$$\tau_{yx} = \mu^v \frac{\delta u}{\delta y} \quad (2.27)$$

where u is the velocity component in the x -direction, and τ is the shear stress in the x -direction due to the gradients in the y -direction. The energy relation is written as

$$q_y = -k \frac{\delta T}{\delta y} \quad (2.28)$$

where q is the heat conduction.

The models used to evaluate with viscosity and thermal conductivity at a given state are known as transport models since the properties affect the way momentum and energy are transported through a flow. In some cases the transport properties can be considered constant, or even neglected but this is highly dependent on the flow case of interest. To calculate viscosity accurately correlations consider viscosity as a function of temperature only. The most famous of these relations is the Sutherlands Law used to calculate the dynamic viscosity of air by using a reference viscosity at a reference temperature [8]. When this relation is not suitable a more accurate implementation, such as the one from Chung et al. [11, 12], is used to calculate the transport properties.

2.5. Compressible Flow Phenomena

The final distinguishing feature of NICFD from ideal fluid dynamics is gas dynamic compressible phenomena. While liquids do not often have changes in density, when the velocity of a gas approaches and passes the speed of sound noticeable density changes can occur. Recall, that the speed of sound is the velocity of a pressure wave through the fluid, and varies in a fluid depending on the state. The relation between the fluid velocity and speed of sound is represented by the Mach number, defined as $M = u/c$. This section describes the basic phenomena seen in gas dynamic flows which are a result of density changes.

2.5.1. Expansion Waves

A consequence of compressible flow are expansion waves which occur when the flow is accelerating beyond the speed of sound. The accelerating particles create lines of different fluid density as they separate. The waves propagate at an angle to the flow velocity which is directly related to the Mach number through

$$\mu = \arcsin \frac{1}{M} \quad (2.29)$$

where μ is the expansion wave angle relative to the direction of flow.

2.5.2. Shock Waves

The occurrence of expansion waves is only one phenomena which must be taken into account when modelling a compressible flow. There are also shock waves. In supersonic flow, when a fluid is travelling faster than the speed of sound, pressure waves can not propagate upstream. Therefore any disturbance or obstruction to the flow can not be communicated to the upstream particles, since the driving force of fluid movement is pressure. However, if there is an obstruction the flow must change, this leads to a discontinuity in flow conditions where the flow instantly decelerates. This discontinuity is called a shock wave, illustrated in Fig. 2.6 for two cases of steady adiabatic flow.

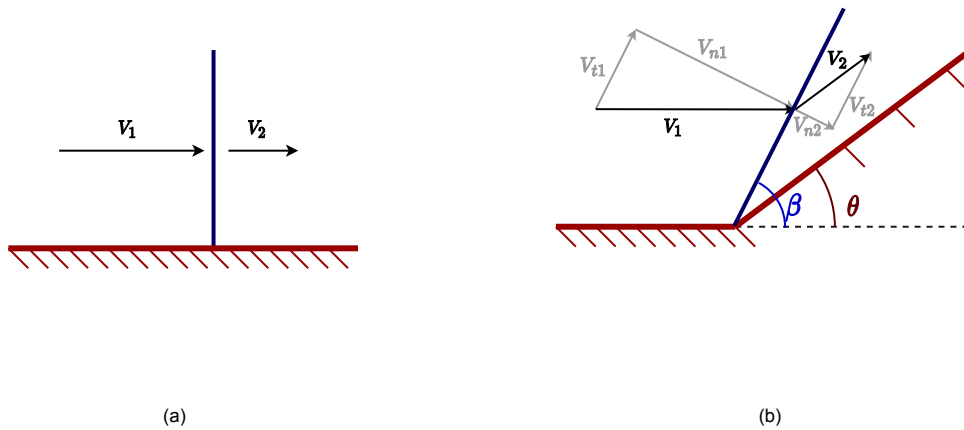


Figure 2.6: Schematics of steady shock waves in compressible flow. In these cases the flow is adiabatic and inviscid, starting from supersonic flow on the left, $V_1 > a$, and resulting in subsonic flow on the right, $V_2 < a$ **a**) Normal Shock wave **b**) Oblique Shock wave with normal and tangential components of the flow velocity with respect to the shock.

The angles of oblique shock waves, β , for a fluid are a function of the flow turning angle, θ , and the inlet Mach number. Subscript 1 represents the flow before the shock and subscript 2 represents after the shock. The theoretical relation of $\beta - \theta - M$ is shown in Fig. 2.7 for MM.

For a given flow turning angle there are two possible solutions, a weak shock and a strong shock. In the usual case the weak shock occurs since it dissipates less energy. If the flow turning angle is larger than the maximum value for the given Mach number then the shock detaches from the surface. The curves on Fig. 2.7 can be represented mathematically by

$$\tan \beta = \frac{\left(1 - \frac{\rho_1}{\rho_2}\right) \pm \left[\left(1 - \frac{\rho_1}{\rho_2}\right)^2 - 4 \frac{\rho_1}{\rho_2} \tan^2 \theta\right]^{1/2}}{2 \frac{\rho_1}{\rho_2} \tan \theta} \quad (2.30)$$

The density ratio $\frac{\rho_1}{\rho_2}$ is equal to the velocity ratio $\frac{V_{n1}}{V_{n2}}$. The equation is derived using trigonometric relations across the shocks in Fig. 2.7 and the conservation of mass.

With no obstruction or change in flow angle the oblique shock angle due to any disturbance is the expansion wave angle presented in Eqn. 2.29.

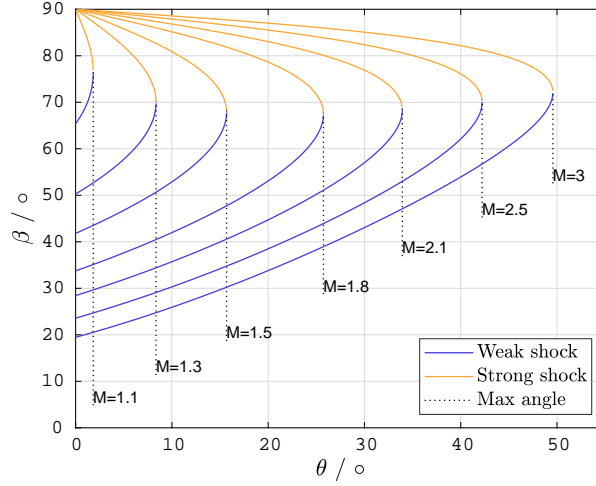


Figure 2.7: $\beta - \theta - M$ diagram for Siloxane MM modelled with the ideal gas law. The angle of a shock, β , is directly related to the flow turning angle, θ , of a flow for a given Mach number assuming a constant specific heat ratio of 1.02605. There are two possible solutions for the shock angle: one is related to the weak shock, and one is related to the strong shock. Both shocks are possible, but the weak is more likely due to the principles of energy conservation. If the flow turning angle is larger than the maximum point on the given Mach curve, then the shock detaches from the surface.

2.5.3. Jump Conditions

A form of the Euler equations can be used to analytically solve the jump conditions of a steady shock. The following relations can be used in combination with an equation of state:

$$\begin{aligned}
 \rho_1 V_{n1} &= \rho_2 V_{n2} \\
 V_{t1} &= V_{t2} \\
 \rho_1 V_{n1}^2 + p_1 &= \rho_2 V_{n2}^2 + p_2 \\
 h_1 + V_{n1}^2/2 &= h_2 + V_{n2}^2/2
 \end{aligned} \tag{2.31}$$

In non-ideal flow, fluid properties are not constant across a shock and thus an iterative process must be used based on Eqn. 2.31. Given the flow conditions p_1 , ρ_1 , and V_1 Grossman [32] proposes the following:

1. Calculate $h_1 = h(p_1, \rho_1)$. Use an appropriate thermodynamic model.
2. Guess a density ratio $\rho_r = \frac{\rho_1}{\rho_2}$ across the shock. Then $\rho_2 = \rho_1/\rho_r$.
3. If the shock is oblique evaluate Eqn. 2.30 given the guessed density ratio. Then $V_{n1} = V_1 \sin \beta$.
4. Solve Eqns. 2.31 to find p_2 , h_2 , and V_{n2} .
5. Calculate $\tilde{h}_2 = h(p_2, \rho_2)$. Use an appropriate thermodynamic model.
6. If $h_2 = \tilde{h}_2$ state two is solved. If not, return to step two with a new guess of density ratio.

2.6. CFD Validation

Even with the theoretical ability to represent a flow of dense organic fluid with equations and submodels, the credibility of the models and numerical methods must be assessed before an engineer can rely on any simulation results. A quantitative evaluation of the compiled flow solver needs to be done through performing validation studies. Coleman explains that validation determines if a model accurately represents reality [15], as opposed to verification which determines if the mathematical model devised has been implemented correctly. This can only be done by comparing an output from the model with the same output from an experiment. Given that a system can have an unlimited number of outputs the validation is done for a set number of system response quantities (SRQ), for example the pressure at a given point.

The first step of validating an established model is quantifying its uncertainty and obtaining experimental results from an identical case; the validation ends with a quantitative validation metric calculated to define the credibility of the model. Work by Eça and Vaz [23, 24] defines the expectations and provide worked examples of validations for RANS CFD code. Other authors have also expressed an interest in validation standards and published documents for reference. This includes Roache [51, 52], Oberkampf and Roy [45], Coleman and Steele [15], American Institute of Aeronautics and Astronautics (AIAA) [3], American Society of Mechanical Engineers (ASME) [4], and Eklund et al. [26]. While different authors present alternate methodologies, the literature agrees that validation has four principle criteria. Validation is done through comparison of software results with experimental data; *Code* verification and *solution* verification must precede the validation stage; validation experiments are kept to the highest standard of rigour, with detailed records of geometry, conditions, and apparatus; and validation metrics must consider uncertainties in the experimental and simulation results [51].

The uncertainties are given as a range of values where the true value is likely to occur. In nature an observable quantity has a value which is most likely to be measured. However, a single measurement could deviate from this exact value, thus the observed quantities are reported as an average expected value which is most likely to be measured, along with a standard deviation. In nature the normal probability distribution, referred to as Gaussian, has equal probability of an observation being above or below the expected value. One standard deviation is defined as where 68% of measured occurrences are observed and 95% of measured occurrences are within two standard deviations. This 95% confidence interval is called the expanded uncertainty, and in this thesis the expanded uncertainties are reported unless explicitly stated otherwise. Details on the terminology and factors of standard deviations related to probability distributions are described by American Society of Mechanical Engineers (ASME) [5] and in the Guide to the Expression of Uncertainty in Measurement (GUM) [37].

An individual model may be validated with a single set of experimental data, however to validate a software a clear domain must be specified and experimental data for conditions throughout the domain must be used to evaluate the validation metrics at all points of the domain.

2.6.1. Validation Hierarchy

The multidisciplinary nature of an engineering system make it unfeasible to experimentally validate entire system models. There are challenging measurement techniques and prohibitive costs of assembling large systems. Instead, to reduce the complexity and increase the resolution which can be made in measurements, subsystems can be considered independently. Once each subsystem has a validated model the system can be reconstructed with the knowledge that any uncertainty or error coming from the model is minimal and only arises from the interfaces between the subsystems. The principle of dividing the system can be continued through breaking subsystems into benchmark cases, and benchmarks further simplified into unit cases. A benchmark case represents a fundamental engineering geometry which is not useful independently and considers two or three phenomena. Each unit case is the simplest case that can be modelled and built experimentally which isolate a single physical phenomena. When doing validation activities for a software, the unit cases should be validated first, then the benchmark cases, followed by the subsystems. Details can be found in Oberkampf and Roy [45].

2.6.2. Validation Metrics

A metric to determine validity of a model includes the comparison error between the simulated results and the experimental result, in combination with a quantified form of the total uncertainty in the physical and computational systems. The metric can be constructed in numerical, graphical, or binary form, depending on the application. While a binary form is simple to communicate to software users, the numerical and graphical forms provide more information and allow for individual interpretation of the metrics for different engineering situations. The two validation metrics currently accepted for comparing the prediction to the measurement are the American Society of Mechanical Engineers (ASME) verification and validation (V&V) 20 standard [4] based on the work by Coleman and Steele [15], Coleman and Stern [16], and the Real Space metric from Sandia Laboratories based on the work from Romero [53, 54].

ASME V&V 20 [4] compares the SRQ comparison error,

$$E = S - D, \quad (2.32)$$

with the validation uncertainty,

$$U_{val} = \sqrt{u_D^2 + u_{num}^2 + u_{in}^2}. \quad (2.33)$$

S is the mean simulation result from running the simulation with different combinations of possible input values sampled from the input uncertainty distributions, D is the mean experiment results, and the u_D , u_{num} , and u_{in} are the experimental, numerical, and input uncertainties, respectively reported in total expanded uncertainty. If the comparison error, E , is less than the validation uncertainty then the solver is validated for that case since the source of model error can not be identified. It indicates the possibility that the model error is zero since the uncertainty bands may shift the experimental and simulation results to being identical. A visualisation of a validated case is in Fig. 2.8a, and an invalid case is in Fig. 2.8b. The metric provides a binary interpretation of validity with no meaning to the proximity of the two values. In this construction of a metric reducing the uncertainty can ironically invalidate a code.

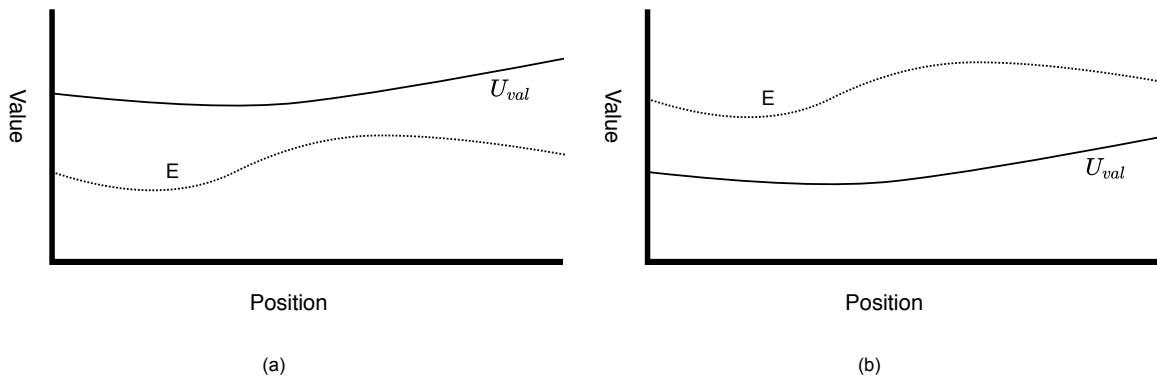


Figure 2.8: Graphical representations of the ASME V&V 20 metric comparing the validation uncertainty with the comparison error between the mean simulation response and the mean experimental response. **a)** Valid case where the validation uncertainty is larger than the comparison error. **b)** Invalid case where the comparison error is larger than the validation uncertainty.

The Real Space metric [54] keeps the experimental and simulation uncertainties separate to give a clear image of what the error means. Romero presents the mean experimental results and the mean simulation results side by side; with u_D bars on the experimental values, and u_{num} and u_{in} together for one set of uncertainty bars on the simulated value, u_S . This metric can therefore define four cases of validity: Zero-order validity where the experimental uncertainty bounds lie within the simulated uncertainty bounds; dubious validity where the limits of the simulated value lie within the experimental bounds; dubious validity where the uncertainty bounds of the two results overlap; and no validity where the uncertainty bounds have no overlapping region. For both dubious validity cases there is a chance that the true value is outside the range of simulated results, thus the true physics are not captured by the solver. The other two cases provide confidence to the user of the model that the simulation will always give realistic values, or always give incorrect values. Visual representations of the four cases are in Fig. 2.9.

The ASME V&V 20 metric gives a simple binary validation by comparing error and uncertainty, which is ideal for code development. It defines whether improvements can be made to the models or if the errors are too mixed within the built-in uncertainty of the code. It does not provide a detailed validation metric for end users of the software. The Real Space method keeps experimental and simulation uncertainty separate for comparison with error. Romero [54] points out the flaws in the ASME V&V 20 [4] method regarding details which can be overlooked by the simplified binary condition. Romero has more information included in the real space metric, but is considered more complicated and takes more time to interpret. This metric can be used for end user validation, and can be used for the software development case of validation if required, although less eloquent. Therefore using the two metrics as complimentary evaluations can provide a more refined validation assessment than either metric independently.

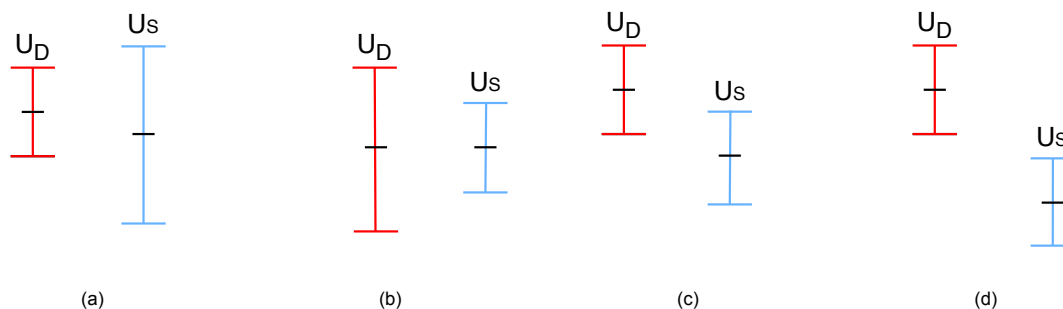


Figure 2.9: Graphical representations of the four validity cases defined by the real-space metric. The experimental and simulation mean values are kept separate with the relation between the uncertainty bars characterising the level of validity for the model. **a)** Valid case where the simulation uncertainty contains the experimental uncertainty, representing that the simulation contains all possible reality; Referred to as zero-order validity. **b)** Dubious validity where the simulation uncertainty is less than the experimental uncertainty. IN this case the simulation only captures a portion of possible reality, indicating that experiment must be improved. **c)** Dubious validity where the uncertainty bars overlap, but do not contain each other. Here the simulation only captures a portion of reality, indicating that the error is significant. **d)** Invalid case where there is no overlap between uncertainty bands.

2.7. Forward Propagation of Uncertainty in CFD Solvers

The core principles of good CFD validation are precise experiments with all sources of uncertainty recorded; and simulations with not only the numerical uncertainty accounted for, but the input uncertainty quantified. This is done through a forward propagated uncertainty quantification (UQ) which defines what the uncertainty of a mathematical model output is, based on the uncertainty of the ‘known’ input parameters. This is a critical component of the validation exercise. For example boundary conditions, non-dimensional coefficients, fluid properties, and geometry can be considered constant values input into a CFD model. However, the values used may have been determined experimentally, have a manufacturing tolerance, or in reality have small fluctuations over time resulting in having a random distribution. These uncertainties can theoretically lead to a difference in the calculated value output by the model and therefore can not be ignored.

Calculating the uncertainty of a response from a linear system can be done using analytical error propagation techniques such as adding absolute uncertainties together when two values are added, or adding the percent uncertainty values when two values are multiplied together. However the NS equations are highly non-linear, thus the direct methodology is not possible for CFD. Instead a statistical approach to uncertainty propagation must be employed. Since each input has a probability distribution the input uncertainty can be evaluated through a Monte Carlo simulation, where every input is sampled randomly over the range of possible values and the results from the model output are statistically analysed to produce a mean response and a standard deviation of the response.

Work from the joint army navy NASA and air force (JANNAF) in 2016 [26], and Montomoli et al in 2019 [41], has examined the advancements in uncertainty quantification with respect to fluid dynamics. However, the standard from ASME for CFD validation [4] recommends the latin hypercube sampling (LHS) or local sensitivity coefficient methodologies for forward propagating UQ since they are well understood and simple to implement. As such, LHS has been accepted by researchers as the default UQ architecture, but other methods are becoming more popular for CFD applications. Leading research done by Congedo, who published his PhD thesis in 2013 [20], focuses on stochastic methods for compressible flows with applications in ORC research. Stochastic simulations refer to a series of model evaluations which provide statistical information on the outputs, for example the mean and standard deviation of a system response. Simulations which are done once, without consideration for the uncertainty bands, are referred to as deterministic simulations. Authors such as Cinella [13, 14] and Gori et al. [30] have applied stochastic methods, such as polynomial chaos collocation, to predicting compressible flows.

Polynomial Chaos collocation is one variant of stochastic collocation (SC) which creates a surrogate model based on the real model which has the same statistical behaviour of the outputs, this allows for faster computations of the output quantities. The concept of polynomial chaos is based on mathematics

from the 1930s, which are outside the scope of this description, where a probability distribution function (PDF) of any shape can be represented as a series of polynomials, similar to how any function can be represented by a Taylor series. Notably, the coefficients of the polynomial indicate the statistical moments. The first coefficient is the mean, the second coefficient is the standard deviation, and the third is the skewness of the output variable [41]. The surrogate model is constructed by taking a set of samples from the original model, and evaluating the statistical moments of the input parameters. Once the surrogate is constructed it can be sampled thousands of times and solved at the speed of a simple polynomial. The sampling of the original model is based on quadrature methods.

In addition to quantifying the magnitude of uncertainty, the sources of uncertainty are also useful for validation analysis. The sources of uncertainty can be identified using a variance based decomposition (VBD) sensitivity study, which determines the influence of model input parameters on the output uncertainty. This is useful to reducing the number of inputs and shortening the simulation time to quantify forward propagated input uncertainties. The sensitivity of a parameter in this chapter is represented by the Sobol Index, where the index is the variation of the system response due to the variation of the input parameter of interest, divided by the total variation of the system response. The primary sobol index,

$$S_i = \frac{\text{Var}_{x_i}[E(Y|x_i)]}{\text{Var}(Y)} \quad (2.34)$$

represents the effect of an input parameter independently of all other parameters. The total sobol index

$$T_i = \frac{\text{Var}(Y) - \text{Var}[E(Y|x_{-i})]}{\text{Var}(Y)} \quad (2.35)$$

represents the effect of an input parameter independently and in combination with other parameters. A value of one in a Sobol index indicates that the parameter is the only one which influences the system output, while a value of zero implies no effect of the parameter uncertainty on the variation of the system response.

2.7.1. UQ of Siloxane MM Supersonic Expansion Model

Iyer [38] conducted a UQ on the flow of non ideal organic fluids while studying the effects of thermodynamic uncertainties on the outputs of NICFD flow solvers and nozzle design. The research from Iyer [38] was done by combining CFX and Dakota [1] using an infrastructure built with visual basic scripts and MATLAB scripts in a windows operating system. The method implemented was an LHS UQ. The results were then verified by using SU2 to reproduce a subset of the flow case samples. The examined case was a high speed isentropic expansion of Siloxane MM through a de Laval nozzle with a wedge placed at the outlet to cause a shock wave, as was done by Head et al. [35]. The uncertain input parameters used by Iyer in the UQ were total inlet temperature, total inlet pressure, critical temperature, critical pressure, the acentric factor, thermodynamic constant κ , the wedge angle, and the four coefficients for the specific heat. Iyer [38] found that the input uncertainties have minimal effect on the ideal region, but have noticeable effects on real gas region. A shock angle uncertainty of $\pm 0.17\%$ and a shock intensity uncertainty of $\pm 0.06\%$ resulted from the input uncertainties in ideal gas region. A shock uncertainty of $\pm 2.6\%$ and shock intensity uncertainty of $\pm 3.1\%$ resulted from the input uncertainties in real gas region.

The most sensitive parameters in the model implemented by Iyer, which included the method of characteristics, were the critical pressure and temperature if the boundary conditions were held constant. However, when the inlet pressure and temperature were considered uncertain, which is an accurate representation of the ORCHID, then the C_p coefficient uncertainties were the most influential. Iyer [38] found the geometry negligible and suggested it could be considered deterministic. The acentric factor and thermodynamic constant κ could also be considered deterministic. Therefore to improve the work the flow turning angle should have been considered deterministic, and the two thermodynamic parameters, ω and κ , could have been excluded from the UQ if their uncertainty was not large. This leaves a total of eight parameters instead of eleven, and if this was done with a sparse grid polynomial chaos surrogate model the computational time would be much faster. The thesis also suggests that a UQ exercise with SU2 should still result in uncertainties in the order of $\pm 3\%$ for the shock angle and intensity, since the maximum and minimum system responses were verified using SU2.

2.7.2. UQ Studies on Thermodynamic models for Real Gases

Cinnella et al. [13, 14] have used a third order polynomial Tensorial Expanded Chaos Collocation UQ to study the effects of thermodynamic models on real gas flow solvers. The first Cinnella et al. [13] paper focused on the uncertainty of the model outputs, while the second paper focused on a sensitivity study of the thermodynamic inputs. Both papers used the same flow configurations, studied the same thermodynamic sub-models, and used assumed Gaussian distributions of input parameter uncertainty. The methodology involved first examining the thermodynamic model output sensitivity to input uncertainties without other considerations, and assumed a standard deviation of 3% on the mean. Second Cinnella et al. [14] examined the changes to real gas dynamic behaviour over a NACA0012 airfoil at $M_\infty = 0.95$ and 0° angle of attack due to the input uncertainties of the thermodynamic models with an assumed standard deviation of 1.5% mean. The smaller standard deviation was used to keep the flow in the non-ideal zone because the flow solver was not equipped for two phase flows, and the flow over the airfoil was close to the two phase region.

In 2009 Cinnella et al. [13] published the work on a UQ of compressible flow with thermodynamically complex behaviour. Three thermodynamic models were used in the study: Redlich-Kwong-Soave (RKS), PRSV, and the five term Martin-Hou (MAH) EoS. The RKS and PRSV models have three uncertain input parameters: the acentric factor, an exponent n , and the reduced ideal-gas constant-volume specific heat at the critical temperature $C_{v,\infty}(T_{cr})$. The outputs of the model using the MAH EoS is sensitive to six parameters: critical pressure P_{cr} , critical temperature T_{cr} , critical compressibility factor Z_{cr} , the normal boiling temperature T_b , the exponent n , and the reduced ideal-gas constant-volume specific heat at the critical temperature $C_{v,\infty}(T_{cr})$.

The results showed that the highest sensitivity area for the system response of pressure were around a shock wave, and in dense gas regions. More complicated thermodynamic EoS were also more sensitive to the input parameter uncertainties. Cinnella et al. [13] concludes with a recommendation to use PRSV EoS because the effects of input uncertainty were only significant in the real gas region of the flow, and the evaluated output uncertainties took a Gaussian distribution with the mean matching the deterministic calculations and a standard deviation of less than 10% on the mean. The MAH model was deemed not suitable for highly non-ideal gas dynamics.

In 2011 Cinnella et al. [14] published a sensitivity study on the thermodynamic uncertainties for dense gas flows using a second order SC UQ. Cinnella et al. [14] also found that a second order polynomial was adequate to conduct the sensitivity study of the airfoil case after examining first to fifth order polynomial expansions. The sensitivities of fluorocarbon (PP10) and a siloxane (D5) due to the RKS, five term MAH, PRSV, and SW equations for siloxane were examined. The uncertain parameters were the same as in the 2009 paper from Cinnella et al. [13], with the addition of 16 material values required for the SW EoS. Siloxane D5 has input uncertainties of 1-2% on critical point data, and 6% uncertainty on the ideal gas specific heat. As with the first study the standard deviation of other parameters were assumed to be 3% of the mean. However, since the true PDFs were unknown the sensitivity study was done for normal and uniform distributions for a MAH analysis. The results were similar but with a higher sensitivity using normal distributions, thus a Gaussian distribution was assumed for all remaining experiments as a conservative estimate.

The results showed that the most sensitive region is around the shock wave for all models, but MAH EoS is too sensitive and should not be used for design work. The simple PRSV and RKS models had close to deterministic means and lower stand deviations than the SW EoS, thus the PRSV was recommended from the analysis. The study of Siloxane D5 transonic flow over an airfoil used the drag coefficient and pressure coefficient as SRQs. A 3% change of input may lead to 6% change in output of drag coefficient near the high temp and pressure region when using the SW EoS.

2.8. Experiments in Non-Ideal Compressible Fluid Dynamics

Experimental facilities that are capable of recreating the flow conditions of Iyer [38] and Cinnella et al. [13, 14] are limited. The combined temperature and pressure requirements with organic working fluids is not yet common for wind tunnels. The two leading facilities which have published preliminary experimental research in NCFD are the Test-Rig for Organic Vapours (TROVA) and the organic rankine cycle hybrid integrated device (ORCHID).

The TROVA is a blow down wind tunnel facility [58] which uses siloxane MDM vapour with the maximum operational design conditions of $p_{des} = 50$ bar, and $T_{des} = 400$ °C [59]. The facility records

pressure, temperature, and the flow field in a nozzle test section. Samples are recorded during transient flow but are considered steady state snapshots since the timescale of thermodynamic variation is much larger than the molecule flow timescale, defined by the flow velocity [30]. The experimental data is obtained from the specially designed nozzle test section which includes nine pressure measurements and a window for capturing images [60]. The TROVA uses schlieren imaging [60] to visualise the flow field and post-processing to extract Mach number and therefore the flow velocity.

The ORCHID was built in 2016 [34] and has two test sections which can be alternately used with the remaining balance of plant. The nozzle test section is for studying classical NICFD, and the turbine test section is for studying ORC machines. The ORCHID is designed to create a continuous fluid flow for steady state analysis, have no time restrictions on experiments, have stable boundary conditions, achieve fully supersonic flow, and achieve real ORC conditions seen in current ORC designs. The facility is designed for using Siloxane MM at maximum design conditions of $p_{max} = 25$ bar, $T_{max} = 320$ °C, and $Q_{max} = 400$ kW_{th} to create supersonic flows in the order of magnitude Mach 2. The nozzle test section can measure sixteen static pressures using a pressure scanner and has a window to allow visualisation of the flow using the schlieren technique.

2.8.1. SU2 Accuracy Assessment

The first NICFD experimental data comparison with SU2 was published in 2017 by Gori et al. [29]. The team makes a comparison of predictions with the experimental results from the TROVA but there is no mention of uncertainties or any validation metric in the paper. This does not meet the standards described by Eça et al. [23, 24] and is therefore not covered in detail. Another assessment was completed in 2019 with results published in 2020 by Gori et al. [30] which does include some uncertainty calculations. However, the accuracy assessment of a single case does not constitute a validation of SU2.

In the paper published in 2020 Gori et al. [30] compares the isentropic expansion of siloxane MDM through a nozzle with the identical case created in SU2 assuming inviscid flow, adiabatic flow, constant back pressure, and centre line symmetry using static pressure and the Mach number in the nozzle as system response quantities. The assessment considered MDM at a compressibility from 0.633 to 0.98. The work however does not claim to be a validation, rather it is an accuracy assessment of the SU2 software through comparisons of the TROVA data and SU2 simulation results. The model input uncertainties and the systematic experimental uncertainties are considered but a comprehensive validation exercise is not conducted. Gori et al. [30] used two runs of the TROVA with five snap shots each to produce ten data sets. Each data set includes the total pressure and temperature recorded with 95% confidence intervals in the settling chamber, a schlieren image to be used in calculating the Mach number, and static pressures recorded with uncertainties at four locations.

Gori considers the total pressure and temperature at the inlet of the test section as uncertain and presents a sensitivity study of the parameters using sobol indices. Once the uncertainty of the input parameters to the TROVA were calculated using instrument specifications these were propagated through the model using a polynomial chaos expansion UQ method to produce a mean value and uncertainty bar for each model SRQ. The Polynomial Chaos Expansion UQ used 4th order polynomial surrogates, and a non-intrusive spectral projection library, to reduce the computation time of the UQ. A grid convergence study was done before running the UQ to ensure grid independent solutions, but the numerical uncertainty was ignored for the rest of the analysis. The implemented thermodynamic model was the SW EoS optimized for MDM and the uncertainty of the thermodynamic model was considered negligible.

Gori et al. found there was a general agreement of experimental and simulated results, but that the error increases in the non-ideal region. They also report a large experimental uncertainty on the Mach number, compared to a relatively small uncertainty due to the simulation inputs. This could be attributed to the resolution of the schlieren images and the neglect of all uncertainties other than total pressure and temperature in the simulated SRQ.

The method used by Gori et al. [30] seems to be based on the textbook from Oberkampf and Roy [45], but it is not complete to the level prescribed by Roy in his paper [55]. The work does not complete the development of uncertainties and comparison error. Gori et al. [30] neglect the thermodynamic model and numerical uncertainties with vague or no justification. Even the listed uncertainties are not rigorously supported. However, the paper does not claim to have completed a validation, most likely due to the considerations listed above.

2.8.2. SU2 Validation Framework

In 2017 Head et al. [35] presented a validation methodology based on the ASME V&V 20 method to be used along with the newly developed ORCHID for validating NICFD flow solvers. The researchers describe an envisioned validation campaign and conducts an example validation using pseudo experimental data.

Head first suggests that a simple case should be validated and argues that the thermophysical sub-model should be the first point of interest. This is supported since turbulence and transport can not be tested without an EoS first implemented correctly. Head has designed experiments for the unit case where only the EoS has an impact on the flow. The first experiment suggested is an isentropic supersonic expansion of Siloxane MM through a de Laval nozzle to Mach 2.1, and the second experiment is to create shock waves by inserting a wedge into the test section. In the first case measuring the static pressure through the nozzle along the centre line would be the SRQ, and in the second case the shock angle, based on the schlieren image, would be the SRQ. Head et al. [35] simulates the validation of CFX with the iPRSV EoS for these experiments using pseudo-experimental data obtained by using CFX with an alternate thermodynamic EoS; the SW model. The placement of a wedge in the flow path is also simulated through using a secondary program. Once the flow is solved the shock angle is determined based on Euler relations. The ASME V&V 20 method is then used for the validation exercise to prove the concept.

To calculate the input uncertainty propagating through the solver the researchers implemented an LHS based UQ. Ten parameters are recommended to be used as uncertain inputs to the flow solver: total inlet temperature, total inlet pressure, critical temperature, critical pressure, the acentric factor, thermodynamic constant κ , and the four coefficients for the specific heat. The back pressure was considered deterministic and the probability distribution functions of all the parameters were assumed to be uniform. Using the Dakota software [1] the samples converged after 2800 simulations.

The numerical uncertainty was considered negligible after doing a grid convergence study. Two types of uncertainties were placed on the pseudo experimental data, boundary condition fluctuation uncertainties and measurement chain uncertainties. Values were estimated for each and used as placeholders for conducting the validation process. Comprehensive explanations were given for each value and the equations were given for calculating the final experiment value uncertainties.

The results of the example validation show that the shock angle, β , had a large uncertainty at the throat, implying that the input uncertainties have large affect in the non-ideal region. The uncertainty also increases with wedge angle. Head et al. [35] also suggests that the pressure is less sensitive than shocks to EoS uncertainties. Thus the argument is made that measuring shocks is better to determine validity of SU2 than static pressure.

The representation of the results is another topic the author considered. The modelling error and the uncertainty is presented in different graphical forms such that they can be compared. A common way to present the results is to plot the full magnitude of the system response with respect to an independent variable. However, this often presents difficulties in interpretation since the comparisons are difficult to appreciate. Comparing the error between the simulation and experiment and the validation uncertainties directly provided are more sensitive means to discern where the code and facility might be improved.

The final observation from Head et al. [35] is that the metric can lead to erroneous conclusions, thus a validation using the ORCHID requires an additional metric. Primarily, if the uncertainty is much larger than the error that is not more valid than if the uncertainty is only slightly larger than the error. As Coleman and Steele [15] describe, ASME V&V 20 defines one of the binary states: there is definitively model error which can be improved; or any potential model error is hidden by the uncertainties so no improvements can be made confidently.

Head et al. [35] suggests the fundamental validation case should be creating shock phenomena in the throat region of a de Laval nozzle. However as this increases the system uncertainty, by adding the wedge angle uncertainty, it appears that the basic isentropic expansion case should be validated first. Using the static pressures along the nozzle without a wedge is truly the most basic unit case. Producing shock waves are more difficult to control, but as Head et al. [35] implies, validation with this increase in sensitivity is more significant. A logical course of action is to validate the isentropic expansion case and then immediately study shock wave generation and compare the two campaigns.

Improvements to the framework presented by Head et al. [35] begins with the UQ method presented. Random sampling and LHS is reliable, but it is outdated compared to modern statistical methods. A

stochastic expansion surrogate model is recommended to improve the computation time of the UQ without reducing the accuracy. Also uniform PDFs are an assumption made to comply with the ASME V&V 20 method, and are conservative, but as Oberkampf & Roy [45] explain it is not ideal. Since it is a proof of concept exercise it is not a problem, but when implementing the framework the PDF's should be investigated fully.

2.9. Validity of SU2 for NICFD

The motivation for the construction of the TROVA and ORCHID is to validate software codes capable of predicting NICFD flows. These validated software tools can then be used for designing turbomachines used in ORC waste heat recovery systems. SU2 is one such software which is verified but has not been fully validated for NICFD.

The published literature related to validating SU2 covers both theory and experiments. The procedures for quantifying uncertainty and metrics to evaluate validity are researched and suitable for the purpose of validating NICFD flow cases in SU2. From the software development perspective the metrics from ASME V&V 20 should be used to determine if the solver error is less than the validation uncertainty. However, the code is currently available as open source and there is a current need for ORC turbomachinery design tools. As such the detail presented by the Romero method would be useful to researchers in the field of design, and informative on the quality of the experiment as well. To create these metrics input uncertainties should be found using polynomial chaos UQ methods, and the numerical and experimental sources of uncertainty fully identified.

Experiments recreating NICFD can now also be done at research institutions, and data is published which can be used to compare with SU2 simulations. Unfortunately the accuracy assessment done at the compressible-fluid dynamics for renewable energy applications (CREA)Lab by Gori et al. [30] does not follow the standard metrics outlined by Coleman, or Romero. The comparison done by the researchers is at a preliminary stage and further rigour must be applied to the process of uncertainty quantification and metric calculation. Future validation of SU2 should instead use the ORCHID designed by Head et al. [33], because of the improved resolution of measurements, steady state capabilities, and a pre-designed experiment ready for use in validation of SU2.

Using an advanced uncertainty quantification technique, along with a procedure adapted from the one proposed by Head et al. [35] in 2017, experimental data from the ORCHID at the TU Delft (TUD) can be used to validate the CFD solver SU2 for NICFD. This is a critical step in developing ORC turbomachinery and the first stage of creating novel power and propulsion (PP) technology.

3

Design of a Validation Study for NICFD

To design or analyse a system, a model can be used to save time, physical resources, and money. However, to rely on the results of the model it must first be verified and validated. Since the validation of an entire system model would require an expensive fully built system, the model can be broken into more versatile sub-models which represent critical subsystems and can be more easily replicated experimentally. The studies done to validate a software for subsystem modelling must be carefully designed and follow the same four principles of validation described in Sec. 2.6 of the literature review.

This chapter introduces the concept of a unit test case for validation, and develops the validation study of the SU2 flow solver for non-ideal compressible flows from the high level goal of ORC turbine design optimisation. The framework of the validation study and the quantities of interest are presented with justification for their choice in Sec. 3.1, followed by a description of the physical experiments used to produce the system response quantities (SRQ) in Sec. 3.2. The development of the SU2 configuration used to model the experiments is then presented in Sec. 3.3. The final section discusses the final SU2 configuration which is used to validate against the experiments.

3.1. Validation Study Framework

Before any experiments or model analysis can be done with the intention of validation, the framework of the study must be carefully defined. The case, the SRQ, and the method of assessment must be selected. This section describes how the validation study for modelling a high speed non-ideal organic fluid was done.

The top level procedure is summarised in Fig. 3.1 which is a hybrid approach based on the available literature. The first and second phase, *framework design* and *experiment design*, are based on the concepts described by Oberkampf and Roy [45] which add depth to the American Institute for Aeronautics and Astronautics (AIAA) software validation guidelines [3]. These are fully described in this chapter and provide the basis for all future assessment to be done. The third phase, *uncertainty quantification*, is described in detail in Chap. 4 and is based on the standards of Eça and Hoekstra [22] defined for computational fluid dynamics (CFD) modelling validation. The final phase, *validation*, is based around the evaluation of metrics. The metrics in this study are a combination of the V&V20 standard from American Society of Mechanical Engineers (ASME) [4], the real space construction by Romero [54], and a final engineering interpretation, constructed for the first time in the turbomachinery context based on the theory presented by Oberkampf and Roy [45].

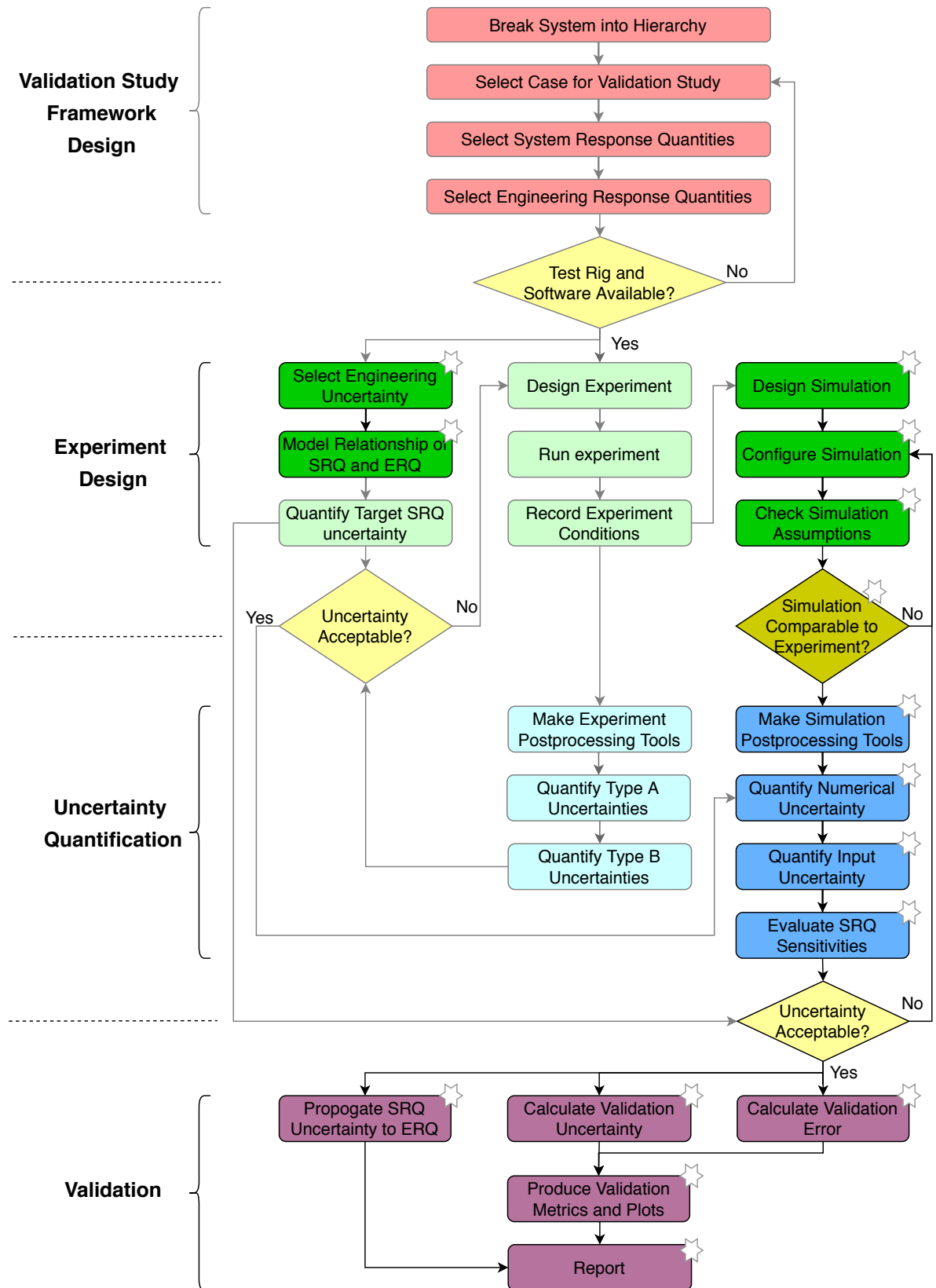


Figure 3.1: Flow chart of the developed validation procedure for this thesis. The procedure is broken into four phases, expressed by different colours in the diagram. The items with a white star in the top right corner are covered in this thesis, while the light colours are either completed by other researchers or omitted for simplicity.

This procedure includes the introduction of an engineering response quantity used to convey the validation metrics in an engineering context. This may be a performance metric or a design value which can be used to interpret the effect uncertainties in the simulation will have on engineering design or analysis. There are three loops in the process based on adjusting the experiment and the simulation to get the acceptable uncertainty bars for the case of interest.

The established metrics rely on the evaluation and analysis of SRQ to quantify comparison errors, E , and uncertainty, U . The new engineering interpretation also deals with uncertainty, but is designed to convey the validation results to engineers in a more intuitive fashion. To distinguish between values directly measured from the system and parameters which must be extrapolated for engineering interpretation two new terms are proposed to classify a SRQ. The direct response quantities (DRQ) is a directly measured response and the term engineering response quantities (ERQ) is introduced to describe a value which is used for engineering system performance metrics, or design metrics. As will be described in Sec. 3.1.3 the ERQ is used to quantify the effect uncertainties in the simulation will have on engineering design or analysis. ERQ and DRQ would both be considered a SRQ, with SRQ being the umbrella term. With the procedure of the study presented the remainder of this section describes the flow case, and lists the DRQ and ERQ chosen for the experiment. Details are given to explain why they were chosen, and how they can be measured.

3.1.1. Flow Case: High Speed Isentropic Expansion

Since validating a model of a turbomachine is multidisciplinary and very complex, the validation of SU2 for NICFD is done for one unit case as defined in Sec. 2.6.1. Consider an organic Rankine cycle (ORC) power plant for waste heat recovery. Given the objective to use SU2 in modelling ORC turbomachinery, let the multistage radial turbine with Siloxane MM working fluid be the system of interest which can be represented using the flow solver. The flow solver does not capture the structural behaviour of the turbine, so can only model the subsystem of fluid dynamics of a single blade row. A full fluid dynamic representation of a turbomachine is complex, involving multiple flow features, meaning benchmark cases must be isolated for validation, such as a converging-diverging nozzle. A nozzle has two interacting flow features, the boundary layer and the isentropic expansion, thus a unit case which can be isolated is the core flow of the nozzle, where the flow can be considered adiabatic and inviscid without any work or heat addition. The breakdown of the turbine system to unit cases is shown in Fig. 3.2.

This breakdown is one of many possible hierarchies which could be used to design the validation campaign for SU2 models of non-ideal compressible fluid dynamics (NICFD). The selection of a converging-diverging nozzle as the benchmark case, and subsequently the core flow for the unit case, is done to isolate the thermodynamic submodels within the NICFD flow regime. A model of the nozzle would not require any transport models, or turbulence models due to the inviscid nature of the flow. However any boundary layer or turbulence unit cases require a reliable thermodynamic model in addition to the turbulence models. Therefore a converging-diverging nozzle was selected by Head et al. [33] to represent one test case which could be used to validate the thermodynamics computational sub-model in SU2.

A nozzle also replicates the flow conditions typically encountered in a stator of ORC turbines. A stator consists of a series of stationary airfoils which are positioned such that the flow must pass between them. The airfoils accelerate and direct the flow in the optimal direction for the rotating component of the machine to extract work. The fluid moving between airfoils in ORC turbines accelerates to Mach one where the area decreases, then the fluid expands to supersonic speeds as the area increases.

The flow experiences three unique flow conditions in the expansion region of the nozzle, defined by the trend in Mach number. This is illustrated in figure 3.3

The flow in the diverging portion of the nozzle can be categorised into the kernel region, the reflex region, and the uniform flow region. The kernel is the initial expansion where the pressure is lower away from the centreline and the Mach number is therefore higher closer to the nozzle wall, at the inflection point of the nozzle the trends invert and the pressure is higher near the wall resulting in lower Mach numbers. This is the reflex region and the flow continues until uniformity is achieved. More details on the flow field is covered by Anand [6].

The flow of Siloxane MM Flow through a Converging-Diverging nozzle, as illustrated in figure 3.3, is the selected experiment for validating the thermodynamic sub-models of SU2 for NICFD. Once the unit case is validated then further investigations into the turbulence and transport model unit cases

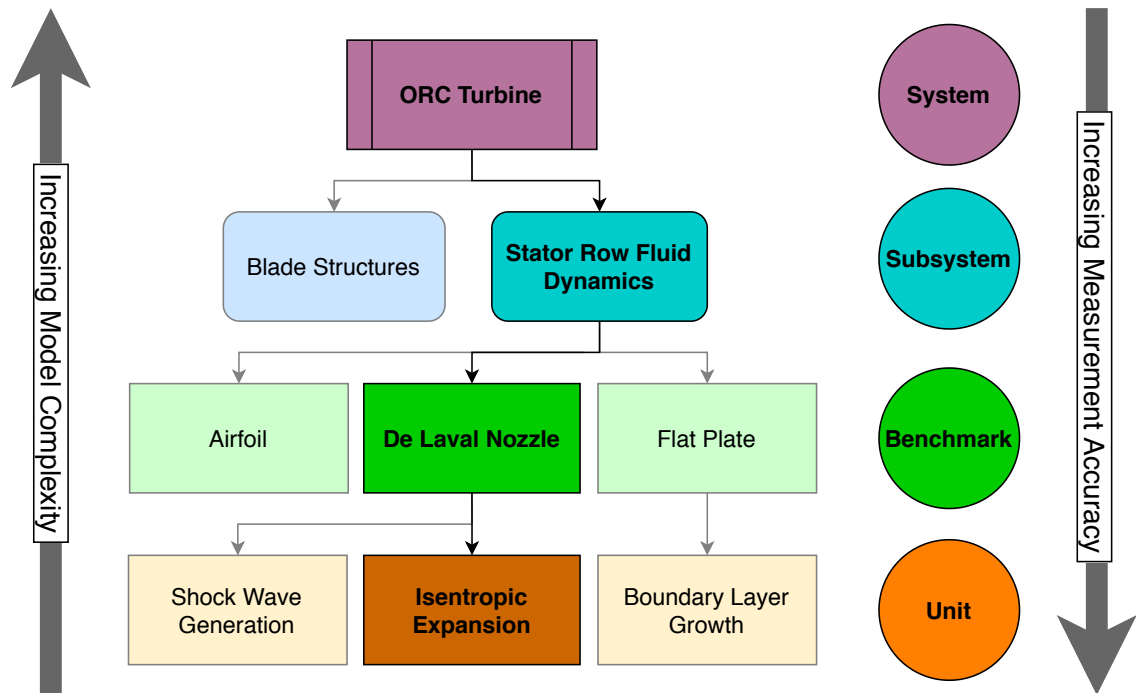


Figure 3.2: Simplified breakdown of Turbomachine system used in an organic Rankine cycle to unit model cases for validation. The highlighted route is the validation case study of SU2 in relation to the end objective of optimising turbomachinery designs. This study focuses on the thermodynamic submodels of SU2 which can be applied to NICFD flows within turbomachines. This hierarchy is adapted from American Institute of Aeronautics and Astronautics (AIAA) [3].

can be done. Once each unit case has been validated then SU2 models can be used to represent an entire blade row subsystem and compared against experiments. Only then can the flow solver be given credibility for turbine optimisation studies.

3.1.2. Direct Response Quantities

The quantities which are used to compare the experiment and model are called SRQ. These can be any value and are at the discretion of the one doing the validation to decide, for example the static pressure at a location or the coefficient of lift over a wing can be recorded for both experiments and simulations. For clarity, in this report, quantities which can be obtained directly without mathematical manipulation will be called DRQ. So of the two SRQ mentioned, only the static pressure could be considered a DRQ, while the coefficient of lift requires a mathematical manipulation of the raw data to obtain. Roy and Oberkampf [55] conveys that for an effective validation the SRQ should be directly obtainable without extra calculation, and Eça et al. [24] explains that they must be representative of the physics being modelled in the software. Therefore the DRQ are values which will be used for calculating the validation metrics which compare the model and the real world physics. Unfortunately, what can be measured experimentally does not always match what can be extracted from the model, thus the selection of DRQ is critical.

In a converging-diverging nozzle with non-ideal compressible flow the values for software validation need to represent the thermodynamics, which includes state features such as the speed of sound. The compressibility effects, such as any expansion waves or shock waves, should also be captured. The output from the SU2 flow solver includes pressure, temperature, density, momentum, and Mach number. Experimentally measurable values include mass flow, inlet temperature, and pressures. Flow velocity and density can also be measured with appropriate instrumentation. Compressible flow features such as shocks can be visualised as density changes using schlieren imaging. Schlieren can also be used to visualise expansion waves, which are directly correlated to the Mach number in supersonic

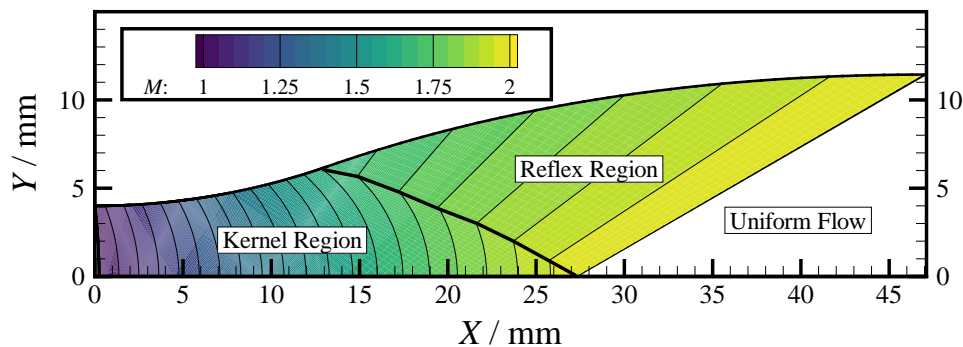


Figure 3.3: Expansion section of a converging-diverging nozzle designed for Siloxane MM as the working fluid with Mach 2.1 at the outlet. The Mach number increases at different rates in the diverging nozzle, resulting in three regions of the flow. In the kernel region the Mach number is lower at the centreline and larger at the wall. In the reflex region the mach number at the wall lower and it increases towards the centre of the flow. The uniform flow region has constant Mach number and constant properties, this is where the flow is fully expanded. Figure taken from Head [34].

flow.

The Mach number captures the compressible flow and thermodynamic behaviour and is available from the simulations and the experiments. The pressure is also a fundamental thermodynamic parameter which is easily measured in simulations and experiments. Therefore the DRQ for the flow of MM through a nozzle are the Mach number and pressure. These can be recorded along the centre line and along the top surface of the nozzle in simulations respectively, and then compared against experimental values. All the pressures are presented in absolute values.

The shock wave angle β of any shock produced due to the introduction of a wedge in the flow would be the best way to show NCFD effects, however they are not considered in the scope of this thesis due to lack of experimental data. The computational structure is provided to allow for β angle validation in the future. This is done through taking the flow conditions at the nozzle outlet from each simulation and using the numerical procedure discussed in section 2.5 to predict the angle of an oblique shock given a flow deflection angle of 0° , 2.5° , 18° , or 26° . The shock solver is coded in MATLAB by Head et al. [35], Iyer [38] and the results are analysed for uncertainty, but not validated.

3.1.3. Engineering Response Quantities

With the DRQ defined validation metrics can be evaluated to determine if the model matches the real physics of experiments. This can constitute a validation of software, however in engineering applications the accuracy of directly measured quantities are often not the relevant parameter of the analysis. The outputs of a simulation may be used to further calculate a parameter, such as using the pressure distribution to calculate a lift coefficient on an airfoil. The individual pressure values, which can be validated as a response since they are directly measured in experiments and simulations, are not useful unless they are taken in context of the entire pressure distribution and non-dimensionalised to become the lift coefficient. This gap between the validation metrics calculated with DRQ and the engineering context may at times lead to misinterpretations of a validation study. From a purely scientific perspective if a model is not valid it can not be used, however from an engineering perspective the verified model without complete validation may have a use in conceptual design or analysis. The best way to determine the suitability of a model should therefore be by assessing the precision of parameters used for engineering analysis which are calculated from the direct system responses. Understanding how much uncertainty would be on a lift coefficient, or another performance parameter, gives more context to the accuracy of the model than the uncertainty on individual pressure values.

Let an engineering response quantity (ERQ) be a parameter calculated from DRQ which could be used as a critical design value for analysis or optimisation. One may immediately think of efficiency as the obvious ERQ, but other ERQ may be heat transfer, drag, mass flow, or in the case of internal flows, entropy generation and loss coefficients. In the turbomachinery case mass flow rate and flow direction are important for design applications, while drag, entropy generation, and work are important for performance analysis.

A thorough explanation of how to use and interpret ERQ in validation studies is given in Chap. 5,

and the remainder of this section lists the ERQ selected for the validation of the SU2 flow solver for NICFD modelling.

The first ERQ will be the mass flow at the throat, which is significant in the geometric design of turbomachines. This is calculated by multiplying density and velocity and area,

$$\dot{m}_{th} = \rho_{th} * u_{th} * A_{th} \quad (3.1)$$

where the subscript th represents the throat location, and the symbol A is the cross sectional area. In the case of SU2 the momentum, ρu , is a flow solver output and the nozzle throat area is a constant. This calculation assumes a uniform momentum distribution at the throat, which is verified with an analysis shown in Appendix A. The mass flow is also easily measured in the ORCHID, thus the ERQ is directly acquired as an DRQ. Mass flow is a unique response in this study since it is an ERQ and an DRQ. Thus the magnitude of the uncertainty bands are important for engineering interpretation, and the mean value is important for validation.

The second ERQ for the SU2 validation of NICFD within the applications of turbomachinery is a performance metric called the loss coefficient [31, pp. 232-233]. Losses in turbomachines are best represented with entropy generation due to irreversibility, and the loss coefficient, defined as

$$\zeta = \frac{T_o(s_2 - s_1)}{\frac{1}{2}u_1^2} \quad (3.2)$$

is a non-dimensional representation of the entropy rise. Since the total temperature is maintained in the flow then the entropy rise can be represented as

$$\Delta s = -R \ln \frac{p_{o2}}{p_{o1}} \quad (3.3)$$

where the subscript o represents the stagnation values, or total values. However, in the case of a converging-diverging nozzle there is no total pressure change since no work is done. Therefore to determine the engineering significance of the SU2 validation we consider an academic exercise of a shock occurring at the exit of the nozzle. This is an extreme case since normally there are a series of oblique shocks occurring through the stator of an ORC turbine. Conducting a study of the shock loss coefficient sensitivity is a necessary academic exercise to illustrate the method of interpreting direct system responses in an engineering context. The entropy rise across a normal shock in an ideal gas is calculated as

$$\frac{\Delta s}{R} = \frac{2\gamma}{3(\gamma + 1)^2} (M_1^2 - 1)^3 \quad (3.4)$$

However in non-ideal gasses the relation is not valid, thus we turn to the iterative method defined by Grossman in Sec. 2.5 where

$$\Delta s = f(p_1, \rho_1, u_1) \quad (3.5)$$

From Eqn. 3.3 the entropy rise in theory can be a function of the pressure when work is done; from Eqn. 3.4 the entropy rise is a function of the Mach number in an ideal gas normal shock; and from Eqn. 3.5 the entropy rise is a function of pressure, velocity and density in a real gas normal shock. The loss coefficient translation from entropy adds a temperature term, which is also produced by the simulation. Thus the loss coefficient from an imaginary normal shock can be used as a generic performance metric for internal flows applications. The uncertainty of the loss coefficient would allow the engineer to understand the magnitude of the performance uncertainty on designs made in SU2.

3.2. Nozzle Test Section Experiments

The isentropic expansion unit case which was selected to isolate the thermodynamic behaviour of a NICFD flow is experimentally represented by the nozzle test section of the ORCHID from TU Delft. Therefore the experimental component of the validation of SU2 for NICFD uses the ORCHID nozzle test section run at steady state design conditions with data recorded by a pressure scanner and shlieren imaging. This validation study uses the data created by Head [34] to define the nozzle profile and boundary conditions of the SU2 model, and the data processing of Beltrame [9] for the analysis of the DRQ.

3.2.1. Converging Diverging Nozzle Profile

The converging-diverging nozzle is designed to accelerate the organic fluid MM. It is designed for inlet conditions corresponding to a stagnation temperature and pressure of $T_0 = 252\text{ °C}$ and $P_0 = 18.4\text{ bar}_a$, and to a back pressure of 2.1 bar_a . The inlet conditions of the fluid correspond to a compressibility factor of $Z = 0.58$ and the design outlet Mach number is 2.0. The rectangular cross section nozzle is 86mm long with a throat height of 8.0mm and constant width of 20mm. See Fig. 3.4 for an illustration of the nozzle geometry.

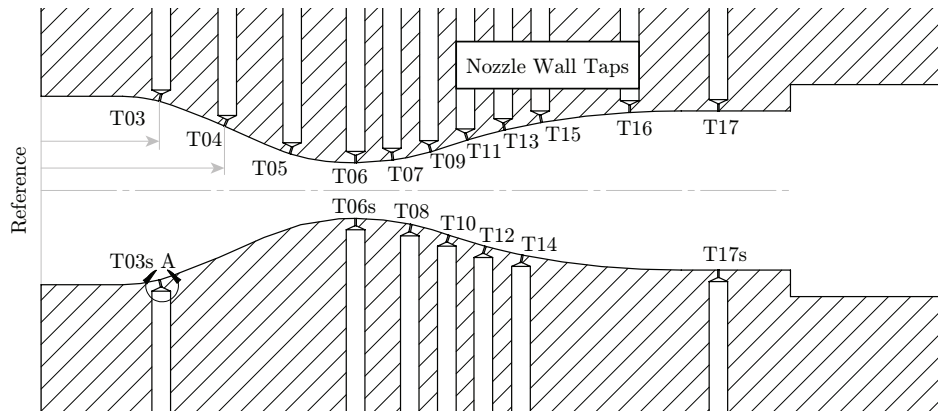


Figure 3.4: Two dimensional cross section of the ORCHID nozzle profile. The inlet on the left is the plane of reference from where all dimensional measurements are taken. Pressure tap locations are also indicated on the nozzle walls. The nozzle geometry is superimposed on plots of flow conditions for the remainder of this thesis as a reference. Taken from Head [34].

Pressure taps are located along the surface of the nozzle walls. The flow is controlled through variations in the thermodynamic boundary conditions of the inlet and outlet. The inlet plane is treated as the reference for stream-wise direction and the centreline is the reference for the span wise direction. The profile is uniform across the width of the nozzle, however the height of the throat, D_{th} , can be different from the nominal case if the assembly is over or under tightened. The profile is assembled as a top and bottom half placed together with gaskets between them and bolts holding it together. Any potential changes in geometry for an experiment are recorded along with the operating conditions.

3.2.2. Test Case Operating Conditions

The operating conditions for two experiments; namely, process run (PR).025-NT.001 and PR.027-NT.001 are reported in Tab. 3.1. The first experiment PR.025-NT.001 represents the on design flow conditions of the ORCHID and PR.027-NT.001 an off design flow condition with half the inlet pressure. Using two flow conditions allow for different isentropes on the T - s diagram to be examined and potentially provide more information about the effects of non-ideality on the flow.

Property	PR.025-NT.001	PR.027-NT.001
$T_0/\text{°C}$	252.7	252.8
P_0/bar_a	18.36	11.10
P_b/bar_a	2.06	1.31
$\dot{m}/(\text{kg/s})$	1.26	0.81
D_{th}/mm	6.66	6.66

Table 3.1: The two experiments considered in the validation study.

The nozzle throat was measured manually after the experiments were complete. Figure 3.5 shows the isentropes corresponding to the two experiments.

The process runs are both well within the non-ideal fluid region, identified by the Γ value less than one, with PR25 inlet conditions starting closer to the critical point. Head [34] provided experimental Mach number data for PR.25, and static pressure data for PR.27. The Mach values are extracted from schlieren image data and pressures are taken from a Scanivalve pressure scanner.

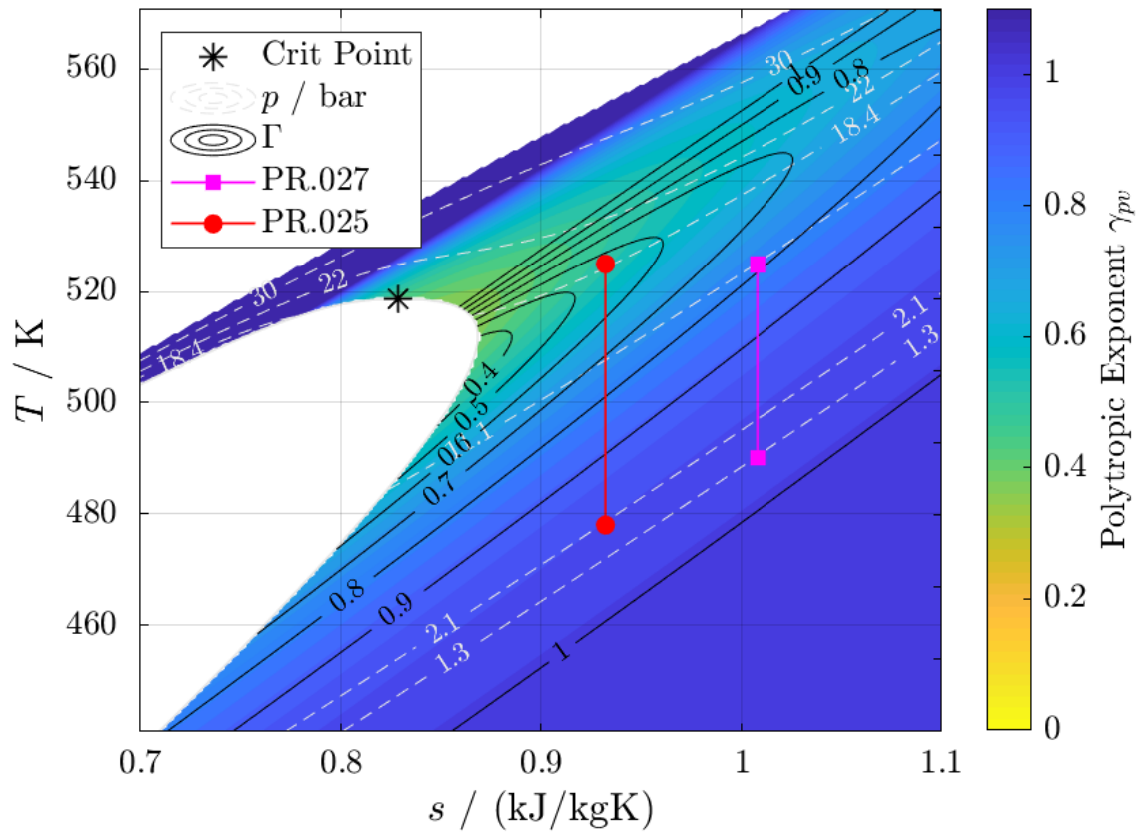


Figure 3.5: T - s diagram of Siloxane MM with process runs 25 and 27 of the ORCHID nozzle test section identified with isentropic lines. The isobaric lines are provided for the two experiments, with γ_{pv} contours and Γ contour lines also identified. Both expansions have a pressure ratio of nine and take place within the non-ideal dense gas region. The critical point is given as a reference.

3.2.3. Data Processing

To interpret the raw data and assess the uncertainty bands the raw measurements required post-processing. The pressure measurements were processed by Head [34] using statistical methods and instrument specifications. The Mach number required more analysis and was thus extracted and processed by a tool developed by Beltrame [9].

The raw measurements of the ORCHID include a camera system used to record the flow of MM through the nozzle test section. A series of mirrors, lenses, and a light source are used to highlight the changes of density in the flow, which is then captured by a camera. This process is called schlieren imaging and is commonly used to observe compressible flow phenomena [56]. In the case of dense organic fluid flows in supersonic conditions the compressible flow results in expansion waves. Schlieren images capture the expansion waves as they are characterised by changes in density, and can be used to determine the Mach number using equation 2.29. Beltrame [9] explains that using this principle the Mach number can be extracted using an image processing tool. The tool identifies the expansion waves in the schlieren image, calculates the angle of the waves relative to the expected flow direction, and converts that angle to a Mach number using equation 2.29. A processed schlieren image is shown in Fig. 3.6.

This image is taken from PR.25-NT.002 and has been processed to highlight the nozzle walls, throat, centreline, and expansion wave angles. The tool compares the expansion wave orientation with the centreline to extract the angles and convert them to Mach numbers. All uncertainties in the measurement chain are accounted for by Beltrame [9].

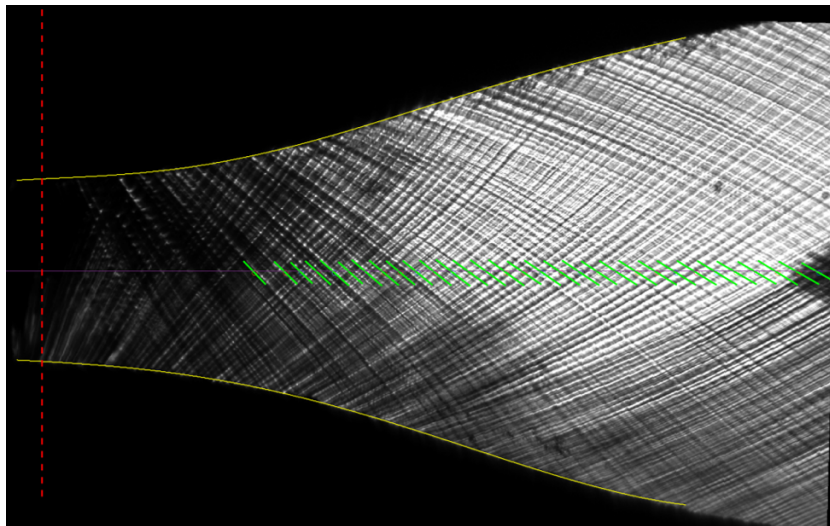


Figure 3.6: Schlieren image of Siloxane MM in the diverging part of the nozzle from PR25 taken from the ORCHID processed by the Beltrame [9] tool. The nozzle profile, centreline, and throat are given to the software which superimposes the reference geometry on the raw image in yellow, purple, and dotted red, respectively. The expansion waves can be seen in the raw image, with the tool identified angles superimposed with green lines. The image has been flipped to agree with the positive flow direction convention of left to right. Taken from Head [34].

3.3. SU2 Model Definition

The SU2 flow solver is used to simulate the nozzle test section of the ORCHID with MM working fluid using either internal EoS implementations or a link to FluidProp coded by Colonna et al. [19]. Fluidprop is a software with different thermodynamic equations of state internally coded, including iPRSV and the SW form for MM. Once set with boundary conditions to match those of the ORCHID from the experiments, the SU2 model can be analysed and compared against the experiments to evaluate the validity of SU2 for NICFD. The exact branch of SU2 is listed in App. F along with the version of FluidProp.

This section describes all the settings necessary to recreate the flow conditions of the experiment and solve Eqn. 2.11. It first presents the assumptions made in the model, then describes the SU2 configuration in detail. The grid development and results of a grid convergence study are explained followed by the selected equation of state (EoS) and the proof of its adequacy for the simulation. The final configuration is a two dimensional Euler flow with a half domain unstructured grid which uses the Peng-Robinson EoS and is solved with the standard finite volume spatial integration methodology. The detailed description is provided at the end of this section.

3.3.1. Assumptions

Before constructing the model of the ORCHID nozzle in SU2 three assumptions were made to simplify the configuration. The flow is assumed to be adiabatic, with no heat transfer between the nozzle surface and the fluid. The flow is assumed to be inviscid, with negligible effects of viscosity and no bulk turbulence. Finally the flow is assumed to be two dimensional, where there is no movement of fluid particles in the third axis direction.

The adiabatic assumption is made since the rate of heat transfer between the fluid and the outside environment is much lower than the rate of flow through the nozzle. A calculation which can be found in appendix A, shows that 36.5 W of energy leave the fluid by conduction compared to the 400 kW in the flow. This is not enough to alter the thermal energy of the system and is thus neglected.

The flow is assumed to be inviscid since the ORCHID nozzle profile is designed to have an isentropic expansion of MM and the boundary layer of the flow does not have time to become significant over the distance of the experiment. Work from Dijkshoorn [21] supports this claim, however to verify the assumption a turbulent calculation was conducted to compare against an inviscid solution. The results showed no significant viscous effects. This can be seen in Sec. 3.3.3 where a RANS and Euler simulation are both compared to experimental results.

Based on the boundary layer displacement thickness on the top and bottom profiles being negligible,

a similar thickness on the flat walls of the test section are assumed. There is also a mesh at the inlet to the nozzle which ensures a uniform flow at the inlet and there is no change in width of the nozzle. This supports the two-dimensional flow assumption although a three dimensional RANS simulation was not conducted to verify the assumption.

These assumptions allow for the omission of transport models in the SU2 configuration, which was the original purpose of the nozzle experiment being selected for validation of the SU2 flow solver. This case deals with NICFD where the assumption of ideal gas is not valid. Thus an appropriate EoS must be selected.

3.3.2. Spatial Discretisation

Dividing the two dimensional region of the ORCHID nozzle into elements is done using the software unstructured mesh generator 2 dimensional (UMG2), an internal code developed at TU Delft for creating an unstructured mesh based on the work of Ghidoni et al. [28]. The grid boundaries were constructed based on the measurements of the ORCHID taken during the experiments and simplified for isolating the region of interest, therefore the modelled nozzle in SU2 deviates from the nozzle design geometry. The nozzle profile is taken as a 69 point spline, then measurements made at the throat in the experiment were used to determine the displacement of the nozzle surface from the centreline. The nozzle outlet was then extended beyond the physical outlet to simplify the solution and avoid dealing with compressible phenomena like expansion fans, which would create numerical issues. Finally a symmetry plane is used since the experimental flow was confirmed to be symmetric by Beltrame [9], Head [34]. The final nozzle shape and sample meshes are shown in Fig. 3.7. Examples of the residuals can be found in App. C.

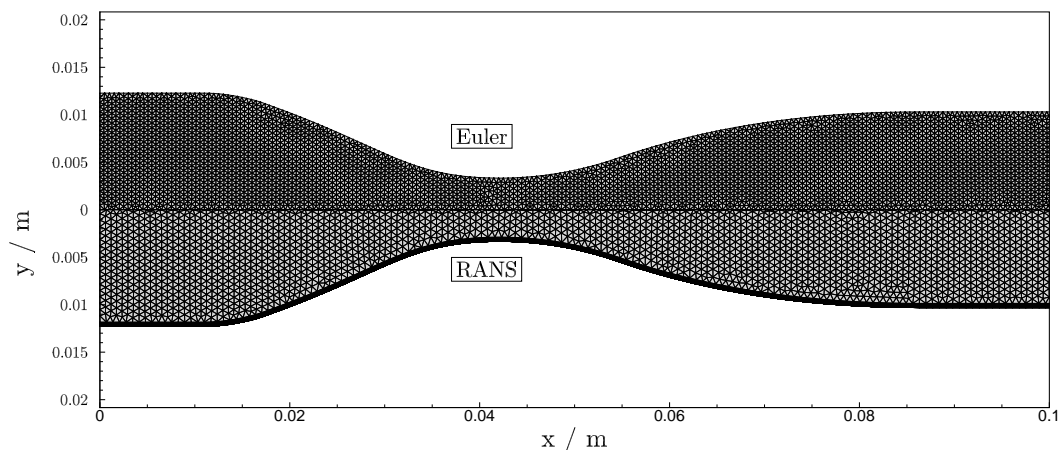


Figure 3.7: Discretised ORCHID half nozzles for the SU2 flow solver. The top mesh is has 10000 unstructured elements with uniform size. This can be used for Euler simulations. The bottom mesh is a hybrid of structured and unstructured cells designed for RANS simulations. The unstructured component is in the free stream and the structured mesh is on the nozzle wall to capture the boundary layer development. There are nearly 15000 elements total in the hybrid mesh.

The top mesh shows an unstructured grid of approximately 10 000 elements which can be used for Euler simulations. The bottom mesh is an example of a hybrid mesh with structured boundary layers used in a RANS simulation. There are 10 000 cells in the boundary layers, and approximately 5 000 cells in the core flow. The boundary conditions of the Euler mesh used for the validation study are listed in Tab. 3.2.

A preliminary grid convergence study using 3035, 6785, 9772, 15 446, 27 373, 61 520, and 110 410 elements determined the mesh most suitable for the validation. The results of the study are shown in Fig. 3.8 where the Mach, pressure, momentum, and density errors are plotted.

The average difference in responses from a mesh with 3000 elements and a mesh with over 100 000 elements is less than 0.4% for the ORCHID nozzle Euler simulation using a Peng-Robinson equation of state. The error decreases with more elements in the mesh, therefore to approach grid independence

Boundary	Setting
<i>Inlet</i>	Riemann Total Conditions
<i>Outlet</i>	Riemann Static Pressure
<i>Wall</i>	Inviscid and Adiabatic
<i>Centre</i>	Symmetry

Table 3.2: Configuration settings for the boundary conditions of the ORCHID nozzle mesh.

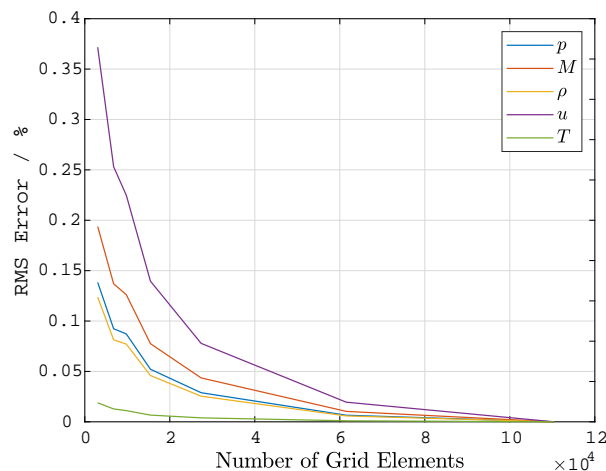


Figure 3.8: Grid convergence study showing the change in SU2 system responses between different mesh resolutions of the ORCHID nozzle. The error values are plotted as a function of number of cells in the grid, showing the trend of grid independence. The error represents the average difference between the finest mesh solution (110000 elements) and the mesh solution with the number of elements listed on the x-axis. It is calculated by taking the square of the difference between the DRQ of the given mesh and the finest mesh at every discrete point along the centreline, then taking the average of the squared differences and calculating the square root. This root sum of squares procedure gives an average error for the system response. The value is non-dimensionalised by dividing by the average value of the variable for the given simulation, and multiplied by 100%. For one variable there is one value of RMS error for each grid. Each variable can then be plotted on the same graph. Seven meshes were examined and compared against the finest mesh for five system variables.

a 10 000 element mesh is selected for the validation study. Using this mesh the numerical uncertainty can not be assumed as negligible, but an uncertainty of the order of magnitude 0.1% is equal or less than that expected from the experiments for all measured parameters. The true numerical uncertainty is not discussed here, but is calculated in Sec. 4.2.

3.3.3. Thermodynamic Model

A preliminary study comparing the results of SU2 simulations using different thermodynamic sub-models was used to determine the appropriate EoS to use in the NICFD nozzle simulations. Deterministic SU2 simulations using the ideal gas law, Peng-Robinson EoS, iPRSV EoS, and Span-Wagner (SW) form of empirical relations were each compared against experimental values. This comparison is not a validation since no uncertainties are considered, however the assessment allows for the most appropriate EoS to be selected for the NICFD conditions of the validation case. The most computationally efficient EoS which provides a prediction close to the mean experimental value over the entire nozzle range will be considered the most appropriate.

The study was done for Euler simulations of the ORCHID nozzle using a 15 000 element mesh to reduce the potential numerical uncertainties. One RANS simulation done as a reference using the FluidProp implementation of the iPRSV EoS, the internally coded SST turbulence model, and the illustrated 15000 element mesh from Fig. 3.7. The comparison of static pressure for PR.027-NT.001, and Mach number for PR.025-NT.001 can be seen in Fig. 3.9. Every Euler simulation was converged second order based on the residuals for each conservation variable reducing six orders of magnitude from the first order solution. The energy residual is converged at -11.5, the density residual is converged at -13.4, the x-momentum residual is converged at -13.6, and the Y-momentum residual is converged

at -14.4. The RANS simulation did not reach the same level of convergence, with only two orders of magnitude residual reduction for the conservative variables from the first order solution to the second order solution. The energy residual reduces to -6, the density residual reduces to -7.2, the x-momentum residual reduces to -7.5, and the Y-momentum residual reduces to -7.3. The turbulence residuals reduced to -1.5, and -8.6. Appendix C has plots of the residual values.

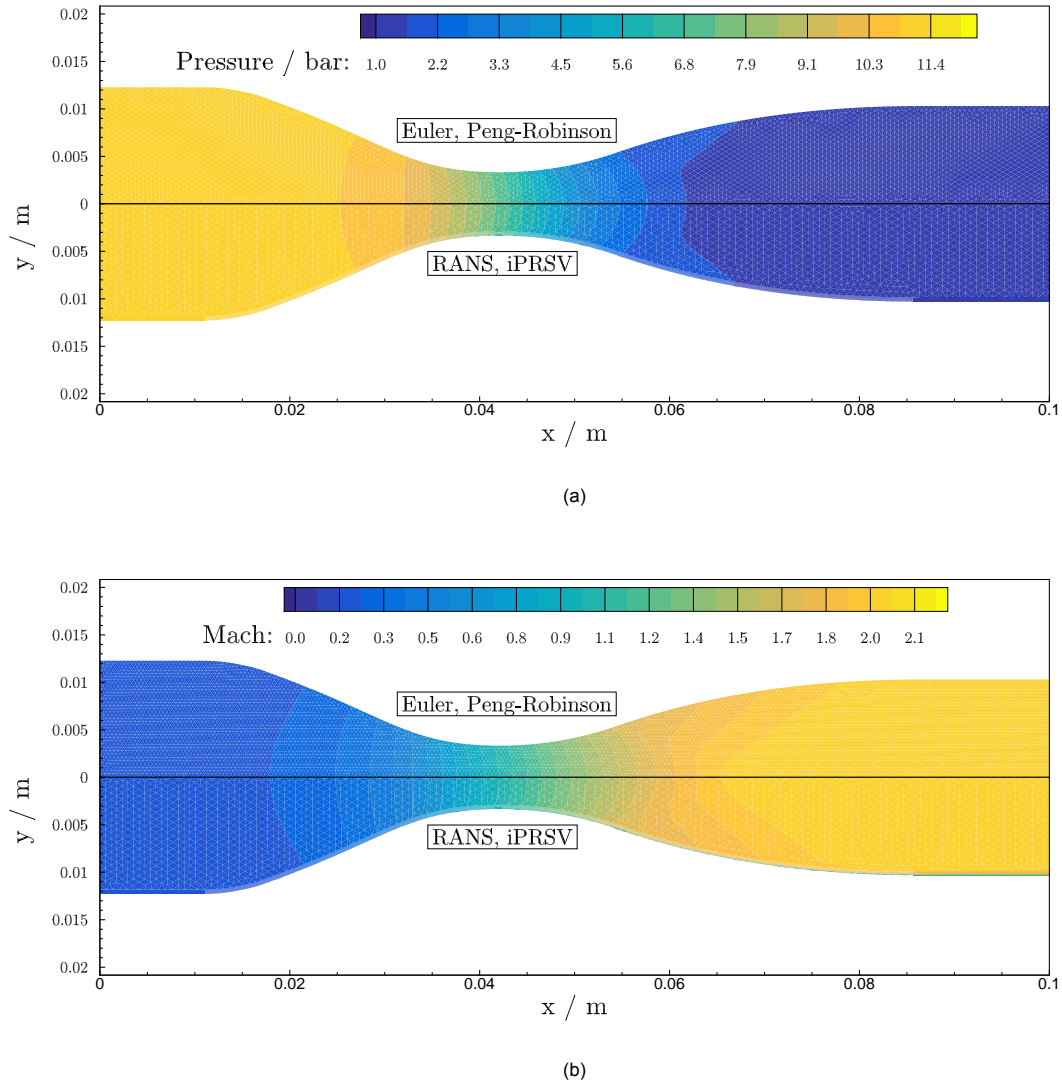


Figure 3.9: Comparison of two-dimensional SU2 simulations for the supersonic expansion of Siloxane MM through a converging-diverging nozzle with inlet temperature of 252°C. The top half of each contour plot is an Euler simulation with the Peng-Robinson equations implemented as the EoS. The bottom half of each contour plot is a RANS simulation with the iPRSV EoS implemented. The meshes are as illustrated in Figure 3.7. **a)** Pressure distribution calculated for PR.027-NT001. Units are bar absolute. **b)** Mach distribution calculated for case PR.025-NT.001.

The viscous RANS simulation took the most time to complete while the ideal gas simulation was the fastest, followed by the Peng-Robinson, iPRSV, and then SW. The ideal gas law and Peng-Robinson models are internally coded in SU2, while the iPRSV and SW models are implemented in fluidprop. The SW model in particular is implemented by RefProp which is packaged and called by FluidProp. As explained in Sec. 2.4 the equations of state require constant parameters based on the fluid characteristics to accurately model the thermodynamic behaviour. Table 3.3 lists the MM thermodynamic properties used in both the EoS implemented by SU2 and FluidProp.

The critical values of MM, along with the molar mass, and acentric factor were taken from Colonna

Parameter	Value
$T_{cr}/^{\circ}\text{C}$	245.6
P_{cr}/bar	19.39
ω	0.419
κ_1	-0.0528519
$MW/(g/mol)$	162.37752
γ_0	1.02605
η_1	48.881
η_2/K^{-1}	732.79e-3
η_3/K^{-2}	-422.02e-6
η_4/K^{-3}	103.31e-9

Table 3.3: Fluid Parameters of Siloxane MM

et al. [17]. The κ_1 value and ω value are taken from van der Stelt et al. [65] and the iPRSV as the most recent. The η coefficients of C_p^{ig} values are also taken from the iPRSV implementation; they are a regression of the fit of the most recently published thermodynamic model for MM by Nannan and Colonna [42], in the form presented by [2]. The γ_0 of MM is determined through the equation:

$$C_p^{ig} = R \frac{\gamma_0 - 1}{\gamma_0} \quad (3.6)$$

where the value of C_p^{ig} is taken from RefProp. γ_0 is the ideal gas specific heat ratio of MM and is only used for the Peng-Robinson equation of state. The Peng-Robinson model implemented in SU2 assumes a constant specific heat ratio, and that isentropic processes are perfectly polytropic.

To appreciate the differences in the configurations the static pressure along the nozzle surface for PR.027-NT.001, and Mach number along the centreline for PR.025-NT.001 can be seen in Fig. 3.10 compared with the experimental results.

From this analysis the Peng-Robinson equation of state will be used as the thermodynamic model which closes the Euler equations for the validation study of SU2 for NICFD. The ideal gas model should not be considered since the ORCHID nozzle operates with MM well within the NICFD region, as seen in Fig. 3.5, and this is supported by the incorrect estimation of the Mach number by almost 0.5 Mach seen in Fig. 3.10c. Unlike the ideal gas simulation, results with negligible differences are found between the Peng-Robinson, iPRSV, and RefProp implementation of SW equations of state for both Euler and RANS solutions. The Mach number is consistently offset from the experimental values, while the pressure has a spike in error near the throat. However, the error is consistent for every equation of state, so the simplest model can be selected. This is consistent with theory as Stryjek and Vera [62] explains that the Peng-Robinson EoS is equivalent to the PRSV in the supercritical flow region. The iPRSV was also only developed to deal with discontinuities at the critical point and provide marginal improvements in other flow regions, therefore the Peng-Robinson should be adequate at this distance from the critical point.

A special note should be made that the internal Peng-Robinson coding in SU2 is polytropic, meaning γ is assumed constant. This assumption could not be made initially based on the region of fluid behaviour, but the polytropic assumption seems to have no effect on the DRQ of interest for validation, thus it is acceptable to use in this case. More discussion on the polytropic assumption can be found in section 3.4.1.

3.3.4. SU2 Configuration

The final configuration for the SU2 validation simulations is a compressible flow Euler simulation with the internally coded Peng-Robinson equation of state used as the thermodynamic sub-model. A 10 000 element mesh is used which is initialised with free-stream conditions and solved using a weighted least squares numerical method for spatial gradients. The convective numerical method is ROE, and every simulation was converged second order with residuals decreasing by at least six orders of magnitude. Appendix G has full configuration files of the Peng-Robinson configuration and the iPRSV configuration

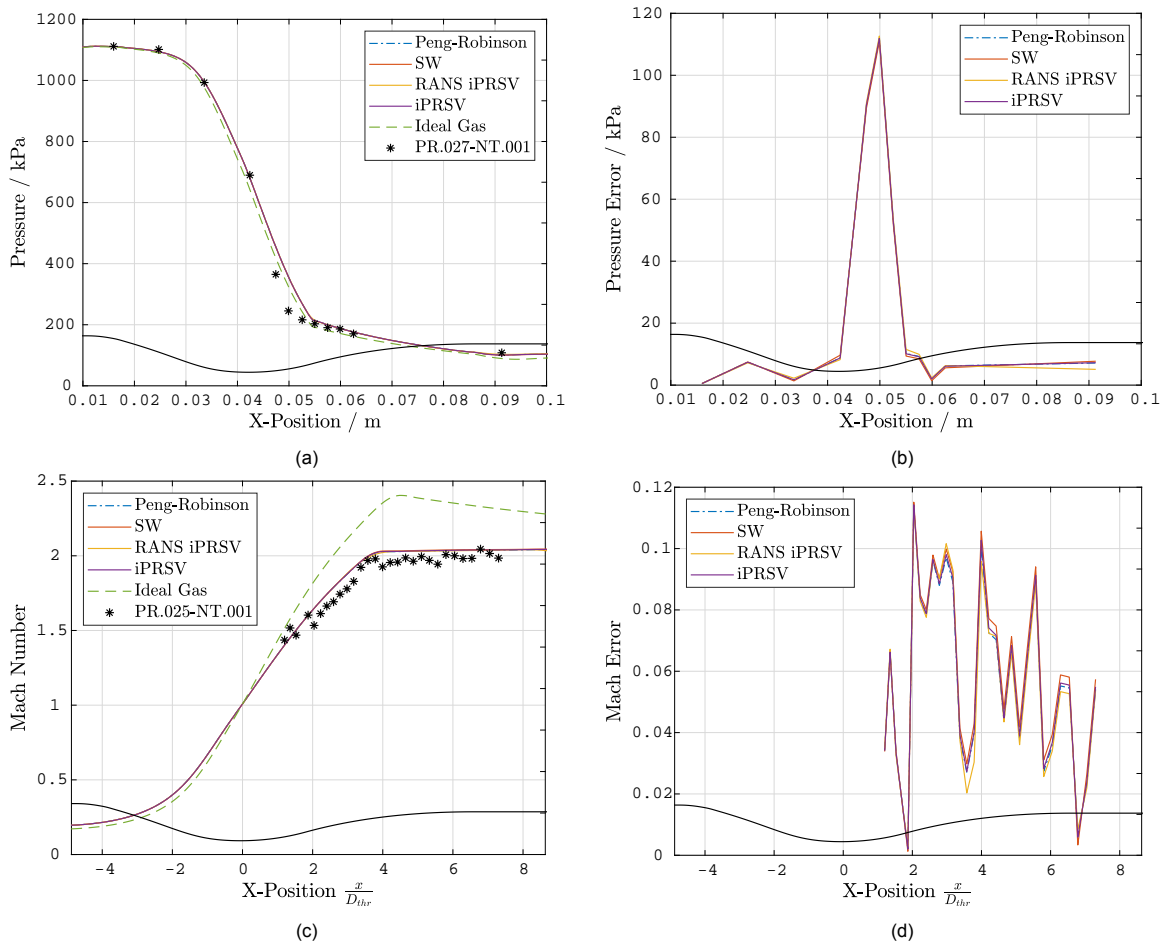


Figure 3.10: Comparison of the different thermodynamic state equations which can be used to close the Euler equations in SU2. Four Euler simulations of Siloxane MM, each with a different EoS, are plotted for the two variables of interest along the ORCHID nozzle test section. The results are compared against a RANS simulation using the iPRSV EoS and against experimental data points. The pressure data is from PR.027-NT.001, and the MACH data is from PR.025-NT.001. The Peng-Robinson, fluidprop SW equation, iPRSV, and ideal gas models are compared with error calculated with respect to the experimental value. **a)** The absolute static pressure along the nozzle surface. **b)** The error of the simulation static pressure with respect to the experimental values along the nozzle surface. **c)** The Mach number along the nozzle centreline. The position is non-dimensionalised with respect to the throat height. **d)** The error of the simulation Mach number with respect to the experimental values along the nozzle centreline. The position is non-dimensionalised with respect to the throat height.

for PR.025-NT.001 and PR.027-NT.001 respectively. Appendix H includes tips for configuring SU2 to solve Euler and RANS simulations for NICFD.

3.4. Discussion on the SU2 Configuration

The validation case of a converging-diverging nozzle for dense organic fluid can be modelled with SU2 ignoring viscous effects, three dimensional effects, and heat transfer to the surrounding system can all be ; but compressibility and thermodynamic non-ideality must be considered. Changes in density, as well as the complex relation between the thermodynamic state properties, impact the model solution. This is by design so that any sources of error between the simulations and experiments must be due to the thermodynamic model, the SU2 flow solver, or the experiment. Since the thermodynamic models have been constructed against empirical measurements, and the experiment is a true representation of physics, the SU2 flow solver can be isolated as the source of error in any discrepancy. There is a possibility of experiments having errors and uncertainties, however the ORCHID and the instrumentation used allows for the highest possible quality of measurements. Uncertainties are adequately quantified and known.

For the given test cases the thermodynamic EoS used to close the Navier-Stokes (NS) equations in the SU2 model is not important as long as non-ideality is considered. The viscous and 3D effects can also be ignored and assumed negligible. Figure 3.9 illustrated the negligible effects of the thermodynamic model and viscous effects. The only observable difference between the two simulations is the Mach number of zero along the nozzle wall for the RANS simulation. This arises due to the no-slip condition, however does not affect the pressure measurement since static pressure is constant perpendicular to the streamlines, and the Mach number is only considered on the nozzle centreline.

3.4.1. Thermodynamic Model

While the Peng Robinson Equation of state is the best model for the given isentropes and selected DRQ, movement towards the critical point may require using the iPRSV or SW. Any isentrope to the right of the nozzle flow on the T - s diagram can be assumed to become more ideal and require less correction from the ideal gas model. A validation of SU2 using the Peng-Robinson equation at this point would validate the iPRSV as well. However, considering that the Peng-Robinson EoS is computationally more efficient there should be no need to consider using the iPRSV and definitely no need for the SW model when examining pressure or Mach number. When the isentrope is closer to the critical point there are potentially more differences in the thermodynamic models, so the iPRSV or the SW must be considered for expansions which occur to the left of the PR.025-NT.001 isentrope in Fig. 3.5.

Another note is that the constant gamma assumption is not correct, however for the variables of pressure and Mach it does not matter. The constant gamma assumes a polytropic process, which is not true due to the variation in gamma which is seen in the T - s diagram of Fig. 3.5. This means the relation of enthalpy and temperature will be incorrect in the simulation. However, due to the construction of SU2 solver the calorific equation of state is only used to calculate the temperature, not to solve the flow conditions. Therefore the temperature variable is not accurately estimated by the solver. This is visualised by Fig. 3.11 where the outlet temperature deviates by over two degrees Kelvin when using the polytropic Peng-Robinson EoS.

If the temperature is a variable of interest the iPRSV or the PR with a non-polytropic implementation will be required to complement SU2.

3.4.2. Viscous Effects

In reality the isentropic core is influenced by viscosity, as the boundary layer grows to a maximum displacement thickness of 0.8 mm by the end of the nozzle [21]. However, the boundary layer has no impact on the DRQ. The static pressure on the wall of the nozzle is not affected by flow velocity at the wall as long as the flow is tangential to the surface. This is specifically designed in the nozzle plus the simulations show no point of separation or indication that the flow is never tangential. Figure 3.10d shows that the development of a boundary layer changes the Mach number distribution on the mid-plane by less than 1% at the exit. Therefore the inviscid assumption is adequate for this validation study.

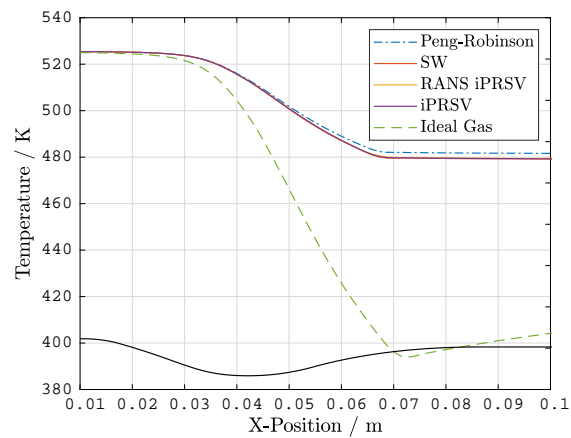
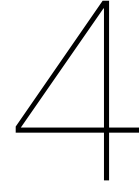


Figure 3.11: Comparison of the temperature along the centreline of the nozzle calculated using different thermodynamic state equations which can be used to close the Euler equations in SU2. Four Euler simulations of Siloxane MM, each with a different EoS, are compared against a RANS simulation using the iPRSV EoS. The ideal gas law is off by nearly 80K at the outlet, while the Peng-Robinson EoS also deviates from the accurate models due to the polytropic constant γ approximation.



Uncertainty Quantification of the SU2 Flow Solver

To appreciate the precision of a model every source of uncertainty must be accounted for and quantified. This process of uncertainty quantification (UQ) is a critical step in any validation activity, since no validation metric can be calculated without uncertainty values. The quality of validation is thus a direct function of the level of rigour applied to the UQ. In the case of CFD flow solvers the uncertainties arise from the experiments, simulation inputs, meshing, and the numerical methods of solving the NS equations.

Generally, uncertainty is broken into experimental and simulation components represented by the subscripts D and S , respectively. While it is common practice to divide uncertainties into systematic and random, the terms allow room for interpretation so are not used in this thesis. Instead, the uncertainty can be broken into Type A and Type B. Type A includes all the uncertainty in an experiment which can be determined from the statistical analysis of measurements, such as the mean and standard deviation, while type B uncertainties cover the remaining sources of experimental uncertainty which are not captured statistically. For example the reported accuracy of an instrument is considered Type B. The process of identifying and quantifying the experimental uncertainties relies heavily on book keeping and thorough statistical analysis. Details of the procedures are described by ASME [5], and are set by the GUM [37].

This chapter presents the full quantification of the uncertainties in the campaign to validate SU2 using the Peng-Robinson EoS for the NICFD flow in a converging-diverging nozzle. An analysis of the SU2 model prediction uncertainties is presented in detail, and the experimental measurement uncertainties are reported to provide a complete picture of the DRQ accuracy. The uncertainty of the ORCHID experiments is covered in detail by Head [34] and Beltrame [9]. The procedure introduced in Sec. 4.1 to quantify each type of uncertainty is generic and can be applied to any flow solver, however the analysis of Sec. 4.2 is only done for the case of interest. The uncertainties of the Mach number along the centreline of the ORCHID nozzle in PR.025-NT.001 and the pressure along the nozzle wall in PR.027-NT.001 are presented in absolute and relative form, in addition to a sensitivity analysis to determine the largest sources of uncertainty. The effect of the DRQ uncertainties on the uncertainty of the losses due to the theoretical shock introduced in Chap. 3 provides an engineering context for the analysis and is reported in Sec. 4.3.

4.1. Quantifying Model Uncertainty

Simulation uncertainty is divided into numerical (*num*), and input (*in*). This section describes how these uncertainties are identified and quantified in the SU2 flow solver with a software infrastructure using methods proven in literature. The numerical portion of simulation uncertainty encompasses all the approximations which must be made during a computational assessment; this includes approximations in the discretisation, truncation, and iteration of a simulation. Discretisation uncertainty arises since discrete value must be assigned to each cell in a mesh even though in true physics the value may be continuous over the domain. Truncation is the removal of digits at the end of a number due to the bit

limit in a computer, and iteration refers to uncertainty from taking a solution from an iterative process which may not be converged to the final solution. The iteration and discretisation uncertainties can be calculated using Richardson Extrapolation as described by Eça and Hoekstra [22]. This method uses the solutions of the same simulation over sequentially finer grids to approximate the total uncertainty level due to discrete errors at a given grid density. This process has been automated with a tool from ReFRESKO [39] which requires the input of simulation results and provides the approximate uncertainties of each output variable through using the method proposed by Eça and Hoekstra [22].

The input portion of simulation uncertainty is the result of input parameter uncertainties being forward propagated through the model to the outputs. Constant values in the simulation, for example boundary conditions or fluid properties, are not exact. The boundary conditions and closure coefficients of the thermodynamic sub-models are determined through experimentation where there are fluctuations in measurements over time, and instruments have limited resolutions. Any possible change in the model constants will have an impact on the final model responses. Evaluating the value of input uncertainty can be done in a structured fashion through LHS, however there are more efficient methods which have been established for NICFD. As discussed in Sec. 2.7 Cinnella et al. [13, 14] have used stochastic expansion UQ techniques to establish the uncertainty of dense organic gas flows, and more methods targeted for NICFD solvers in ORC design have been presented by Congedo [20].

A simplified example of input uncertainty calculation and sensitivity study using SC can be found in App. B where the polynomial form of the calorific equation of state seen in Eqn. 2.24 is examined. The study shows that SC produces results equal to the LHS and VBD approach of calculating system response statistics and input sensitivities for a polynomial system. The study also concludes that only one coefficient of the polynomial, η_2 , is important to include in the uncertainty quantification study.

4.1.1. Applied Numerical Infrastructure

The numerical uncertainty is calculated using the Richardson extrapolation method, which is implemented by the ReFRESKO software [39]. The implemented method to calculate the SU2 model input uncertainty is a third order polynomial chaos SC method with Smolyak sparse grid sampling, done using Dakota [1] on a Linux operating system. These programs are wrapped within a series of Python and MatLab scripts to interface them with the SU2 simulations and results. Figure 4.1 presents a top level flow chart of the input uncertainty calculation infrastructure. Python is used as the interfacing language between Dakota and SU2 with calls to a MATLAB shock wave calculator developed by Head et al. [35], Iyer [38] based on the jump conditions for a steady shock wave described in Sec. 2.5. The code is developed especially for SU2 in Linux and can be reused to assess the uncertainty of different test cases. The code also produces Sobol indices for the responses of interest. Appendix E presents detailed flow charts with script names, and the method to connect SU2 results with the ReFresco executables. A full list of the software versions, hardware, and scripts used for the infrastructure can be found in App. F.

4.1.2. Infrastructure Verification

To verify the infrastructure for quantifying the uncertainty of the SU2 solver an assessment was done three times for PR.025-NT.001. This included running variants of the code to prove the independence of the results from the UQ method, and using different thermodynamic models to determine if the models produced different levels of uncertainty. Table 4.1 describes the differences of each study done along with the number of function evaluations required by the code to converge on the final uncertainty values of the system responses. Each function evaluation is a complete run of SU2 until second order

EoS	UQ method	Uncertain Inputs	Evaluations
iPRSV	LHS	9	>2000
iPRSV	SC	9	1571
Peng-Robinson	SC	6	573

Table 4.1: Uncertainty quantification studies conducted to verify the UQ framework for SU2 NICFD forward propagated input uncertainty quantification. The studied were all done on a model of the ORCHID nozzle test section using PR.025-NT.001 as the reference flow condition.

convergence, which has different run times dependent on the hardware available. On the machine

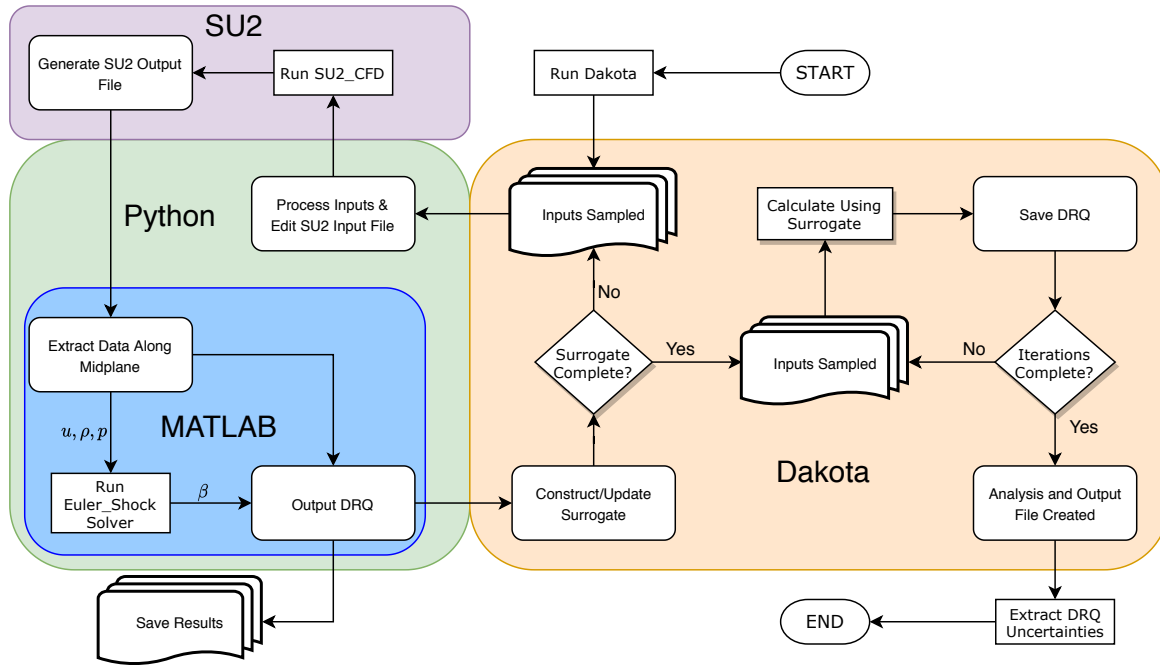


Figure 4.1: Applied framework to implement a sparse grid stochastic collocation UQ for SU2. The code, implemented in Linux, accepts PDFs of SU2 model inputs and evaluates the uncertainties of the DRQ along with the Sobol indices for the given configuration of SU2.

described in App. F the SC UQ with the Peng-Robinson model took 5.23 hours. The number of uncertain inputs differ depending on the choice of the EoS. The iPRSV EoS includes nine constants to construct the thermodynamic model, which are reported in App. E. The six uncertain model inputs used in the Peng-Robinson EoS are listed in Tab. 4.2.

The results from each study were identical and will be shown in Sec. 4.2.2, specifically Fig. 4.5a. From this example study the sparse grid SC UQ implemented in Dakota [1] was verified as the framework around which to build the uncertainty quantification infrastructure required to calculate the simulation of uncertainty of SU2 for NICFD conditions. The study also confirms the results from Chap. 3 indicating that using the Peng-Robinson EoS is identical to using the iPRSV EoS for modelling case PR.025-NT001.

4.2. Model Uncertainties for Non-Ideal Compressible Flow

For the flow case defined in Sec. 3.3 the simulation uncertainties of the Mach number along the centre-line and the pressure along the nozzle surface are determined using the infrastructure and methodology described in Sec. 4.1. The significant sources of uncertainty arising from the SU2 simulation of NICFD flow using the Peng-Robinson EoS in the ORCHID nozzle is the discretisation and forward propagated input. In this case the truncation is considered negligible because the simulation was run with double precision and the uncertainties due to iterations are negligible due to the convergence of the residuals. The steady conservation equations were solved second order until the residual levels for all variables were reduced six orders of magnitude. An example of the residual convergence is given in App. C. This section presents the numerical uncertainties for the DRQ and a sensitivity analysis of the model inputs, in particular the fluctuating boundary conditions and closure coefficients of the thermodynamic sub-model. The simulation uncertainty is then combined with the experimental uncertainty to determine the final total validation uncertainty.

4.2.1. Discretization Uncertainty

Calculating the discretization uncertainty resulting from the 10000 element mesh used in the SU2 simulation uses the same data from the grid convergence study in Sec. 3.3. The results from identical

simulations with a 3, 7, 10, 15, 30, 60, and 120 thousand element mesh were input to the uncertainty quantification code described in Sec. 4.1 to evaluate the uncertainty of the system responses using Richardson extrapolation. U_{num} for the Mach number along the nozzle centreline, pressure along the nozzle profile, and oblique shock angle for an imaginary wedge placed in the flow are presented in Fig. 4.2. β is calculated by taking the values of flow parameters from the mesh and then using them as inputs to the shock solver.

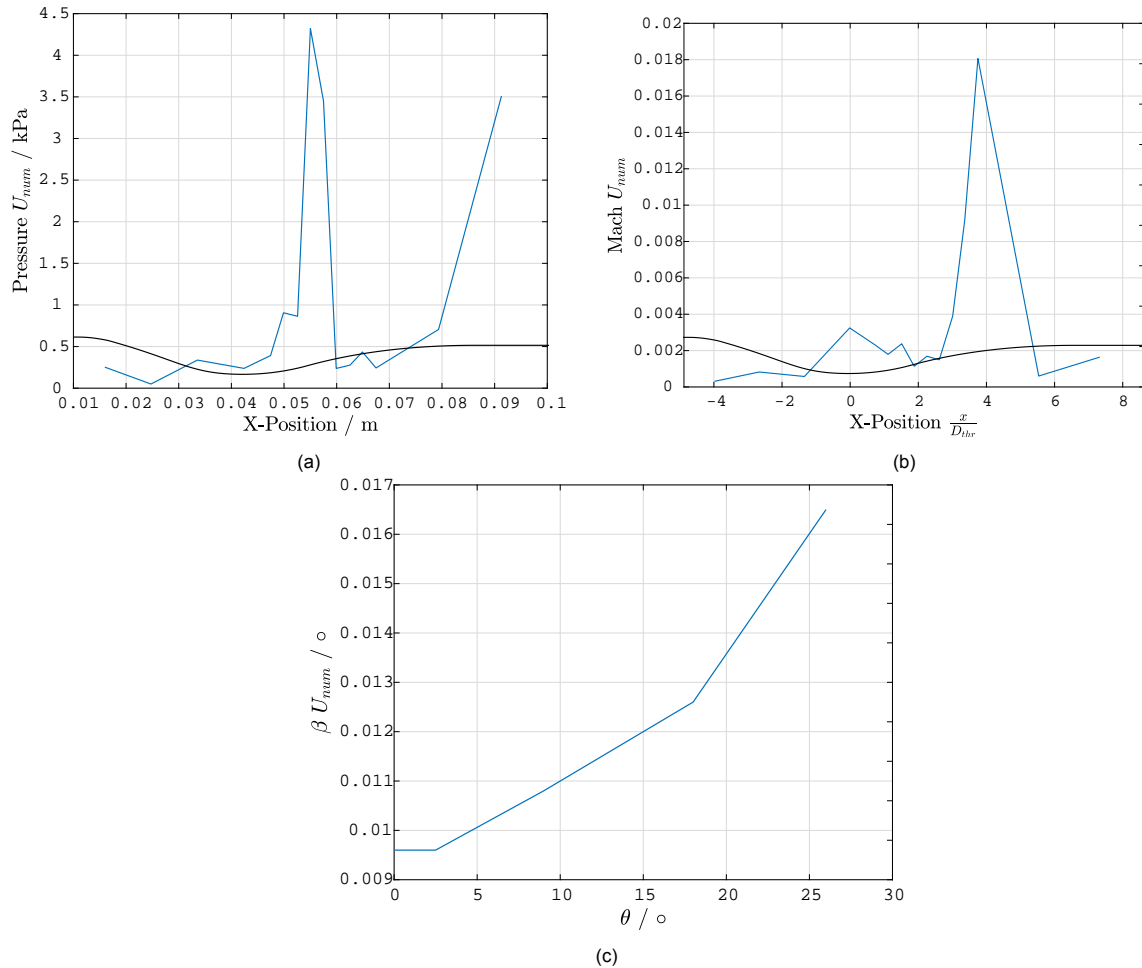


Figure 4.2: Total expanded numerical uncertainty of direct system responses calculated on a 10000 element mesh in SU2 using the Richardson Extrapolation method of Eça and Hoekstra [22]. The flow is a converging-diverging nozzle with Siloxane MM as the working fluid. The inlet flow is at Mach 0.2 and the outlet is Mach 2, with an expansion ratio of approximately nine.

The uncertainty is calculated at discrete points along the nozzle and connected with linear sections for clarity. The nozzle profile is superimposed to illustrate the relative position of the uncertainty values along the nozzle. **a)** Pressure along the nozzle surface for PR.027-NT.001. **b)** Mach number along the centreline of the nozzle for PR.025-NT.001 **c)** Oblique shock wave angle uncertainty for different flow turning angles created by a wedge at the nozzle outlet. The shock angles are solved using the jump conditions across a steady shock for non-ideal gas dynamics.

The oblique shock angle uncertainty seen in Fig. 4.2c does not include any uncertainty from the MatLab shock calculation. The iterative method of the solver may be another source of uncertainty, however the settings used in the fzero function result in an uncertainty of orders of magnitude less than the mesh discretization uncertainty¹. Thus the only source of numerical uncertainty for the angle β is the uncertainty values arising from discrete errors in the mesh. The total numerical uncertainty is also less than 0.02 degrees everywhere, which is negligible.

The pressure uncertainties are small for the majority of the flow except for two locations. The second spike is caused by a course mesh adjustment made at the outlet which was introduced to aid

¹The tolerance used on fzzero in Matlab is set to 2.2204e-12, so the uncertainty arising from the calculation procedure used to solve the jump conditions for a steady shock is orders of magnitude lower than the input uncertainty.

in simulation convergence. This uncertainty does not influence the analysis to follow since it is outside the domain of interest. The first, and largest, spike occurs in both the pressure and the Mach number. This is found at the end of the kernel region, shown in Fig. 4.3. The location of the transition line at the centreline is 0.07 m. This corresponds to the non-dimensional position of 3 on Fig. 4.2b where the spike in Mach uncertainty is located. The transition on the nozzle surface is at 0.055 m which matches the spike in uncertainty on Fig. 4.2a where the spike in pressure uncertainty is located. This implies

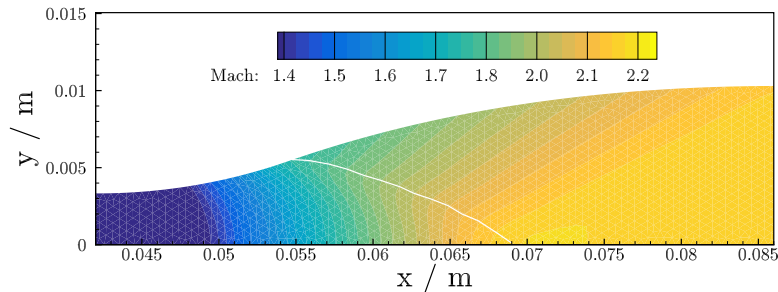


Figure 4.3: Kernel transition for PR.027-NT.001 illustrated by a white line overlaying the contour plot of the Mach number. The Mach number has a change in gradient at 70 mm along the nozzle centreline, and 5.5 mm along the nozzle surface which represents the transition from kernel region to reflex region.

that increasing the mesh resolution in this location is required in order to capture the change to reflex or uniform flow. However, an increase in mesh density will result in increased computational times. The uncertainty is thus included in the analysis and accounted for in the validation metrics. In the future the mesh density at the exit should be kept consistent with the remainder of the nozzle grid. More importantly, if the computational resources are available, the mesh should be refined along the kernel transition line.

4.2.2. Forward Propagated Input Uncertainty

The input uncertainty of the SU2 flow solver is evaluated using the probability distributions of the boundary conditions of the ORCHID measured by Head [34] and the thermodynamic closure coefficients from literature. Uniform distributions were assumed for the uncertainties if there was not enough experimental data to extrapolate a full distribution. Table 4.2 lists the uncertain inputs to the two SU2 models analysed.

Model Input	PR.025-NT001 Uncertainty	PR.027-NT001 Uncertainty	Assumed Distribution
T_o	± 0.729 K	± 0.690 K	normal
p_o	± 3511 Pa	± 1920 Pa	normal
T_{cr}	$\pm 3\%$ in $^{\circ}\text{C}$	$\pm 3\%$ in $^{\circ}\text{C}$	uniform
p_{cr}	$\pm 5\%$	$\pm 5\%$	uniform
γ	$\pm <1\%$	$\pm <1\%$	uniform
ω	$\pm 15\%$	$\pm 15\%$	uniform

Table 4.2: Uncertainties of inputs used for the SU2 model of the ORCHID nozzle test section using the Peng-Robinson Eos.

The boundary conditions, T_o and P_o , include the Type A and Type B uncertainties from the experiment. The back pressure is treated as deterministic due to the physics of a supersonic expansion. After the throat of a nozzle where the flow chokes the supersonic expansion of a fluid the static pressure decreases as a function of the nozzle profile independently of the back pressure at the end of the nozzle. If the pressure within the nozzle does not match the outlet pressure then either a shock occurs, reducing the pressure and resolving the flow discontinuity, or the flow suddenly expands at the outlet in the form of expansion waves. In all simulations done in this study the effects of over or under expansion are assumed to be far downstream. The potential uncertainty due to geometry is neglected due to machine tolerances being high², and precise measurements of the facility. The thermodynamic

²a standard 5-axis milling machine can produce parts with errors less than 10 μm [27]

constant uncertainties are directly taken from the work of Colonna et al. [17], however the uncertainty of γ is not reported and had to be calculated from the C_p uncertainty by using Eqn. 3.6. Cinnella et al. [14] reports $\pm 3\%$ uncertainty of C_p over the temperature range of the ORCHID experiments, thus was used as a reference. The acentric factor has no reported uncertainty except for Iyer [38] who reports 15% uncertainty with no effect on the system responses. However, since the model used in the thesis is different from the one reported here, the same 15% value is taken and treated as uncertain.

The Sobol indices produced from the SC UQ studies define which of these input uncertainties are significant to the resultant system response uncertainties. These are shown in Fig. 4.4. The three plots show the variation of the Sobol indices for the static pressure, Mach number, and shock wave angle along the non-dimensional nozzle position and the flow turning angle. Even though the stagnation

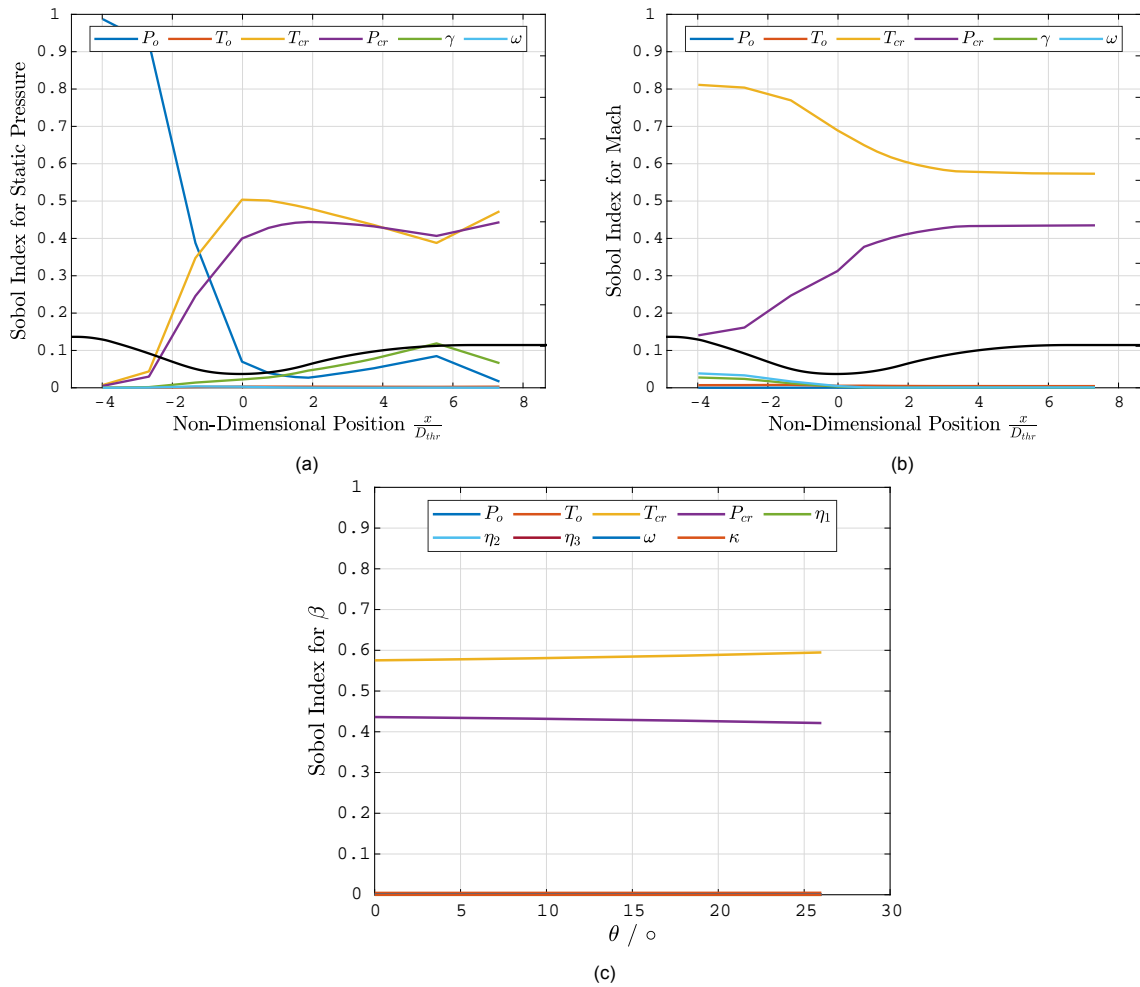


Figure 4.4: Sobol indices representing the relative influence of uncertain input parameters on the system responses of a converging-diverging nozzle with Siloxane MM as the working fluid modelled in SU2 assuming two-dimensional flow using the compressible Euler equations. The inlet flow conditions are at Mach 0.2 and the outlet is Mach 2, with an expansion ratio of approximately nine. **a)** The effect on the uncertainty of pressure of PR.027-NT.001 calculated along the nozzle surface using the Peng-Robinson EoS. **b)** The effect on the uncertainty of Mach number of PR.025-NT.001 evaluated along the centreline using the Peng-Robinson EoS. **c)** The effect on the uncertainty of the oblique shock angle calculated at the outlet of the nozzle for PR.025-NT.001 using the iPRSV EoS.

pressure appears to be the dominant parameter for calculating the static pressure at the inlet in Fig. 4.4a, this is a trivial result since the pressure near the inlet must be controlled by the boundary condition. The resultant Sobol indices show that for each DRQ the critical values most influence the system uncertainty. T_{cr} decreases in influence along the nozzle as the flow becomes more ideal, and P_{cr} increases in influence. The importance of the critical point values may be related to the phenomena of choked flow since the influence appears to be consistent once the flow becomes supersonic. There is a

slight kink in the trends in Fig. 4.4a, however this may be due to the large rise in numerical uncertainty at the outlet which is discussed in Sec. 4.2.1. In general, the thermodynamic model is more significant than the boundary conditions when evaluating the uncertainty on the outputs considered. However, it is only the pressure and temperature values of the critical point which effect the system responses.

The DRQ uncertainties calculated by the UQ are shown in Fig. 4.5. Figure 4.5a shows that un-

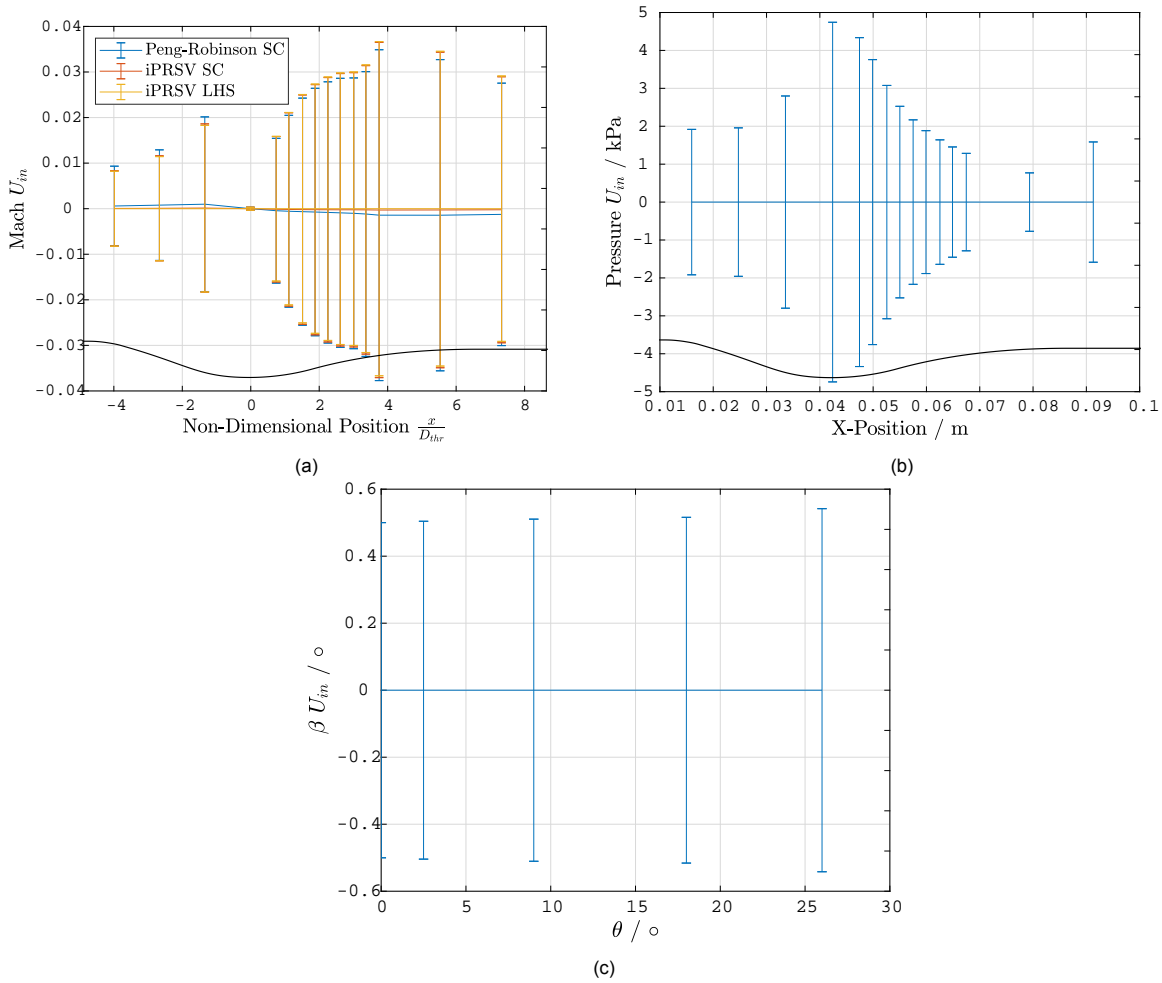


Figure 4.5: Expanded input uncertainties for the system responses of a converging-diverging nozzle with Siloxane MM as the working fluid modelled in SU2 assuming two-dimensional flow using the compressible Euler equations. The inlet flow at Mach 0.2 and the outlet is Mach 2, with an expansion ratio of approximately nine. The nozzle profile is superimposed for reference.

a) The Mach number uncertainty calculated along the nozzle centreline for PR.025-NT.001 evaluated using the Peng-Robinson EoS. The results from three different UQ studies are superimposed to illustrate the independence of the results from the UQ method and EoS selected. **b)** The pressure uncertainty calculated along the nozzle surface for PR.027-NT.001 evaluated using the Peng-Robinson EoS. **c)** The uncertainty of the oblique shock angle calculated at the outlet of the nozzle for PR.025-NT.001 using the iPRSV EoS.

certainties of the DRQ evaluated using all of the configurations listed in Tab. 4.1 are the same. There is a slight deviation of mean response between the Peng-Robinson EoS and the iPRSV, however the difference is negligible, e.g., the maximum deviation in the Mach number is 0.001 and is located at four throat heights past the nozzle throat. The SC UQ methodology also changes the uncertainty bands by an indiscernible amount when compared with the LHS. Since the SC required the fewest simulations, this method is chosen for the analysis to follow. Furthermore, the uncertainties in the DRQ γ_{pv} , μ , ρ , T , and u are also recorded since they can be directly measured in future experimental work, but are presented in App. D.

Figure 4.5c shows that the uncertainty in the shock wave angle increases as the flow turning angle increases. This is consistent with property variations over shocks of higher strength. Therefore the EoS becomes more relevant when the flow field becomes complex. The magnitude of the uncertainty

is however fairly consistent, meaning the percent uncertainty of the oblique shock angle decreases at larger deflection angles. The magnitudes of the Mach number and pressure uncertainties show opposite trends as a function of nozzle position. The Mach number has no uncertainty at the throat, where the flow chokes, while the pressure has the largest uncertainty at the same location. The trend in the Mach appears consistent with physics, since the flow must choke at exactly Mach 1 at the throat. As the flow accelerates through the expansion the influence of the thermodynamic model increases and the uncertainty of the critical values, which were seen to have the most influence on the output uncertainty, can have more effect. The magnitude of the uncertainty bands are also consistently less than 0.04 Mach, the significance of which will be examined in section 4.3. The pressure also has a maximum uncertainty of nearly 5 kPa, which for a deterministic value of nearly 800 kPa at the throat is equivalent to an uncertainty of $\pm 0.6\%$. An uncertainty of less than one percent is usually considered acceptable, however the uncertainties from all sources must be aggregated before a determination can be made.

4.2.3. Total Uncertainty of the DRQ

The total expanded uncertainty in the Mach number and pressure can be determined from the numerical and experimental contributions. This is determined using the root sum of squares providing that each contribution is independent from one another.

Figure 4.6 shows the total post-processed uncertainties along the nozzle for each DRQ. The total

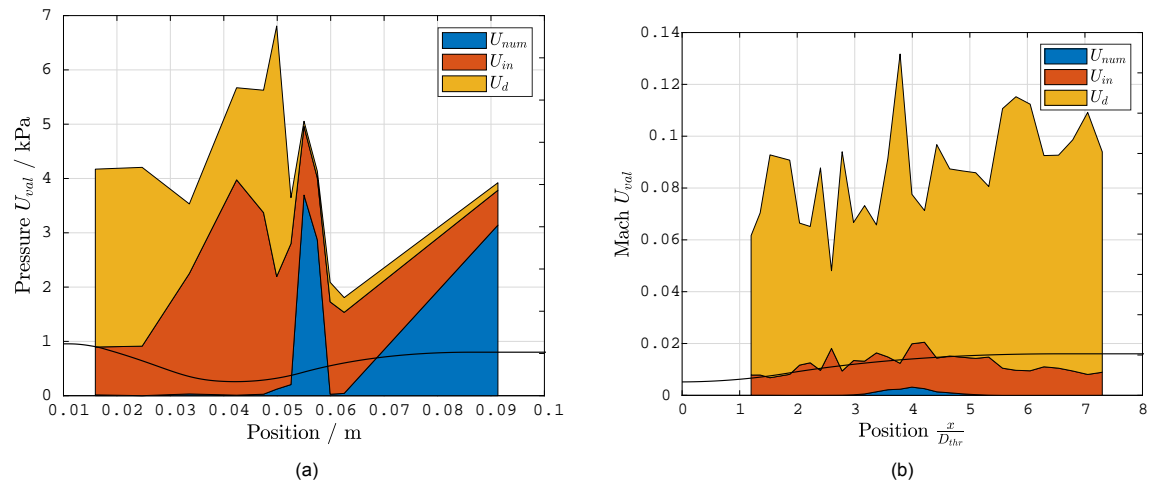


Figure 4.6: Total expanded uncertainties for the system responses of a converging-diverging nozzle with Siloxane MM as the working fluid. The inlet flow at Mach 0.2 and the outlet is Mach 2, with an expansion ratio of approximately nine. The proportion of the uncertainty due to the numerical, input, and experimental uncertainties is highlighted in blue, red, and yellow, respectively. The nozzle profile is superimposed for reference. **a)** The pressure uncertainty calculated along the nozzle surface for PR.027-NT001. The simulation components of the uncertainty are evaluated using the Peng-Robinson EoS. **b)** The Mach number uncertainty calculated along the nozzle centreline for PR.025-NT-001. The simulation components of the uncertainty are evaluated using the Peng-Robinson EoS. Only the diverging section of the nozzle is presented.

area under the curve presented in each plot is the total expanded uncertainty for the given DRQ, with the proportion of the total uncertainty caused by each component highlighted in a different colour. For example, in Fig. 4.6a at the inlet the total uncertainty of the pressure is ± 4 kPa, and the majority of the uncertainty arises due to the experimental uncertainty, while at the outlet the uncertainty is again approximately 4 kPa, however the source of the uncertainty is mostly numerical. From the pressure plot it can be interpreted that the highest uncertainty in pressure value is at the throat, which is due to the simulation and the experiment, however the issue of mesh resolution around the kernel transition can be seen at 0.055 m from the inlet, where the numerical uncertainty suddenly rises. This is an area of the nozzle to observe when calculating the validation metrics, however the magnitude of the uncertainty at the kernel transition point is still less than the uncertainty at the throat. It should be noted that the uncertainty remains between an absolute value of ± 7 kPa and ± 2 kPa throughout the nozzle, which is a range of $\pm 0.4\%$ of the recorded local static pressure at the inlet to $\pm 4\%$ of the local static pressure at the outlet, respectively.

The uncertainty in the Mach number differs from the pressure in that the majority of the uncertainty is due to the experimental value. This arises due to the high degree of uncertainty in the spatial resolution of the data set, and challenges optimising a schlieren image over the entire brightness gradient of the nozzle. The details of the experimental uncertainty in the Mach values are explained by Beltrame [9]. The Mach number is also only considered between the throat and the uniform flow region as it is from where experimental data is available. The trend of the absolute Mach number uncertainty is to increase along the nozzle, as the value of Mach number increases, and the change in uncertainty from ± 0.06 to ± 0.11 is proportional to the change in Mach number from 1.25 to 2.1. This proportional uncertainty is consistently $\pm 5\%$ of the local value, which appears much more significant than the static pressure uncertainty. However, the true significance of these uncertainties can not be appreciated until they are examined from an engineering context.

4.3. Engineering Significance of System Response Uncertainties

The relevance of the uncertainty in a DRQ cannot often be appreciated. Therefore, the significance of the uncertainty is better translated into a quantity relevant to engineering analysis, e.g., an ERQ. The engineering significance is determined by interpreting the uncertainty of the pressures and Mach numbers in the simulated nozzle as an uncertainty on the mass flow rate, and uncertainty on entropy generation across a normal shock in the supersonic section of the nozzle. As explained in Sec. 3.1.3 these ERQ are meant to illustrate the effect of the simulation output uncertainty on the design and performance of a turbomachine, or more generally an internal flow device. The magnitude of the ERQ uncertainty, U_{Eng} , will indicate the significance of the validation uncertainty and provide a reference to determine if the validation comparison error calculated in the next chapter is consequential for turbomachinery applications. This section presents the mass flow uncertainty, the process of determining the loss coefficient uncertainty from the DRQ uncertainty, and reports the relationship between non-ideal shock losses and the DRQ. While an uncertainty quantification using Dakota was used to propagate the DRQ uncertainties to the loss coefficient, the mass flow was directly assessed in the initial UQ reported in Sec. 4.2.

4.3.1. Mass Flow Uncertainty

Mass flow rate is a fundamental design parameter which relates the geometry and performance of a turbomachine. For a given velocity triangle of a turbine, the mass flow rate defines the cross sectional area of the flow path. Engineers use the mass flow in the design process for solution verification and geometry design, therefore any uncertainty on the simulated value can impact the design process. Using the relation identified in Sec. 3.1.3 the mass flow was calculated as an output in the CFD analysis when doing the UQ. Mass flow only has one value for the entire simulation, as the mass flow is constant through the nozzle, therefore PR.025-NT001 & PR.027-NT001 are compared to see if the mass flow uncertainty is a function of inlet pressure. The uncertainties of mass flow are summarised in Tab. 4.3.

This uncertainty does not include any uncertainty from the non-uniformity of flow at the throat, which

	\dot{m} / (kg/s)	U_{num} / (kg/s)	U_{in} / (kg/s)	U_d / (kg/s)	U_{val} / (kg/s)	U_{val} %
PR.025-NT001	1.03	± 0.0011	± 0.019	± 0.0031	± 0.0193	± 1.87
PR.027-NT001	0.59245	± 0.000614	± 0.00387	± 0.0007	± 0.00398	± 0.67186

Table 4.3: Mass flow calculated at the throat of a converging-diverging nozzle with Siloxane MM as the working fluid modelled in SU2 using the Peng Robinson EoS.

is explained in Sec. 3.1.3 and proven in App. A. Thus the analysis of mass flow numerical uncertainty only includes the uncertainties of the x-momentum calculated by SU2 at the centreline. The sensitivity of mass flow rate to the uncertain inlet parameters are given in Fig. 4.7. The sensitivities also indicate that the critical values are the only parameters which affect the input uncertainty.

Each percent uncertainty in the mass flow measurement translates to a percent change in the cross sectional area required. This is because the equation is a linear system and to propagate uncertainty through multiplication percent errors for each parameter are added together. For the case of ORC turbomachinery 1% uncertainty will be used as the threshold for significance.

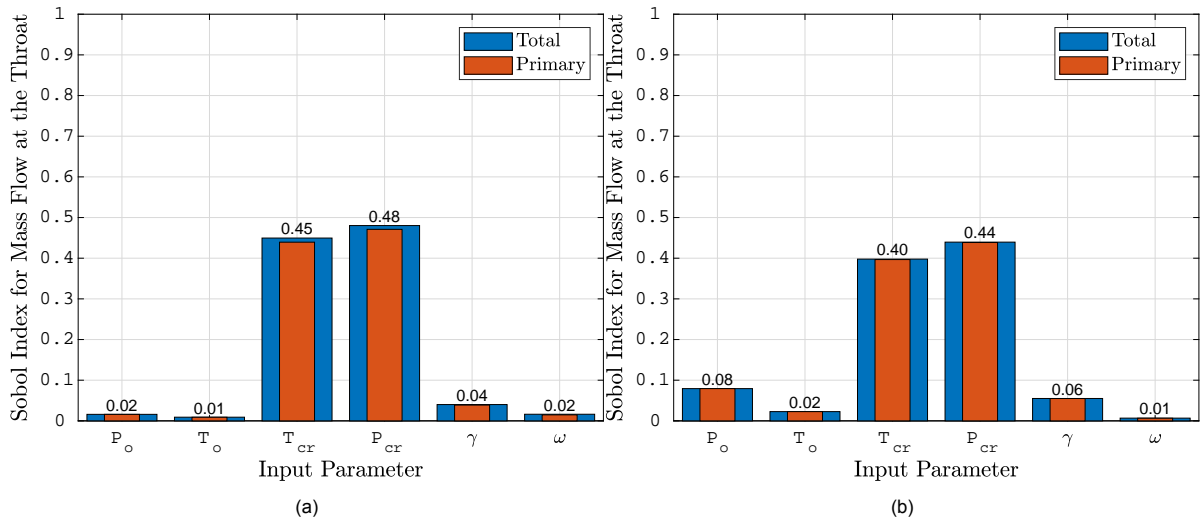


Figure 4.7: Sobol indices representing the relative influence of uncertain input parameters on the mass flow at the throat of a converging-diverging nozzle with Siloxane MM as the working fluid modelled in SU2 using the Peng Robinson EoS. **a)** PR.025-NT001 with an inlet pressure of 18 bar. **b)** PR.027-NT001 with an inlet pressure of 11 bar.

4.3.2. Loss Coefficient Calculation

The second engineering response quantity, entropy rise in the form of a loss coefficient, is a performance metric used by engineers in turbomachinery design. Since the validation test cases treated thus far have no sources of loss, owing to the fact that it is an isentropic expansion, the loss coefficient is calculated as a theoretical loss occurring over a steady normal shock in the nozzle³. For example, take the pressure tap locations in the ORCHID nozzle test section highlighted in Fig. 4.8 superimposed over the Mach contour from PR.025-NT001. The flow conditions from the centreline at each of these loca-

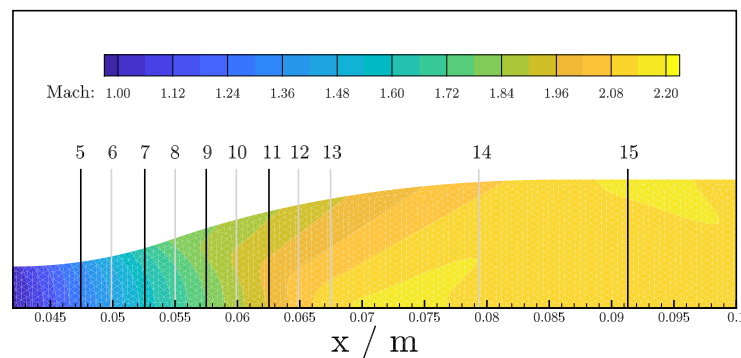


Figure 4.8: Locations of pressure taps along the ORCHID test section nozzle profile superimposed on the contour plot of the Mach number from PR.025-NT.001. Theoretical steady normal shocks are placed at each of the indicated x positions, and the loss across them is calculated using the conditions corresponding to the centreline as the conditions before the shock. Black lines are analysed in detail in Sec. 4.3.4.

tions provides cases representative of physics in a real ORC Turbine. If the back pressure is off-design, for example during start-up or shut-down, there is a theoretical possibility of a shock occurring at any of these points. Since shocks did not occur in the simulation or experiment, the following analysis is an academic exercise to illustrate the capabilities of an ERQ, and the results are meant to indicate the utility of the analysis. As such the theoretical shocks are treated as discontinuities perpendicular to the

³The alternate loss coefficient methods were analysed, including total pressure drop and ideal normal shock loss, but only the steady non-ideal shock is presented as the results are the only ones which have physical meaning.

flow direction with uniform properties across the shock front. This simplification allows the loss coefficient to be calculated using the entropy rise calculated using the centreline flow conditions instead of finding an average entropy rise. The uncertainty calculated for the loss coefficient can be interpreted as the uncertainty of estimated turbine performance parameters optimised using the adjoint solver of SU2.

As seen in Sec. 3.1.3 the loss coefficient can be calculated directly from the DRQ, however, in the case of a non-ideal flow expansion, loss coefficients are not a direct response from the CFD analysis. To evaluate the loss coefficient across a shock at any of the locations indicated in Fig. 4.8 a function was built externally to SU2. For this analysis the inputs to the loss calculator are the SU2 model outputs and the function being analysed is the real gas normal shock solving method from Sec. 2.5 in combination with an entropy calculation using the iPRSV EoS, and non-dimensionalisation using Eqn. 3.2. The output is a series of loss coefficients. The shock solver used is the one developed by Head et al. [35], Iyer [38], the iPRSV EoS is called using RefProp [44], and the codes were linked using a Python script. Figure 4.9 shows the procedure to calculate the loss coefficient in flow chart form.

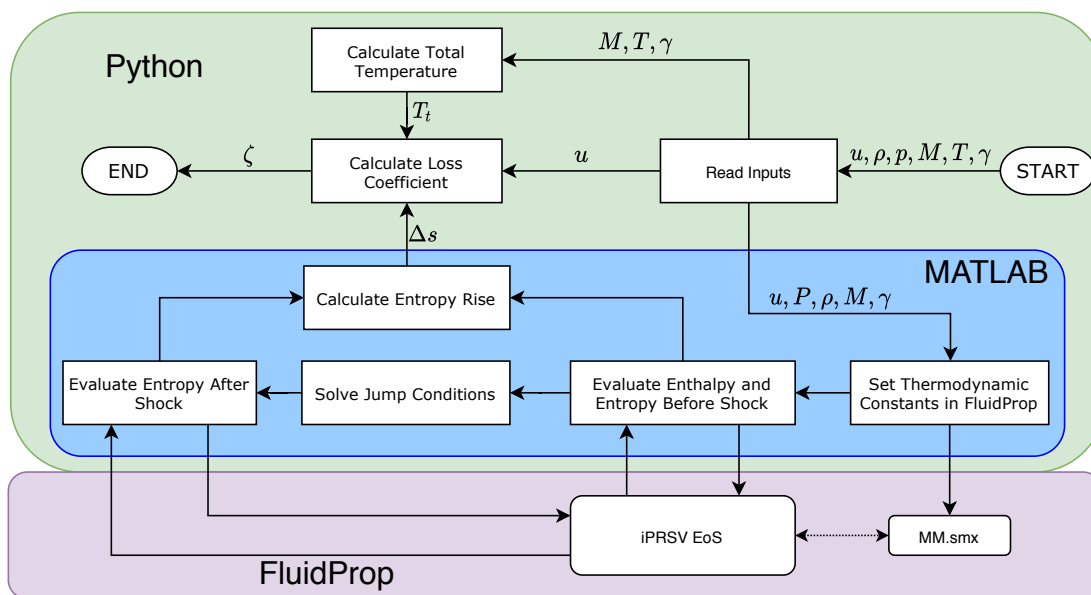


Figure 4.9: Applied framework to evaluate the loss coefficient across a normal shock. The code accepts the conditions before a shock and evaluates the entropy rise across the shock before non-dimensionalising the value.

4.3.3. Loss Coefficient Sensitivity Analysis

To determine the effect of DRQ uncertainty on the output of the loss coefficient calculation another UQ exercise is required. This is done using Dakota [1] linked with the function described in the previous section using a Python script, similar to the UQ described in Sec. 4.1. The loss coefficient is initially calculated using the conditions at the nozzle outlet for PR.025-NT.001. All the inputs are considered uncertain to conduct a sensitivity study and remove variables with negligible influence from the detailed analysis. The uncertain inputs to the loss coefficient calculation are: Mach, static pressure, density, velocity, temperature, ideal specific heat ratio, critical temperature, critical pressure, and the most influential coefficient of the ideal gas specific heat polynomial. The results from the sensitivity study of App. B justify only using the single coefficient. The first six inputs and their uncertainties are taken directly from the output of the UQ done for the PR.025-NT001 model built in SU2 using the iPRSV EoS, and the remaining thermodynamic parameters are taken from Tab. E.1.

Consider position 15 of the nozzle for Case PR.025-NT001, using $P_o = 18.36$ bar and $R = 51.202$ J/kg·K. The inputs to the analysis of the property change across the shock is listed in Tab. 4.4.

Figure 4.10 shows the Sobol indices from the sensitivity study based on the uncertainties of Tab. 4.4. Dominant influence is seen from three flow quantities: pressure, density, and velocity.

Flow Parameter	Mean	Standard Deviation
M	2.0386	0.0146
P/Pa	187884	2113.5
$\rho/(kg/m^3)$	8.0972	0.1563
$U_x/(m/s)$	307.75	3.9160
T/K	477.11	2.3282
γ	1.0353	0.0010
Thermodynamic Parameter	Minimum	Maximum
T_{cr}/K	511.3	526.1
P_{cr}/bar	18.42	20.36
η_2	0.7108	0.7548

Table 4.4: Input uncertainties used to calculate the loss coefficient due to entropy rise across an imaginary shock located at the outlet of a converging-diverging nozzle with Siloxane MM as the working fluid. The first six uncertainty distributions for flow parameters are normal, the remaining thermodynamic parameters have uniform uncertainties.

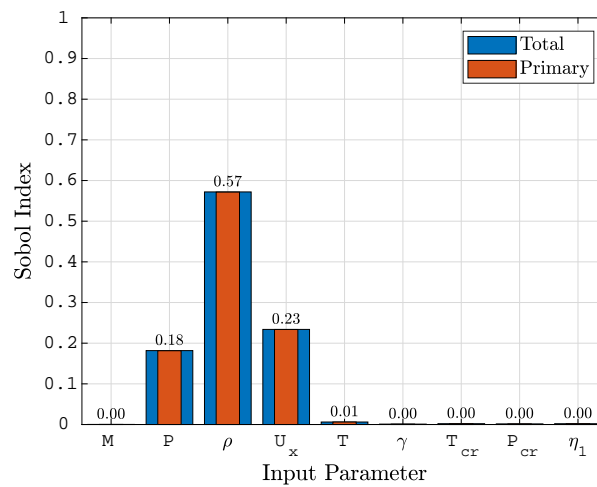


Figure 4.10: Sobol indices representing the relative influence of uncertain input parameters on the loss coefficient calculated across a non-ideal steady normal shock with Siloxane MM as the working fluid using an iterative shock solving method and the iPRSV EoS. The sensitivities are calculated for a shock occurring with inlet conditions of Mach 2, pressure at 1.9 bar and temperature of 477 K.

From the full nine parameter study it can be seen that the thermodynamic model has no significant effect on the numerical procedure used to solve the jump conditions over a steady normal shock wave in a non-ideal gas. For this case all uncertainty in the final loss coefficient arises from the pressure, density, and velocity of the flow before the location of a theoretical shock. Therefore the thermodynamic model is considered exact with no uncertainty, along with the ratio of specific heats, for the remaining detailed analysis. This leaves five parameters, $ERQ = f(M, P, \rho, U_x, T)$. The Mach number is included since it is a measured DRQ in this thesis, and the temperature is included because it had an effect on the loss coefficient, although minimal, and the computational power was available to run multiple UQ with five input parameters.

4.3.4. Loss Coefficient Uncertainty

As seen in the previous section the entropy rise across a normal shock is a function of Mach number, static pressure, density, velocity, and temperature, all direct outputs from an SU2 model. Therefore the uncertainty of that entropy rise must be a function of the same parameters. Rising entropy in a process, which can be represented by a non-dimensional variable such as the loss coefficient, is an indication of increased randomness in a flow, which is a good indicator of machine performance. To create an entropy rise from the ORCHID nozzle flow, and thus a loss coefficient, an imaginary steady shock can

be placed anywhere in the nozzle and the theoretical performance metric can be used to determine the significance of the error or uncertainty in an SU2 model.

The UQ study described in the previous subsection was repeated over a range of conditions, but using the five input variables. The twelve positions in the nozzle illustrated in Fig. 4.8 were examined to consider the effect different flow conditions would have on the uncertainty propagation. Figure 4.11 displays the result of the study using the uncertainty values produced in the UQ study of the ORCHID nozzle from Sec. 4.2 as the inputs.

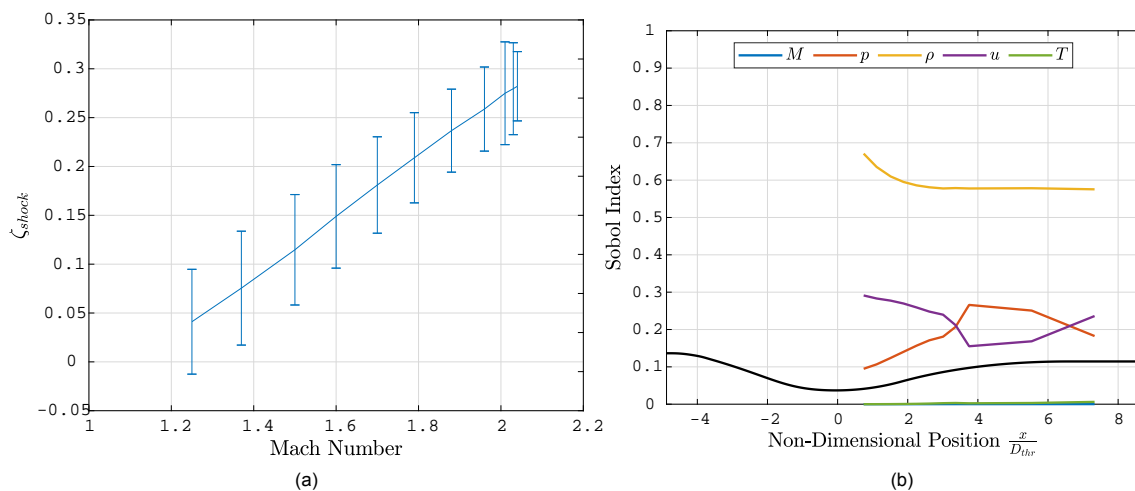


Figure 4.11: Loss Coefficient across a non-ideal normal shock located in different positions of a converging-diverging nozzle with Siloxane MM as the working fluid. **a)** The loss coefficient value and expanded uncertainty as a function of the Mach number before the shock. **b)** Variation of Sobol indices representing the relative influence of uncertain input parameters on the loss coefficient uncertainty. The nozzle is superimposed for reference.

As can be expected the losses are higher across a shock at higher Mach number. Additionally the sensitivity should be higher in the non-ideal region. This is confirmed in Fig. 4.11a where a subtle increase in the uncertainty bands is noted as the Mach number decreases. At Mach 1.25, close to the throat and within the kernel region, the uncertainty on the loss coefficient is 0.0537. At the outlet of the nozzle in the uniform flow region where the Mach number is 2.04 the loss coefficient uncertainty is 0.0355. There is an exception to the trend when Mach is equal to two, however this coincides with the end of the kernel region where the uncertainty values are higher due to the discretization. Using the Sobol indices from Fig. 4.11b we see that for the iterative shock solving procedure the density uncertainty is very important in the loss approximation across shocks. This is consistent with the standard deviations of all the variables put into the analysis. The standard deviation of density is 1.93% compared to the 0.72% and 1.12% of Mach and Pressure, respectively.

The absolute value of the loss coefficients provide a sanity check for the implementation of the analysis, however the objective is to assess the variation in uncertainties.

4.3.5. DRQ to ERQ Uncertainty Maps

To assess the effect of Mach number and static pressure uncertainties on the performance metrics of turbomachinery the UQ can be repeated again, but with only one input parameter considered uncertain. The loss coefficients produced in these cases will have uncertainty bands exclusively from the variation in the Mach number or the static pressure, based on which parameter was considered uncertain. A UQ study was done at five Locations, indicated by the black lines in Fig. 4.8 and the single variable input study was repeated at each of those positions for different magnitudes of input uncertainties. This allowed for a map of DRQ uncertainty to ERQ uncertainty to be developed. For example, take the top line of Fig. 4.12c. The flow conditions at the centreline of the ORCHID nozzle test section in line with pressure tap fifteen were taken as the reference values, meaning a Mach number of 2.04. An uncertainty quantification assessment on the loss coefficient was done with all inputs constant, except for the Mach number which was given an uncertainty of 1%. The response was a loss uncertainty of 0.0004. The study was repeated but with an uncertainty of 2% on the Mach input. The corresponding

loss uncertainty was 0.0008. This was repeated for different Mach number uncertainties until the linear relation was mapped. This procedure was repeated for a different location corresponding to the Mach number of 1.88 to produce the second line in red. Overall five positions were considered and the procedure was done for Mach and static pressure, resulting in the plots of Fig. 4.12. These maps can be used to interpret the DRQ uncertainty in the context of the engineering parameter.

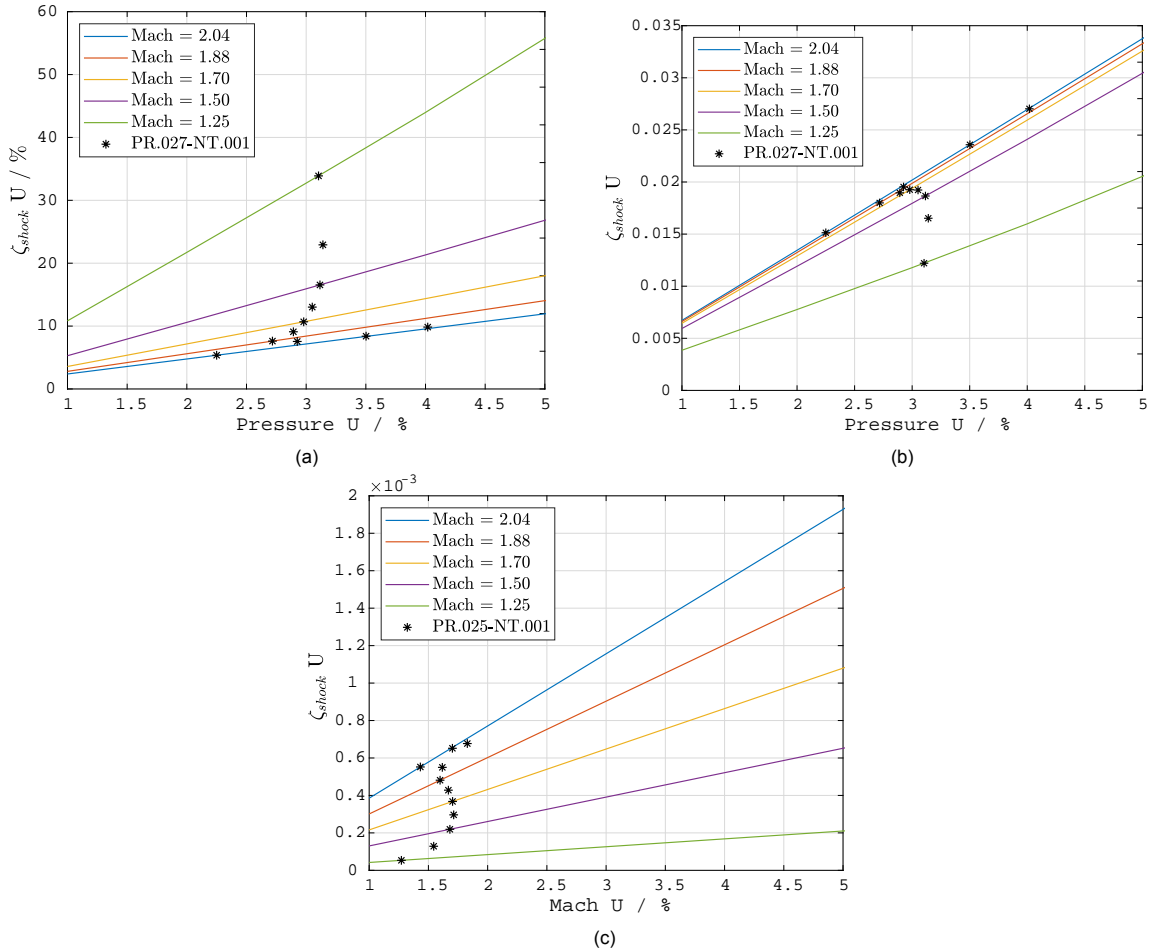


Figure 4.12: Relation of a flow parameter uncertainty to the loss coefficient uncertainty calculated across a non-ideal steady normal shock located in a converging-diverging nozzle with Siloxane MM as the working fluid. The shock is calculated using an iterative numerical procedure summarised in section 2.5, and using the iPRSV EoS. The flow conditions from the SU2 model of the ORCHID nozzle are presented with black stars. **a)** Map of pressure uncertainty to loss coefficient uncertainty. PR.027-NT001 results are superimposed as black stars. **b)** The same as a), but in absolute uncertainty instead of percent. **c)** Map of Mach uncertainty to loss coefficient uncertainty. PR.025-NT001 results are superimposed as black stars.

Figure 4.12 presents the uncertainty of the loss coefficient as a function of the DRQ uncertainties. Figure 4.12a and Fig. 4.12c are produced using the UQ procedure described at the beginning of this subsection, first with only the pressure input uncertain, and second the Mach number input uncertain. Once the lines were built, the flow conditions and uncertainties given by the ORCHID nozzle analysis could be plotted as points superimposed on the constructed map. In these plots the uncertainty of the loss coefficient is only due to the single DRQ variations.

These plots confirm what was always assumed, that increasing the uncertainty of the DRQ increases the uncertainty of performance metrics. The plots however provide a relation which can be used to quantify the uncertainty of an SU2 result in an engineering context. For a given absolute Mach number (could also be a set γ_{pv}), represented by a line, these plots map DRQ uncertainty to ERQ uncertainty. For example, if the pressure uncertainty is $\pm 4.5\%$ at Mach 1.25 in the SU2 solution of MM, then if you were to calculate a steady normal shock at that point the uncertainty of the loss coefficient would be at least $\pm 50\%$. It could be higher because this study is done with only the pressure being uncertain. If

the uncertainty of density and velocity were included then the uncertainty would be higher. The trends from Fig. 4.12a show that at higher Mach numbers the uncertainty of pressure reduces in significance, but Fig. 4.12c shows the uncertainty of the Mach number increases in significance at higher absolute Mach numbers. The SU2 results from the ORCHID nozzle test section simulations are superimposed using only the simulation uncertainty, which is what is important in this context since the simulation is what is used for design optimisation.

From the perspective of a turbomachinery designer, uncertainty of ± 0.01 on the loss coefficient could matter for optimising designs, any coarse resolution may not allow the true optimum to be identified. For performance analysis applications an uncertainty of ± 0.1 may be significant for estimating losses. These numbers are subjective and will vary from engineer to engineer, and with the maps available any engineer can define their own value for their given purposes. However, for the purposes of this analysis, values of loss coefficient uncertainty below ± 0.01 will be considered negligible.

When looking at the results from the DRQ UQ, seen as black stars, we see that the pressure uncertainty is always significant for this method of calculating entropy. The trend of Mach uncertainty is however less important due to the value of loss coefficient uncertainty never going above ± 0.002 . In a turbomachinery context this is not significant and flows above Mach 2, where the highest uncertainty exists, are not expected in ORC applications. Therefore the pressure uncertainty is not acceptable if the pressure needs to be used for further analysis, but the Mach uncertainty is fine.

This result is critical if the results from SU2 are ever to be used to further predict performance of a flow feature using the Grossman method. If an alternate method is used, or the shock is solved within the SU2 flow solver itself, then the maps of Fig. 4.12 are not relevant. Despite the narrow applicability of this analysis, the maps gives context to the DRQ results when no other context is available. This was an academic exercise, and could be improved in future validation campaigns if real loss metrics can be calculated instead of using a theoretical loss mechanism. The analysis could also be improved by using a direct relation instead of an iterative method. However this is a reasonable analysis to conduct, showing that the uncertainty of SU2 can not be ignored.

4.4. Discussion on SU2 uncertainty quantification

The outcome from the uncertainty quantification activities executed on the SU2 flow solver are discussed in this section. A review of the implemented methodology and sources of improvement are provided, followed by a review of using the methodology to assess the selected DRQ. The uncertainties and sensitivities associated with the ORCHID nozzle test section modelled in SU2 will be examined, and finally the results of the attempt to establish an engineering significance metric are evaluated.

4.4.1. Tools and Methods

Overall the methodology implemented is effective and can be used for the future studies of NICFD with SU2. The code infrastructure implements an SC forward propagated input uncertainty quantification, and uses the Richardson extrapolation for determining numerical uncertainties. In future cases the iteration and truncation errors of a simulation from SU2 should be negligible, as they were in this case, so the infrastructure can be used. The code requires the unstructured mesh to be manually created, and for a set of reference simulations be conducted prior to using the coded tools. For example the first order solution of the SU2 run using the mean inputs must be established in order for the simulations done in the UQ loop to be completed rapidly. The code attempts to restart from a reference solution on every iteration. There are ways to adapt the code and create a more robust infrastructure which would reduce the need for manual configuration at the beginning of the process, however due to the potential variety of future SU2 models which must have quantified uncertainty the depth of code which would need to be created is beyond the scope of a single research project. As such, any future user of the code will need a basic understanding of SC, Richardson extrapolation, SU2, Matlab, and Python to effectively use the procedure.

Using a third order Stochastic Collocation was an effective choice for this study, even for situations where the number of inputs rise above the seven or eight. With each additional input which must be assessed the sparse grid sampling algorithm took exponentially more samples. At the threshold of nine samples the number of evaluations required to create the surrogate model approached on the number of evaluations used by a Latin hypercube sampling method, however the Latin hypercube samples only produce statistical moments, not the sobol indices. SC combines the statistical analysis of the LHS and

VBD modules within Dakota, and produced accurate results. It is recommended to maintain using the third order SC approach for all further assessments of SU2.

The ReFresco software for determining the numerical software is also straight forward to implement with the established code, so should be continued to be used in further uncertainty assessments. The code is robust enough such that even when the number of elements in a mesh do not exactly double on each iteration an uncertainty can still be calculated. The fundamental theory for determining the numerical uncertainty of one grid is based on having a consistent increase in the grid size, but it is not trivial to control the exact number of cells in a mesh with standard mesh generation tools, especially in an unstructured context. The Matlab code automatically constructs the necessary input files, runs the executable, and extracts the output numerical uncertainty given the set of results manually simulated on each grid size of interest. The process of determining the exact numerical uncertainty can thus be done in no more than a couple of minutes longer than the SU2 simulations take to run independently. One potential flaw is that the code assumes a uniform cell size, so if there is a future study done with refined cell size at locations of interest the one evaluating the numerical uncertainty of the grid will need to include an additional step of accounting for the variation of cell size in the mesh. This may include in the simplest process establishing the uncertainty due to different mesh sizes and then using the uncertainty at each location of interest taken from the same location on a uniform mesh at that level of discretisation.

4.4.2. Magnitude and Sensitivity

The results from the uncertainty study of SU2 simulations provided uncertainties on the same order of magnitude as the experimental uncertainties for the given DRQ. This makes sense as the simulation uncertainty is a direct function of the experimental uncertainties, in addition to the thermodynamic uncertainties. Any additional uncertainty on the simulation value is due to the uncertainty of the thermodynamic constants or the numerical discretisation. The discretisation could be removed by refining the mesh even further than was done, but as was introduced in Sec. 2.6 and will be seen in Chap. 5 having a simulation uncertainty slightly larger than the experimental uncertainty is optimal for validation studies. This raises the unique characteristics of simulations done for validation that the target level of uncertainty is not zero, but rather the target value is the same as the experimental value. If the experimental uncertainty is reduced then the simulation uncertainty can be reduced, but there is no reason to lower the simulation uncertainty below that of the experimental value. The increase in computational cost would actually reduce the confidence on the validation. It must be understood that validation is focused on a model capturing behaviour observed in real physical situations, therefore a simulation with no uncertainty can never be considered valid. The zero uncertainty simulation may have benefits in a purely theoretical standpoint, but for engineering this is not necessary and could be considered irresponsible. This is why the concept of an engineering metric is introduced for the validation study, the engineer is the one most likely to need an accurate uncertainty value and need an understanding of the uncertainty levels. A theoretical physicist, or a software developer may be satisfied with a direct system response, but the engineering context is what allows a software to be used for real world applications.

In the specific case of the uncertainties associated with a NICFD supersonic flow with no viscous effects or external heat transfer, it can be interpreted from the results that the thermodynamic model will have an impact on the uncertainty and can not be neglected. In these flow cases it appears that the critical point of the fluid is the cause of simulation uncertainty, which is likely due to the critical point being a fundamental characteristic of a compound. As experiments are done to reduce the uncertainty of the critical point values the uncertainty of cubic equations of state will reduce. There is then an argument to neglect the uncertainty from all other thermodynamic properties, such as the acentric factor or the κ and η constants used in the thermodynamic sub-models. For performance analysis this can be done, as the uncertainty may change less than 10% and in industry this can be accounted for by the safety factor added to important calculations. However for the level of rigour required for a full validation campaign the thermodynamic properties should be included. For example in the Peng-Robinson equation of state the ideal gas polytropic exponent does have an influence on the DRQ uncertainty despite having much lower influence than the critical values. The boundary conditions also have a much lower influence than the critical values, except for when evaluating the same properties in the flow field. The pressure at the boundary of the control volume will have an influence on the pressure through the flow. Therefore the boundary conditions should always be included. One exception is the back pressure for a converging-

diverging nozzle, as the physics of the situation will remain constant through the throat and initial region of the diverging portion of the nozzle independent of the back pressure. Any major deviation in back pressure from the design value could result in a shock within the nozzle, but small fluctuations have no impact until the outlet of the nozzle, which is not the area of interest for this study. The use of a property in the uncertainty quantification as always falls on the final decision of the engineer conducting the assessment, but for future validation campaigns of SU2 models using the iPRSV EoS in NICFD applications seven parameters are recommended to be considered uncertain: $T_{cr}, P_{cr}, T_o, P_o, \eta_0, \eta_1, \eta_2$.

Special attention should be directed towards the uncertainty values in the kernel region of nozzle flow. The uncertainty changes from the throat until the end of the kernel indicating that the flow in this region is complex and sensitive to changes.

4.4.3. System Responses

Using the static pressure and the Mach number of a nozzle flow appear to be complimentary system response which provided different information on the flow but a related enough to provide an assessment of the flow features. In future cases having additional properties assessed may be useful, but the minimum responses of static pressure and Mach have given useful observations. The different levels of accuracy which can be obtained from each parameter is interesting and supports the argument that only having one response quantity to validate against could provide a skewed result on validation. In NICFD flow the state variables pressure, temperature, and density are representative of the thermodynamic behaviour and should be assessed in combination with a variable representative of compressibility such as expansion waves or shock waves. In this case the expansion wave uncertainty assessment was done, and is provided in App. D, but the Mach number is a direct function of the expansion wave angle so the two can be interchanged.

Whichever parameters are selected to analyse, the significance of the uncertainties should be interpreted in an engineering context. Using a simulated shock wave may not always be suitable, or relevant, but the exercise is important to carry out nonetheless. The exact process of calculating the engineering metric can be improved based on the case of validation, where a true value of performance is better than a theoretical loss. Using a standard metric across different validation studies of SU2 may be a benefit in order to compare results. It is recommended to stay in the field of turbomachinery when deciding on an engineering response to use as the metric of context. The generation of maps similar to those in Fig. 4.12 can be done independently of a validation study, such that engineers could interpret previous and future validation cases which do not have an engineering context for their own purposes. An engineer always does the interpretation of significance using their personal experience and judgement, however having a standard translation allows the process to be done quicker and with more confidence. Work needs to be done to determine the most relevant and versatile ERQ, which may be the loss coefficient, that can be assessed as a function of the different direct system responses of SU2 and provides context in the turbomachinery field. The numerical method used is an iterative method which assumes Euler relations, so is not globally applicable, but the resultant map is an excellent example of the target analysis which should be done in parallel with validation activities. The maps will be used in the assessment of the validation metrics constructed for the static pressure and Mach number calculated with the SU2 flow solver.

5

Validation of SU2 for NICFD Simulations

To assess the predictive capability of a CFD flow solver, such as SU2, the results of a simulation must be compared to experimental data with complete uncertainty bands included. As discussed in Chap. 3, the first step of the validation study is to devise and run an experiment. This is an iterative process which requires preliminary simulations and trial experiments. Once the final experiment is conducted, one must record the experimental conditions, identify and categorise all the experimental uncertainties, and construct the model definition for the flow solver. Once measurements are acquired the experimental data must be processed and the uncertainty quantified. The simulation uncertainties are quantified with a grid convergence study and an uncertainty analysis. Finally, the quantities of interest are recorded and the validation metrics are calculated using the recorded uncertainty values and mean results. The metrics provide a clear indication of the model accuracy and precision compared to true physics, i.e., the measured quantities.

This chapter presents a validation through the use of industrially accepted validation metrics for the model definition and DRQ presented in Chap 3. A description of the selected validation metrics is given first, then the values are computed for the Mach number along the nozzle centreline and the static pressure along the nozzle surface. The test cases considered provide a first assessment of the predictive capabilities of the SU2 flow solver, and in future test cases the metrics can be used to further ensure the software is able to predict correctly the flow physics over a larger range of operating conditions characterised by NICFD. Statistical indicators used to discern a practical threshold for code validation in the field of NICFD is introduced for the first time in this work.

5.1. Engineering Uncertainty Threshold

There are two industrially accepted metrics which are used to evaluate the accuracy of a numerical model, given context by the engineering response function introduced in Sec. 3.1.3. The validation metrics are ASME V&V 20 and the Real Space method which are introduced in Sec. 2.6.

Critics of the established metrics point out that using a binary interpretation of the validation data, i.e. being valid or invalid, buries important information regarding the sources of uncertainty and provides an oversimplification of the analysis. Beltrame [9] has suggested the use of a numerical metric ranging from zero to one associated with the accuracy of a simulation based on a Gaussian function. The metric defines zero as completely invalid with 1 being perfectly valid, and the continuous scale an indication of the level of simulation accuracy. He then defines an accuracy threshold, however the threshold is still an indication of where the uncertainty and error of the accuracy assessment overlap. Another proposal by Hills [36] suggests a metric using a weighted r^2 norm with a mathematically defined threshold. The advantage of this is the ability to be applied to multivariate, correlated data, but again does not establish the threshold of validity in an engineering context. The limitation for these metrics is they do not provide any context for the magnitude of error and uncertainty for engineering applications, they define validity in a purely mathematical form.

To interpret the metrics calculated using the ASME V&V 20 and Real Space methods in an engineering context, the engineering response quantities (ERQ) can be used. Instead of a purely scientific

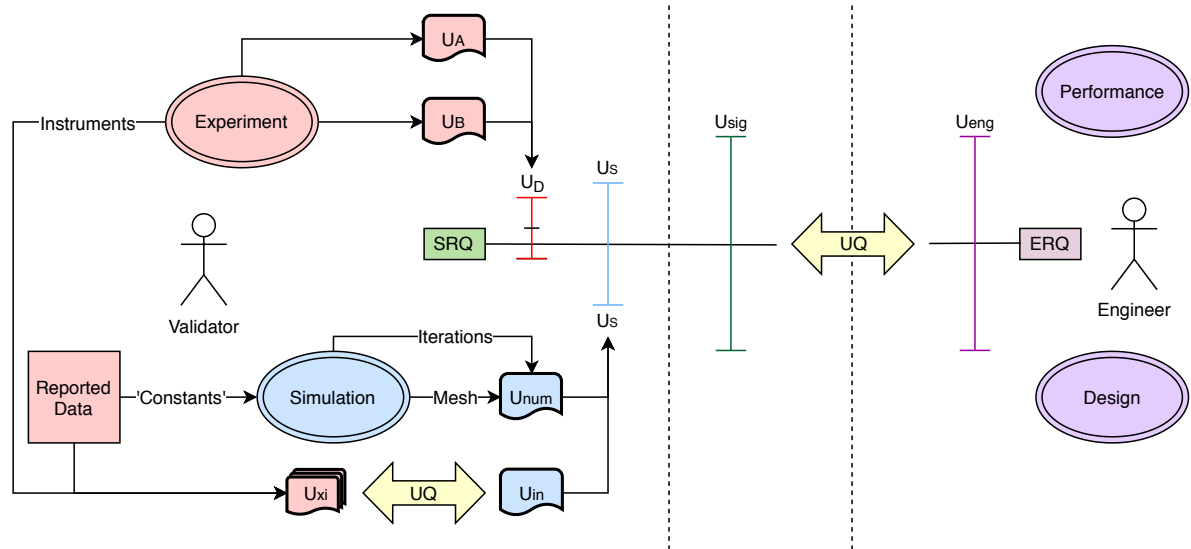


Figure 5.1: Validation uncertainty diagram. The sources of uncertainty in a validation campaign are identified and related to the forms of uncertainty relevant to validation metrics. The experimental sources of uncertainty are coloured in red while the simulations sources of uncertainty are highlighted in blue. The diagram illustrates the focus of the validator in producing the uncertainty bands and comparing the results of simulation and experiment for a given system response quantity, while the focus of an engineer is to determine the value of a design or performance metric, called ERQ, to a given level of accuracy. The ERQ uncertainty can be converted to an SRQ uncertainty using a UQ, thus defining an upper limit of precision called U_{sig} .

interpretation of validation, a reference value which defines the performance or design of an engineering system can allow engineers to determine if the model is adequate for their purposes.

Looking at Fig. 5.1 recall that U_{num} , a function of the grid, iterations, and truncation error in CFD, is the uncertainty which can be easily controlled. Relaxing the numerical criteria, e.g., the mesh size and convergence criteria, expands the uncertainty bands of the simulation and theoretically speeds up the computation. Now consider that the experimental uncertainty of an SRQ is a value set by the quality of the equipment, illustrated in Fig. 5.1 as the red uncertainty bar. In an target case the experimental uncertainty should be small and bounded by the simulation uncertainty, illustrated in Fig. 5.1 as the blue uncertainty bar. The optimal relation between them is therefore $0 < U_D \leq U_S$.

Recalling that $U_S = U_{num} + U_{in}$ there is then a logical problem. If the quality of the validation reduces when the simulation uncertainty becomes smaller than the experimental uncertainty, and by increasing the numerical uncertainty the simulation becomes faster, then the conclusion must be to sacrifice all numerical accuracy (within the mesh, iterations, and truncation) for the fastest valid simulation. This is obviously not feasible and results in a simulation where the SRQ are valid, but have huge uncertainty bands. There must therefore be an upper limit to the magnitude of a simulation uncertainty band which, when used, allows for useful simulations to be conducted. A globally defined uncertainty limit to achieve useful simulations does not exist, but rather the uncertainty limits for a useful simulation can be developed for the particular case under validation, based in an engineering understanding of the physics. What is reasonable depends on the situation, and different engineers will take different views of the same situation, therefore the only solution is to use the Engineering Response Quantity defined in Sec. 3.1.3 for creating this upper uncertainty threshold.

Each ERQ will have an engineering accepted uncertainty, U_{Eng} , defined as the uncertainty which is related to a significant effect on an engineering design or analysis. The ERQ selection is dependent on the situation, and the threshold of U_{Eng} is case dependent as well. Thus the ERQ and U_{Eng} value must be selected during each validation campaign before final metrics can be constructed.

If an ERQ is related it to a DRQ, as done is Sec. 4.3.5, then the U_{Eng} of the ERQ can be backward propagated to the DRQ to define a significant uncertainty, U_{Sig} , for that DRQ. U_{Sig} defines an upper bound to the uncertainty on the simulation output which would have an impact on the engineering design or performance of the system. This becomes the absolute upper bound of U_S to be used in the validation. If U_S is below U_{Sig} , then the software can be validated using the ASME or real space

methods. If not, then the ASME and real space methods are not to be trusted and the experiment or flow solver must be improved before a case can be validated. A summary of the relationship between all the sources of uncertainty and the proposed engineering uncertainty of the ERQ is presented in Fig. 5.1. If there is no engineering application which can be used to define the thresholds on U_{Sig} , and thus U_S , the simulation uncertainty is instead forward propagated to produce an engineering uncertainty.

The final U_{Eng} values in this report, calculated using a UQ framework, present the best possible accuracy of the SU2 flow solver for predicting the loss coefficient in a 2D organic fluid expansion. Users of the software can independently determine if this level of accuracy is adequate for their purposes.

5.2. Results of DRQ Validation

Upon completion of the SU2 model analysis from Sec. 4.2, and the mapping of the DRQ to ERQ from Sec. 4.3.5, the validation metrics can be constructed using the data from Head [34]. Validation metrics are calculated for three variables, measured over test cases described in Chap. 3. The variables are the Mach number along the centreline of PR.025-NT.001, the pressure along the nozzle profile of PR.027-NT.001, and the mass flow from both experimental runs. As described in Sec. 5.1 the DRQ means and standard deviations from the UQ are combined with the DRQ numerical uncertainties, experimental means and experimental standard deviations to produce the validation metrics. The comparison error is calculated with Eqn. 2.32, and the validation uncertainty is calculated with Eqn. 2.33.

This is done as a function of nozzle position, and as a function of the polytropic exponent γ_{pv} . γ_{pv} will be the only measure of non-ideal behaviour used as it has a clear physical meaning for internal flows and turbomachinery, and is an excellent metric of non-ideal behaviour directly connected to the fundamental derivative of gas dynamics. The value of γ_{pv} is directly calculated using

$$\gamma_{pv} = \frac{\rho u^2}{pM^2}, \quad (5.1)$$

which is derived by Tosto et al. [64]. The uncertainty of γ_{pv} is calculated by the UQ in Sec. 4.2. Figure D.6 in the appendices contains the results of the γ_{pv} UQ for PR.025-NT001 along the centreline, and Fig. D.9 contains the results of the γ_{pv} UQ for PR.027-NT001 along the nozzle profile.

The experimental value of γ_{pv} is taken through an interpolation process. The simulation DRQ values have a related nozzle position and value of γ_{pv} , thus the simulation data is used to map each nozzle position to a related γ_{pv} . This mapping can be used to plot the experimental DRQ values, which have a position, on the γ_{pv} axis. The experimental γ_{pv} uncertainty is then the maximum position value mapped to γ_{pv} and the minimum position value mapped to γ_{pv} .

The threshold of significant uncertainty for giving an engineering context to these results is extracted from Fig. 4.12 assuming that an uncertainty of more than 0.01 on the loss coefficient from a normal shock is not negligible is a design optimisation context.

5.2.1. Test Case PR.027-NT.001

Figure 5.2 shows the static pressure along the surface of the ORCHID nozzle test section compared against the SU2 model simulation results. There are fifteen pressure taps, three of which are redundant, i.e. there are duplicate measurements at the inlet, throat, and exit. Thus the validation assessment is conducted at twelve locations across the nozzle.

Figure 5.2a is an absolute comparison of the model and the experiment. The mean results from the simulation are plotted, along with the simulation uncertainty bars, then the experimental values are plotted with the experimental uncertainty. Figure 5.2b is a representation of the real space metric, where all the errors and uncertainties are taken with respect to the mean pressure distribution obtained from the simulation. The difference between the experiment and the simulation is what is plotted, with the uncertainty bars for every value remaining the same. Figure 5.2c plots the full scale pressure measurements as a function of the polytropic exponent γ_{pv} . Figure 5.2d is finally the plot of comparison error and validation uncertainty to represent the ASME metric.

The plots show that the kernel region of the flow, from the throat until 0.055 m into the nozzle, has a large comparison error. The rate of change of pressure is lower in the simulation than in the experiment which manifests as a maximum error of 112 kPa at 0.0499 m. The inlet and outlet static pressures from the flow solver have the same order of magnitude as the experiments, with comparison errors of less than 10 kPa.

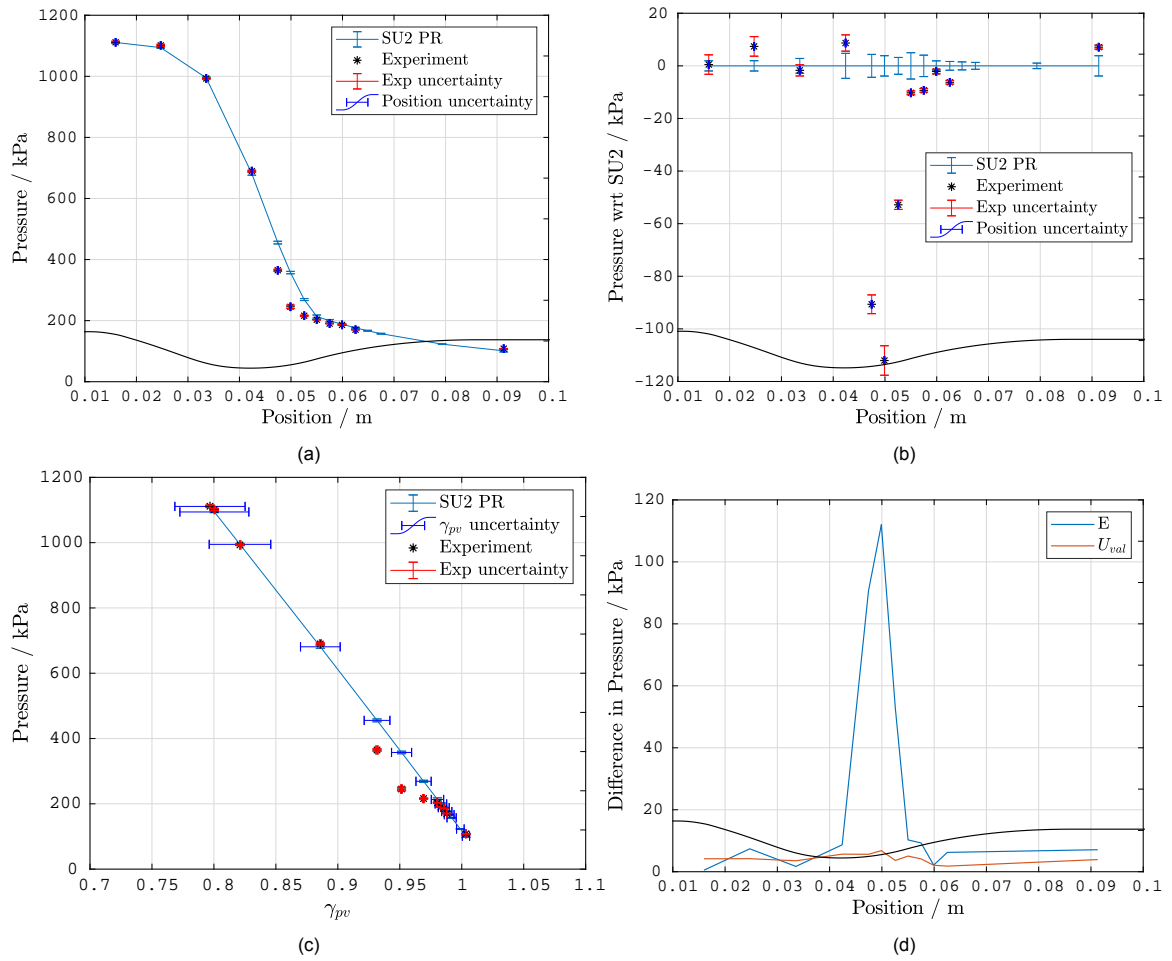


Figure 5.2: Validation plots of static pressure for a converging-diverging nozzle modelled in SU2 using the compressible Euler equations and the Peng-Robinson EoS. The test case is described in Sec. 3.2 and the model definition summarised in Sec 3.3. The mean simulation results along the nozzle surface are compared against the mean ORCHID PR.027-NT.001 pressure tap data. **a)** Absolute static pressure as a function of nozzle position. **b)** Absolute static pressure with respect to the SU2 model mean simulation value as a function of nozzle location. This is a version of the real space metric. **c)** Absolute static pressure as a function of polytropic exponent γ_{pv} . **d)** ASME V&V 20 validation metric plot of absolute static pressure as a function of nozzle position.

The regions of validity, where the modelling error is less than the uncertainty, only includes the inlet of the nozzle and one point of the diverging section. These are the static pressures at locations $x=0.01596$ m, $x=0.03355$ m, and $x = 0.05991$ m. In the geometric frame of reference the relation between the comparison error and validation uncertainty of the static pressure along the nozzle profile is close to valid conditions at the inlet and outlet, but the metrics indicate the model could still be improved.

To interpret these results in an engineering context the analysis from Sec. 4.3 is used. The absolute uncertainty of loss coefficient which is acceptable was set at 0.01, which translates to a U_{sig} of between 1.5% and 3% for static pressure based on Fig. 4.12b. This implied that the static pressure simulation uncertainty must stay below 3% so not to influence the calculation of engineering performance metrics. Since the validation uncertainty is above 3% in most positions, the uncertainty of the SU2 flow solver will negatively impact the design process, although it is the same order of magnitude as the target uncertainty level, 1.5%. One interpretation of this result is that the non valid regions are not reliable for design or performance calculations, while the validated regions may provide useful design insights on pressure distribution, although the level of uncertainty is relevant and can not be ignored.

The invalidity appears to be related to the nozzle profile, and not a function of the non-ideal thermodynamics. In figure 5.2c the simulation and experimental data can be seen to be consistent with

each other at values of γ_{pv} below 0.9, and values above 0.975. The only section of non-validation, between γ_{pv} of 0.9 and 0.975, has data points extracted from within the kernel region of the nozzle. It should be noted that in the γ_{pv} domain all the data points outside the kernel region are valid, while in the geometric domain only a subset of those same data points are valid. For example, the static pressure at $x=0.02472$ m is not valid in the geometric domain according to Fig. 5.2b, but that same point corresponds to a $\gamma_{pv}=0.8$ which is valid according to Fig. 5.2c. This indicates that geometric position in a nozzle flow is not the same as thermodynamic position in a flow. The differences need to be further investigated, but the similarities between the two domains is what should be given focus.

To explain the discrepancy there is either a problem with the experimental set up, resulting in lower pressure being recorded on the pressure taps, or the SU2 flow solver is unable to capture the rates of pressure change in the kernel region of an expansion. There is potential the pressure taps were offset from being perpendicular to the flow and a suction effect from the high velocity fluid lowered the recorded pressure. The pressure taps not being level with the nozzle surface may be due to the vibration in the experimental runs, or overtightening of the nozzle, however this conclusion can not be made with only one set of data. The experiments will need to be run again with further SU2 simulations to establish the cause of the region of large error.

5.2.2. Test Case PR.025-NT.001

The Mach number along the centreline of the ORCHID nozzle test section is compared against the SU2 model simulation results in figure 5.3. There are thirty measurement locations, thus the validation assessment is conducted at thirty locations across the nozzle. Validation results comparing the expansion wave angle are given in App. D along with a second data set of Mach number from the same process run, PR.0.25-NT.002.

Figure 5.3a is an absolute comparison of the model and the experiment. The mean results from the simulation are plotted, along with the simulation uncertainty bars, then the experimental values are plotted with the experimental uncertainty. Figure 5.3b is a representation of the real space metric, where all the errors and uncertainties are taken with respect to the mean Mach number distribution obtained from the simulation. The difference between the experiment and the simulation is what is plotted, with the uncertainty bars for every value remaining the same. Figure 5.3c plots the full scale Mach number measurements as a function of the polytropic exponent γ_{pv} . Figure 5.3d is finally the plot of comparison error and validation uncertainty to represent the ASME metric.

The plots show that the maximum comparison error is 0.111 Mach at $x=2.04$ in the non-dimensional domain. Similarly to the static pressure analysis, the maximum error is in the kernel region of the flow. However, instead of the error reducing in the uniform flow region, as seen with the static pressures, the comparison error indicates a relatively consistent shift in the experimental Mach number from the simulation of approximately 0.06 Mach.

The ASME V&V metric indicates a valid simulation at all points except for six data points in the kernel region of the flow: $X=2.04$, $X=2.226$, $X=2.5959$, $X=2.9795$, $X=3.17$, and $X=3.99$. The results in the geometric and γ_{pv} domain, Figs. 5.3b and 5.3c, show that the Mach number near the throat and in the uniform flow region have high levels of accuracy. The experimental uncertainty is however larger than the simulation uncertainty by a factor of up to three, indicating that the validation does not meet the zero order threshold defined by Romero [54]. This corresponds to when the simulation uncertainty is larger than the experimental uncertainty, and all possible physical realities are contained within the simulation uncertainty band.

The analysis from Sec. 4.3 is then used to put context on these results. The absolute uncertainty of loss coefficient which is acceptable was set at 0.01, which is an order of magnitude lower than the highest loss coefficient uncertainty recorded as a function of Mach uncertainty in Fig 4.12c. This indicates that the uncertainty on the Mach number from the flow solver is negligible in an engineering context. Therefore, validated regions of flow for Mach number prediction are very trustworthy, and the non-valid regions are also adequate for design purposes as long as the uncertainty remains within the same order of magnitude as the comparison error. As such, the results should be considered validated for this flow case despite the comparison error being larger than the validation uncertainty at points of Fig. 5.3d.

To validate the entire flow region using the ASME metric the reason for the offset between the experiments and simulations needs to be identified, and removed. The error in the kernel region implies that even if there is a problem with the pressure taps experimentally, there is a consistent trend towards

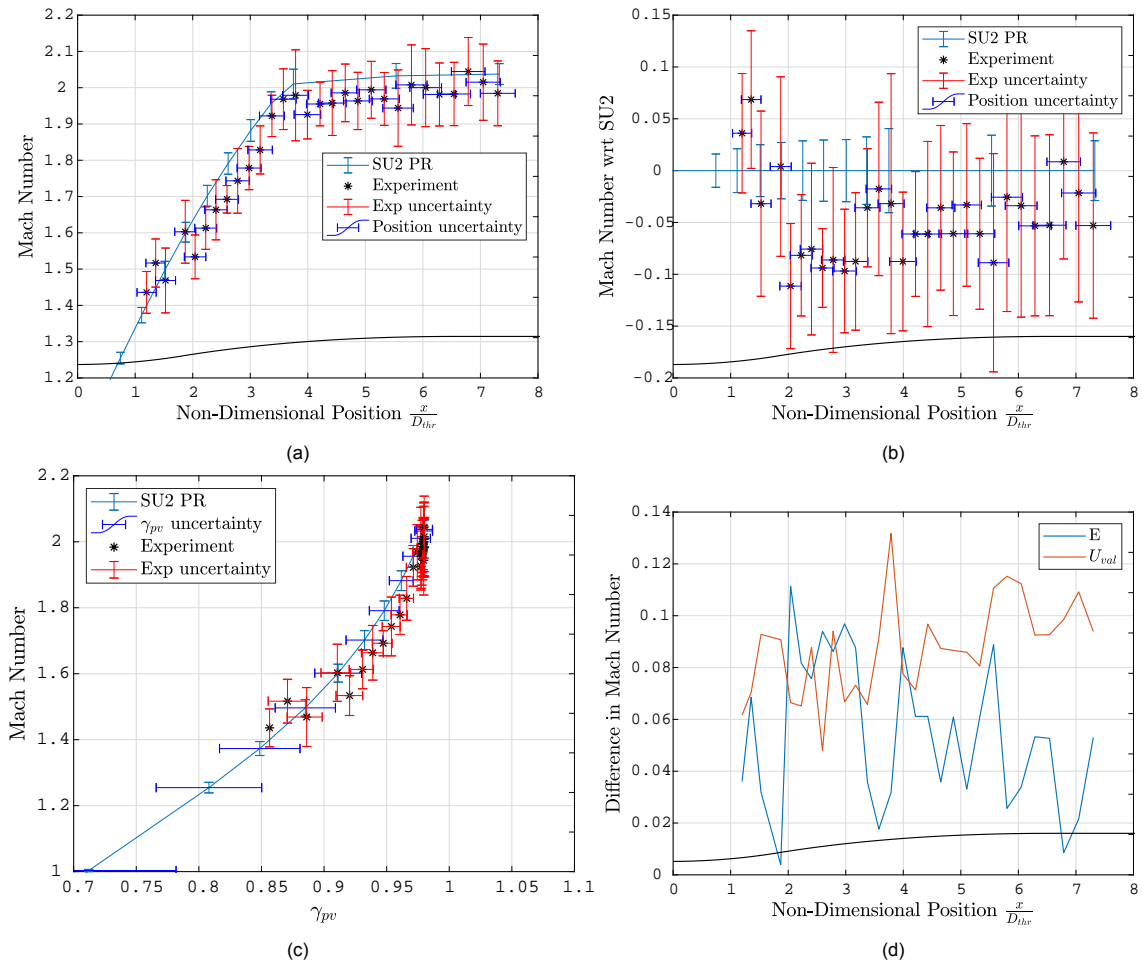


Figure 5.3: Validation plots of Mach number for a converging-diverging nozzle modelled in SU2 using the compressible Euler equations and the Peng-Robinson EoS. The test case is described in Sec. 3.2 and the model definition summarised in Sec 3.3. The mean simulation results along the nozzle centreline are compared against the mean ORCHID PR.025-NT.001 schlieren data. **a)** Mach number as a function of nozzle position non-dimensionalised with respect to the throat height. **b)** Mach number with respect to the SU2 model mean simulation value as a function of nozzle location non-dimensionalised with respect to the throat height. This is a version of the real space metric. **c)** Mach number as a function of polytropic exponent γ_{pv} . **d)** ASME V&V 20 validation metric plot of Mach number as a function of nozzle position non-dimensionalised with respect to the throat height.

inaccurate simulation results in the kernel region of a supersonic expansion. This may be due to internal code of the SU2 software, or there may be something recorded incorrectly from the experiment. A hypothesis for the offset is presented in Sec. 5.3.4. Despite the observed offset, focus should be directed towards reducing the experimental uncertainty to create zero order validation in future experiments.

5.2.3. Mass Flow

The final set of validation metrics is constructed for the mass flow rate. The predicated mass flow at the throat using the SU2 model for the two test cases, PR.025-NT001 and PR.027-NT001, is compared against the experimental mass flow recorded using a Coriolis flow meter on the liquid side of the ORCHID, see Fig. 5.4. The mass flow rate from the model is calculated using Eqn. 3.1 assuming the momentum and at the throat centreline is uniform across the entire cross sectional throat. This assumption is examined in App. A. Figure 5.4a is an absolute comparison of the models and the experiments. The mean results from the simulation are plotted, along with the simulation uncertainty bars, then the experimental values are plotted with the experimental uncertainty. The design value is plotted as a reference. Figure 5.4b is a representation of the real space metric, where all the errors and uncertainties

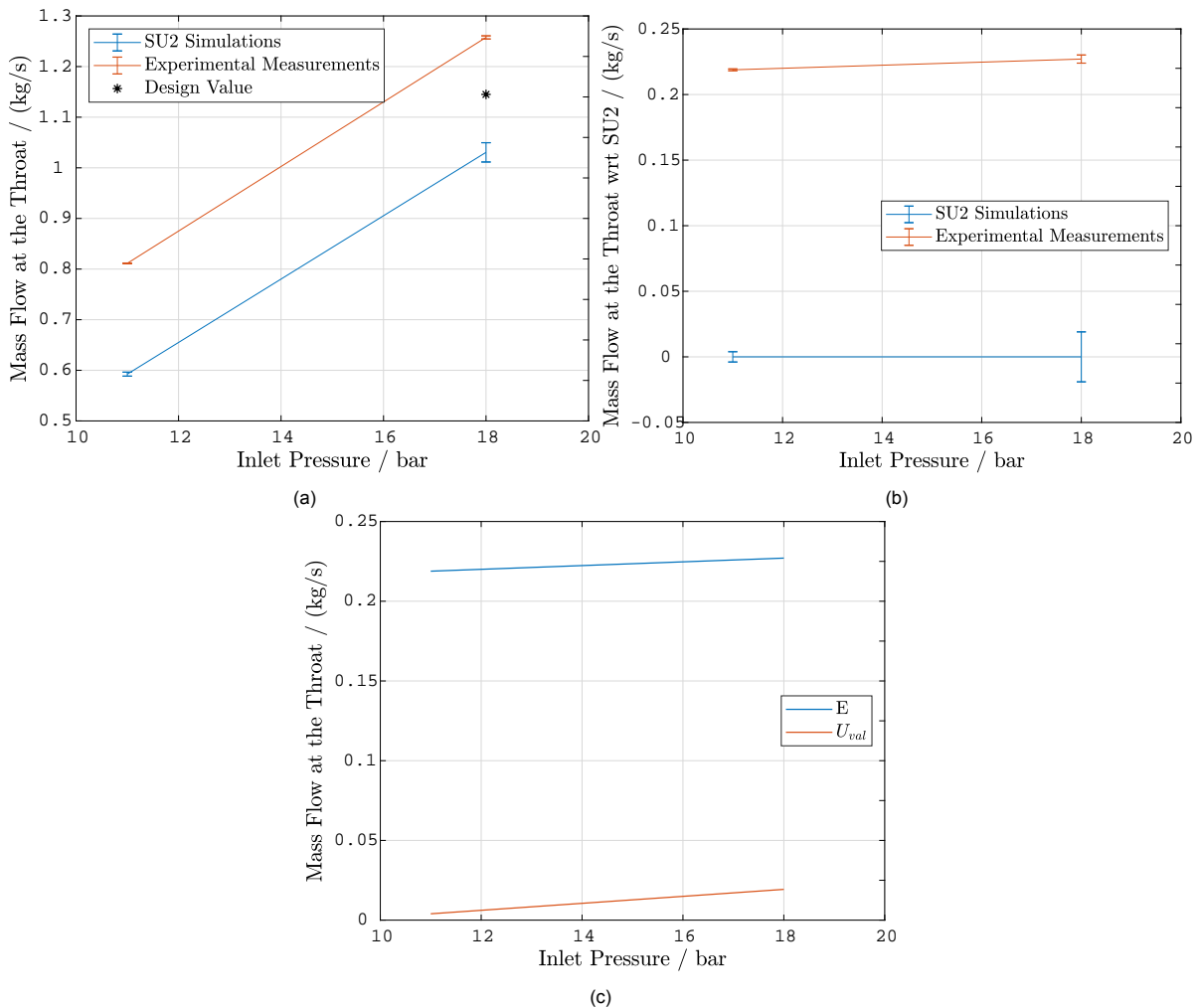


Figure 5.4: Validation plots of mass flow through a converging-diverging nozzle modelled in SU2 using the compressible Euler equations and the Peng-Robinson EoS. The test case is described in Sec. 3.2 and the model definition summarised in Sec 3.3. The mean simulation mass flow at the nozzle throat when operating at a given inlet pressure are compared against the mean measured ORCHID mass flow on the liquid side of the nozzle at the same inlet pressure. **a)** Absolute value of the mass flow with the design value for reference. **b)** Mass flow with respect to the SU2 model mean simulation value. This is a version of the real space metric. **c)** ASME V&V 20 validation metric plot of mass flow.

are taken with respect to the mean simulation result. The difference between the experiment and the simulation is what is plotted, with the uncertainty bars for every value remaining the same. Figure 5.4c is finally the plot of comparison error and validation uncertainty to represent the ASME metric. The flow conditions are identified by the inlet stagnation pressure, 18 bar for PR.025-NT.001 and 11 bar for PR.027-NT.001.

The predicted mass flow should be higher than the measured value since the calculation assumes no boundary layer and that the flow conditions are uniform over the entire rectangular throat region. The momentum at the midpoint of the throat, which was used as the average value, is higher than the values near the walls. However there should be a similar order of magnitude on the mass flow between simulation and experiment since these simplifications should result in small errors, as indicated in App. A. The experimental mass flow results were expected to be outside and below the uncertainty bands of the simulation. However, the trends seen in Fig. 5.4a are the opposite, where the experimentally measured mass flow is larger than the simulated value for both flow conditions.

The large anomaly seen in the plots, between 20% and 25%, may be due to incorrect throat geometry being recorded from the experiment. If the throat height is incorrect in the simulation then the cross-sectional area used in the simulation to calculate the mass flow is also incorrect. This would lead

to a uniform offset between the simulation and experiments, and figure 5.4b would have two horizontal lines due to the change in area having the same effect on both flow cases. This is evident, and it may be possible that at higher pressures and temperatures the throat is wider as the gaskets expand. This hypothesis is examined further in Sec. 5.3.4 where it is found that the mass flow could also be corrected by an increase in throat height by 2 mm.

However, the offset is not perfectly constant and the mass flow is offset by a slightly larger margin for the higher pressure flow case, implying that the throat geometry is not the only problem. A second possibility involves the bypass valve, which is located after the Coriolis flow meter but before the nozzle test section in the ORCHID [34]. The valve allows flow to be diverted for control or safety purposes and thus the discrepancy in mass flow could be due to mass flow going through the bypass instead of the test section.

The true reason for the discrepancy in mass flows may be a combination of geometric errors and an open bypass valve, however the experiments will need to be done again with more data acquisition to determine the cause.

Regarding the uncertainty of mass flow in an engineering context, the magnitude of the simulation uncertainty is on the order of 2%, which should not be ignored for the application of turbomachinery design in the context of ORC since it is above the 1% value defined in Sec. 4.3. Once the source of error is identified for the flow rate any regions of invalidity determined by the metrics should be considered invalid. The regions of validity can be used but while still taking into account the uncertainty of the simulation.

5.3. Discussion of SU2 Validation

This section reviews the evaluation of the validation metrics for SU2 simulations of NICFD. Although the results vary for the different system responses, they are definitive when combined with the newly introduced engineering threshold. The Mach number predicted along the nozzle centreline for expansions of siloxane MM are reliable in the context of turbomachinery, while the static pressure along the surface is not predicted accurately. The largest area of concern, as with the UQ study, is in the kernel region of the flow. The acceleration of flow through the nozzle from the throat until the nozzle geometric inflection point has physical behaviour which is not completely captured by SU2. There is a possibility that the discrepancy found in the mass flow rate is related to the discrepancy in static pressure, if there is a geometric deviation from the physical experiment to the SU2 model. *The only conclusion which can be drawn is that the experiments must be done again with additional data acquisition regarding geometry and flow rates.* Even with no doubts in the geometry and flow rate the study would need to be conducted over more expansions at different pressure ratios, inlet pressures, and regions of non-ideality. Then the point of validation expands to become a region over which the software can be used to predict NICFD. The study methodology, flow case, and metrics used in this study are discussed in detail to advise the future validation activities.

5.3.1. Methodology

The general procedure outlined in Fig. 3.1 was followed for this validation campaign. The process is simple to carry out and quick to complete since the code for the uncertainty quantification and validation metric calculation is complete. Once the experiments are done the simulations can be immediately carried out and metrics which are useful to engineers established. By including the iterative process of assessing the uncertainty prior to moving on to each phase of validation the validation will only produce relevant data. This requires close working proximity between the experimentation and simulation, which is the one flaw of this validation study. The experimental data was acquired months before the SU2 model was constructed and analysed, leaving limited opportunity for an iterative feedback to improve the experiments and model while conducting the simulation.

The experiment and the simulation must maintain separation in order to maintain the integrity of the validation, so it is recommended to have separate individuals conduct the experiments and the simulations while they maintain close communication. The experiment must be run completely and then provide input to the simulation, after which the simulation must be analysed completely before giving feedback to the experiment. Doing this process before evaluating the validation metrics may save time by reducing the delay to obtain better quality experimental data. In this case the results must be interpreted without addressing the questions regarding the experimental geometry and mass flow.

In the future the mutual reliance may diminish, however for optimal efficiency of validation activities there should be two teams, working in parallel, running experiments and simulations then providing instant feedback.

5.3.2. Converging-Diverging Nozzle Flow

As stated in Sec. 3.1 the flow case of a dense organic fluid through a converging diverging nozzle is the first point of validation required for validating SU2 models for NICFD conditions. The ORCHID design conditions provided a specific variant of the flow case, which can be used as a reference for future studies. PR0.25-NT.001 located the expansion isentrope well within the non-ideal region, the effects of which were successfully captured by the Peng-Robinson equation of state for the response quantity of Mach number. The second isentropic expansion, PR.027-NT.001, was also non-ideal but closer to ideal when using the measures of non-ideality. Despite being closer to the ideal gas region the static pressure was not accurately captured when using any thermodynamic model. These two cases should then continue to be investigated to determine the true level of accuracy of the SU2 flow solver. The experiments should be repeated, and the validation study done again but with more response quantities recorded and compared for both isentropes. The density and velocity are recommended. The true assessment of validity can then be established and an intelligent decision can be made about the next isentropic expansions to investigate.

5.3.3. Metrics

The ASME V&V 20 metric was the easiest to interpret, and could be integrated with the engineering uncertainty threshold. However the proposed numerical representation of this relation between uncertainty and error from Beltrame [9] could be a further improvement on the metric which would provide a quantitative assessment of validity. The real space metric, however gives the reader an understanding of if the model is over or under predicting a physical quantity and allows judgement to be made on the quality of the experiments and the simulations separately. This is important for validation as knowledge on where to focus resources is important. For example in the future when validating using the Mach number the experiment should have the most attention, while for static pressure the simulation and SU2 software may require more attention. The real space metric can also integrate the engineering uncertainty threshold without much alteration. Overall the metrics compliment each other and will be used by different people in different situations. Thus it is recommended to use both perspectives when providing a report on validation results.

A new perspective on validation metrics for NICFD, in addition to applying an engineering context, is to compute both the numerical and experimental uncertainty bands as function of the non-ideality parameter γ_{pv} rather than the nozzle geometry. By plotting the uncertainty metrics as a function of the polytropic exponent, or even the fundamental derivative, the metrics can be interpreted independently of the exact flow geometry. This is appealing, however the evidence indicates that the comparison error for these particular test cases are a function of the nozzle geometry, in particular the kernel region, therefore plotting the metrics as a function of γ_{pv} or Γ is not relevant. An interesting observation is that the γ_{pv} axis has more validated points, which is due to the way that γ_{pv} is a calculated flow parameter, instead of a geometric constant. This may represent the flow solver more accurately an imply that the flow solver correctly captures the effects of non-ideality, but may determine the level of non-ideality at a geometric location incorrectly. Using a γ_{pv} or Γ domain should be investigated further to determine if the results can be replicated across different flow cases, showing independence of the SU2 solver from the geometric case, or if the defining feature of the model behaviour is the geometric location.

Finally the engineering response quantity was useful for the assessment of the validation metrics. By providing context to the uncertainty and the error values the borderline cases, where validity is dubious or slightly beyond the acceptable bounds defined by the ASME V&V 20 metric, could be clearly interpreted as valid or not. In a borderline case where the uncertainties are well below the threshold of significance, the simulation can be treated as valid from an engineering point of view, although academically the results may be dubious from the software. Conversely, if the threshold is much lower than the uncertainty of a response quantity which has dubious validity, it would not be trusted by an engineer. The U_{eng} and U_{sig} values give a strong metric for final decision making.

5.3.4. Hypothesised Source of Error

The preliminary hypothesis to explain the large error between the simulated and experimentally measured mass flow is that the throat geometry is not correctly represented in the SU2 model. This hypothesis can be examined with a preliminary study to investigate the effect of using a different nozzle geometry in the simulation.

The nozzle profile is constructed to machine position in two halves then assembled with a gasket between them held together by bolts, thus the only source of geometric error is the spacing between the top half and bottom half of the nozzle. This is represented by shifting the half nozzle profile along the y axis in the model. To determine the amount of shift to add to the model geometry, the methodology described by Spinelli et al. [58] for nozzle design can be used. Implementing the adiabatic and isentropic assumptions imposed on the nozzle flow, described in Sec. 3.3, the energy conservation equation can be written in the form

$$M = \frac{\sqrt{2 [h_t - h(\rho, s)]}}{a(\rho, s)}. \quad (5.2)$$

Since the flow must be choked at the throat the Mach number must be one. For the isentropic expansion the total enthalpy and entropy are also constant. Therefore, using the enthalpy and entropy of the design case, there is a unique solution of density. With this analytically determined density value the throat area was calculated by Head et al. [33] for a design mass flow rate using equation 3.1. The inverse function can be used to determine the throat area given a measured mass flow rate. This area is used to determine the throat height since the nozzle width is set. It is assumed that there is no flow over the bypass valve. Therefore the mass flow measured by the flow meter in the liquid state is assumed to be equal to the mass flow over the nozzle in the vapor state assuming steady conditions.

The experimental mass flow rate in the design case indicates the height should be 8.13 mm instead of the 6.66 mm used in the simulation. The value of 6.66 mm was measured when the ORCHID was not operational, indicating that the height expands during operation, either due to pressure or temperature. Figure 5.5 presents a deterministic comparison of the original model, new model with shifted nozzle, and the experimental data of the Mach number along the centreline. The inlet and outlet of the nozzle are also shifted by the 1.3 mm.

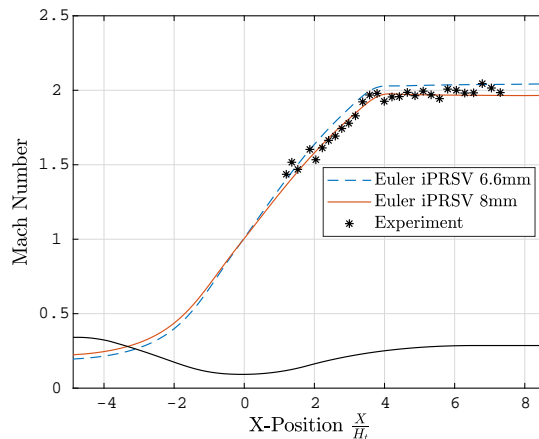


Figure 5.5: Comparison of two simulations with experimental results of the Mach number along the centreline of a converging-diverging nozzle modelled in SU2 using the compressible Euler equations and the Peng-Robinson EoS. The test case is described in Sec. 3.2 and the model definition summarised in Sec 3.3. The two models use the same nozzle profile as the experiment, but have different throat areas. The model of a nozzle with a 6.66 mm throat is in blue dashed lines, while the model with a 8 mm throat is in solid red. The nozzle profile is superimposed in black to provide a reference.

The simulation using the corrected geometry to match the mass flow measurements shows better association with the experimental data. This supports the hypothesis that the model did not match the geometry of the experiments. The experiments will need to be conducted again with precise measurements of the throat height made during the runs. See [34, Ch. 8] for the recommended approach.

6

Conclusion

The validation of the SU2 flow solver for classical non-ideal compressible fluid dynamics (NICFD) is required to advance the research into efficient organic rankine cycle (ORC) turbomachinery design. The work reported in this thesis assessed the predictive capabilities of two SU2 models, determining if the simulations of NICFD in the context of internal flows represented real physics. Furthermore, the methods and outcomes of the work provide feedback to the software developers on the quality of the SU2 code, informing them of aspects which could be improved.

An infrastructure has been developed to assess the validity of the SU2 two dimensional flow solver with clearly defined metrics, which for the first time interprets the model uncertainties through an engineering lens. The infrastructure was used to assess the flow solver predicting classical non ideal compressible flow characteristics seen during the expansion of Siloxane MM through a converging-diverging nozzle using compressible Euler equations, no heat transfer, and the Peng-Robinson equation of state. Two test cases were considered, using Mach number along the centreline and static pressure along the nozzle surface as the direct system response quantities (DRQ) which could be compared between the simulations and experiments. The model definition was developed in Sec. 3.3. Section 4.1 describes the infrastructure.

The numerical uncertainty was evaluated using the principles of Richardson extrapolation proposed by Eça and Hoekstra [22] which is implemented by ReFresco [39], and the forward propagated input uncertainty quantified using a sparse grid stochastic collocation implemented in Dakota [1]. These uncertainties in combination with the experimental ORCHID data from Head [34], and data analysis tools from Beltrame [9] provided the necessary inputs to construct the ASME V&V 20 [4] and Real Space [54] metrics. The metrics were given context with a novel Engineering Response Quantity (ERQ) analysis based on determining the effects of system uncertainty on performance parameters, in particular the theoretical loss across a steady normal shock in the nozzle presented as a non-dimensional loss coefficient.

In this thesis a first step was made towards the goal of validation for the SU2 flow solver. The completed work did not validate all models of classical NICFD constructed with the SU2 software, however it established one point of experimental comparison within the domain of classical NICFD. The detailed answers to the research questions are presented in this chapter, along with recommendations for improving validation research activities, and suggested future work to build on these results towards a fully validated SU2 suite used in the design optimisation of ORC turbomachinery.

6.1. Research Answers

This research has proven that the SU2 flow solver can be validated to predict high speed non-ideal flows of dense organic vapours and supercritical fluids. This can be done for any given experiment with the infrastructure provided. There are now two sets of validation metrics which can be used in the future efforts to validate the software for all possible flow conditions and ranges. The two sets of metrics provide answers to the initial research questions:

1. **How accurately can the SU2 solver predict transonic flows of non-ideal organic fluid?**

The comparison error between the simulation and experimental Mach number ranges from 0.004 to 0.111 along the nozzle centreline. The largest experimental uncertainty is 0.125 Mach at 3.79 throat heights past the throat, which corresponds to 6%, and the simulation has a maximum absolute expanded uncertainty of ± 0.04 at 3.75 throat heights past the throat, which corresponds to less than 2%. The simulation uncertainty is negligible in an engineering context as it translates to a potential uncertainty of less than $1e-3$ on a loss coefficient calculated across a theoretical steady normal shock. Section 5.2.2 discusses these results in detail.

For the static pressure along the surface of the nozzle the comparison error between the simulation and the experiment ranges from 0.5 kPa to 112 kPa. The smallest error is found in the converging section of the nozzle, and the largest error is in the kernel region of the flow. The static pressure could be predicted with a maximum uncertainty of $\pm 5 \text{ kPa}$ at the end of the kernel region of the nozzle, equivalent to approximately 3% of the local value. This is significant in an engineering context for turbomachinery design as it translates to a potential uncertainty of 0.02 on a loss coefficient calculated across a theoretical normal shock. There is room to remove uncertainty through refinement of the mesh, at which point the maximum uncertainty would be at the throat. Section 5.2.1 discusses these results in detail.

The metrics thus indicate that the prediction of transonic flows of non-ideal organic fluid is accurate enough for the Mach number, but not accurate enough for the static pressure in the context of turbomachinery design.

The mass flow has an uncertainty of up to 2%, which in the context of turbomachinery optimisation is not to be ignored. However, the mass flow deviates between experiment and prediction, which is likely owed to the throat dilating by 1.3 mm during PR25.025-NT001. New experiments need to be run before a final assessment on the accuracy of mass flow predictions can be made. Sections 5.2.3 and 5.3.4 discuss these results in detail.

2. What effect does forward propagation of model input uncertainties have on the probability distribution of the SU2 simulation results of dense organic flows?

The largest component of the overall pressure uncertainty is a result of the uncertain boundary conditions and thermodynamic closure coefficients, with a maximum uncertainty of ± 5 kPa, equivalent to approximately ± 3 % at the throat of the nozzle. The model input parameters which provide the highest contribution to the static pressure uncertainty are the thermodynamic properties. The critical pressure and temperature each have Sobol indices of 0.45, while the remaining influence is from the acentric factor and ideal gas specific heat ratio. The only exception is at the inlet to the nozzle, where the fluctuating pressure boundary condition is the dominant source of any uncertainty on the static pressure prediction in the converging section of the nozzle. After the throat, where the flow is choked, the thermodynamic constants are the dominant influence for the uncertainty of the predicted flow quantities.

Experimental uncertainties are larger than the simulation uncertainties for Mach number along the nozzle centreline, with an average uncertainty of ± 0.1 Mach compared to the simulation uncertainty of ± 0.03 . Therefore focus should be directed to lowering the experimental uncertainties, and simulation uncertainties do not need to be reduced. The most important input parameters which provide the highest contribution to the predicted Mach number uncertainty are again the critical pressure and temperature, since they define the behaviour during and after choked flow. Unlike the static pressure there is no other input value of interest besides the critical values.

Section 4.2 contains the details of these results.

3. What is the domain over which the SU2 solver can be applied when solving non-ideal dense organic vapour flows?

The results from Chap. 5 can not independently define a clear domain of applicability for SU2 models in the NICFD flow regime. Instead they provide the valid prediction points for two isentropic expansions of MM through a nozzle at 525 K: an expansion from 18.4 bar to 2.1 bar, and an expansion from 11.1 bar to 1.3 bar. According to the ASME V&V 20 metric the Mach number prediction along the centreline of the nozzle for the high pressure expansion is valid at all points except for in the kernel region of the flow, in particular at $X=2.04$, $X=2.226$, $X=2.5959$, $X=2.9795$, $X=3.17$, and $X=3.99$. X is the the number of throat heights past the throat location. The static

pressure prediction along the nozzle surface of the low pressure case is only valid at $x=0.01596$ m, $x=0.03355$ m, and $x = 0.05991$ m of the nozzle. In the context of turbomachinery design the Mach number along the centreline can be predicted by the flow solver, but the static pressure along the wall can not be predicted. In the future this data in combination with additional case studies can be used to determine regions of the Siloxane MM T - s diagram where SU2 models are suitable.

From these preliminary results the non-ideality of the flow defined by the polytropic exponent γ_{pv} appears to not have an impact on the prediction accuracy, but rather the geometric regions of flow in the nozzle affect the credibility of the flow solver predictions. The most uncertain system responses are at the throat and the end of the kernel region, and the comparison error also increases in the kernel region for static pressure. In summary, the two-dimensional compressible Euler solutions for isentropic expansions of dense organic fluids modelled with SU2 are accurate before the throat and past the kernel region of a nozzle. The absolute value of γ_{pv} was not correlated to the accuracy. This implies that model credibility could be either a function of the change in non-ideality over time, $\frac{\delta\gamma_{pv}}{\delta t}$, or change in non-ideality over space $\frac{\delta\gamma_{pv}}{\delta x}$.

The Peng-Robinson equation of state (EoS) is adequate for predicting most thermodynamic quantities for MM at 525 K and 18.4 bar, and any conditions farther from the critical point. Temperature is the only quantity which is not precisely estimated. The iPRSV EoS is potentially required for NICFD closer to the critical point. A model built in SU2 may require the SW form of the EoS or lookup tables if operating within close proximity of the critical point.

6.2. Recommendations

This section describes recommended practices and actions to take for repeating the UQ study from Chap. 4 or other validation activities involving NICFD. This is for SU2 modelling, ORCHID experiments, and metric calculations. Suggestions to improve this study are listed as either ways to reinforce the conclusions, or flaws with the method which must be corrected.

- Assess more than one DRQ for a given process run. PR.025-NT.001 only had Mach number data and PR.027-NT.001 only had static pressure data. A greater number of DRQ which are measured at the same time would allow a clearer picture of the validity to be found.
- Compare the Mach number near the surface of the nozzle profile. The Mach number prediction is only compared against experiments in the kernel and uniform regions, not in the reflex region. Pressure was accurate in the reflex region, and confirming this accuracy with the Mach number in the same flow conditions would help define the domain of applicability for SU2 in regions where gas dynamics and thermodynamics must be modelled with complex equations. This will be challenging due to the boundary layer.
- Do the simulations with mesh refinement at the kernel transition line. The numerical error found at the transition between the kernel region and the other regions of flow could be removed with mesh refinement. This transition potentially needs to be treated like a shock wave. The mesh was not fine enough at the transition of the kernel region to capture the true changes in fluid behaviour.
- Calculate the numerical uncertainty with a fully uniform mesh density. The simulations done used a coarse mesh at the outlet to increase the rate of convergence, and despite it being at the exit it may have had an impact on the Richardson extrapolation. Also, if the subsequent grids used in the grid convergence study can be made to have exactly double the number of elements every time the calculation may be more accurate for estimating the uncertainty. In this case the discretisation was not the main source of uncertainty for the validation, however in future studies the numerical uncertainty should be calculated with more rigour. The larger uncertainty in these simulations may have helped the validation metrics move towards a valid state.
- Check the statistical dependency of U_{in} , U_D , and U_{num} . Currently the uncertainties are assumed to be independent so they can be aggregated using the root sum of squares. This assumption may not be valid for the numerical and input uncertainties, as one can see small increases in the

input uncertainty in Figs. 4.5a and 4.5b aligning with the spikes in numerical uncertainty seen in Figs. 4.2b and 4.2a. However, the spikes in the input uncertainty plots are not significant so the uncertainties were assumed as independent in this thesis. In future work a study needs to be done to determine the level of dependence between the numerical uncertainties and the input uncertainties, or a finer mesh with negligible uncertainty should be used. This however may lead to unreasonable computational times considering that the uncertainty is of a magnitude which is acceptable.

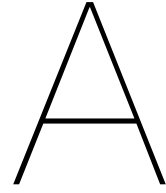
- The throat height must be measured during the experimental campaign. The height in this thesis was based off a measurement taken after the experiments and thus could be incorrect. Either use a measured mass flow to inform the height, measure the throat during flow to see if expansion occurs, or have real time measurements of the geometry to allow the model in SU2 to be more accurate and remove doubt about the error causes.
- Investigate if input uncertainty distribution types affect the UQ. Assumptions were made to treat uncertainties of inputs as normal or uniform, it must be determined if this assumption affects the results. Work from Cinnella et al. [14] provides a starting point for this investigation.
- Use γ_{pv} in the normal shock loss estimation calculation to change the ideal loss estimate to potentially a true loss estimate. γ_{pv} is meant to be a real replacement for γ which can convert ideal relations to real relations. This concept is based on the work from Nederstigt [43].
- Repeat the UQ analysis with variable throat size as a variable, it may be uncertain. Geometric uncertainty was ignored for this study, considering the machining of parts was so precise. However, the vibrations, thermal expansion, and tightening effects on gaskets could possibly have added an uncertainty bar on the geometric constants used in SU2. This should be investigated and confirmed.
- Run the UQ with RANS instead of Euler equations to get a real pressure loss coefficient from non-isentropic flow. The current assessment of ERQ is only mathematical, so is useful for a translation of DRQ to ERQ, but is not physically meaningful to this case. If RANS is done then the meaning becomes physical and results could be more interesting. This does not invalidate the current study of ERQ, but rather provides extra substance analysis.

6.3. Future Work

Considering that this research did not fully validate the SU2 flow solver for all NICFD flow simulations this section lists the future projects which should be based off the procedures and results.

- Add density and velocity measurements to the experiments. These two parameters can then be DRQ for SU2 model validations. This can give more information as to how the errors are occurring in the code for easier corrections in the software.
- Repeat PR.025-NT.001 and PR.027-NT.001 with more measurements. Record the Mach number, pressure, geometry, density, and velocity for an on design nozzle test section run and two off-design runs. Do one of the off-design runs at a higher pressure, and one at a lower pressure. Then use the created infrastructure and method to analyse the data.
- Validation of the SU2 flow solver using shock angle as a DRQ. Place a wedge in the nozzle flow and record the shock angle with the schlieren images. Assess the validity metrics using the developed infrastructure and include the real entropy rise across the shock as an ERQ. This would provide a better indication of the ability to capture compressibility effects in flows solved with SU2.
- Multiple experiments need to be analysed at different state conditions for Siloxane MM. This would allow a map to be created, superimposed on the T - s diagram, where the most appropriate thermodynamic models can be used. Calculate the validation metrics for a sample of expansions ranging from critical conditions at the inlet, to fully ideal conditions at the inlet. A large data set will allow an observation to be made if there is a pattern of γ_{pv} vs validity. In the future the interpolation and extrapolation of validation regions based on a finite number of validated cases will be required for the flow solver. The interested reader can begin with the paper by Merle and Cinnella [40].

- Plot the the DRQ validation metrics against γ_{pv} , Γ , and nozzle position to investigate what causes the invalid predictions. The proximity to the critical point, rate of change of γ_{pv} , and region of flow field are all possibilities. This also allows examination of different flow cases uses the same non-dimensional parameter as a reference.
- Study the effects of software uncertainty on loss correlations and loss prediction. Conduct a UQ using the different equations of loss prediction for turbomachinery in order to define the accuracy thresholds for different flow parameters solved for by SU2. This dives deeper in the concept of ERQ.
- Extract the speed of sound from experiments using measured Mach number and velocity measurements. The speed of sound is a thermodynamic quantity which can be validated, instead of velocity and density which validate the implemented conservation equations.
- Conduct an experiment of an expansion starting in the classical ideal flow region defined as $\Gamma > 1$ and expanding through the non-ideal region. This may not be possible due to current physical limitations of experimental facilities.



Proof of Assumptions

A.1. Adiabatic Flow

The nozzle test section of the ORCHID is well insulated except for the windows which are used to visualise the flow with schlieren imaging. The windows are made of silica glass (SiO_2) and would be the principle source of heat loss. As a conservative estimate consider that the pane of glass on both sides of the nozzle is completely exposed, and this allows for uniform heat loss across the entire surface. The glass panes are each 120 mm x 60 mm in area and 40 mm thick. For heat loss calculation the system will be treated as a rectangular plate with constant material properties in contact with static room temperature air. The fluid MM is considered to be on average 500K which is the same temperature as the inner surface of the glass, and the outer surface experiences free convection.

Variables

k_{SiO_2}	$1.38\text{W}/\text{m}\cdot\text{K}$	https://www.crystran.co.uk/optical-materials/silica-glass-sio2
h_{air}	$20\text{W}/\text{m}^2\cdot\text{K}$	Conservative Estimate
ΔT	200K	Head [34]
L	0.04m	Head [34]
A	0.0144m^2	Head [34]

Equations & Solution

$$\dot{Q}R_{\text{system}} = \Delta T \quad (\text{A.1})$$

$$\frac{1}{R_{\text{system}}} = \frac{1}{R_{\text{conduction}} + R_{\text{convection}}} \quad (\text{A.2})$$

$$R_{\text{conduction}} = \frac{L}{kA} \quad (\text{A.3})$$

$$R_{\text{convection}} = \frac{1}{h_c A} \quad (\text{A.4})$$

Therefore,

$$\dot{Q} = \frac{\Delta T}{\frac{L}{kA} + \frac{1}{h_c A}} \quad (\text{A.5})$$

$$\dot{Q} = \frac{200\text{K}}{\frac{0.04\text{m}}{(1.38\text{W}/\text{m}\cdot\text{K})(0.0144\text{m}^2)} + \frac{1}{(20\text{W}/\text{m}^2\cdot\text{K})(0.0144\text{m}^2)}} \quad (\text{A.6})$$

$$\dot{Q} = 36.5\text{W} \quad (\text{A.7})$$

The enthalpy of the flow is on average approximately 400 kJ/kg, and with a mass flow of approximately 1 kg/s the amount of energy flowing through the system is $400 \text{ kJ/kg} * 1 \text{ kg/s} = 400 \text{ kW}$.

$0.0365 \text{ kW} \ll 400 \text{ kW}$, so heat loss through the silica glass panes can be considered negligible in this simulation.

A.2. One Dimensional Mass flow

prove one dimensional mass flow equation is good enough (use the integral approach and see the difference). Using Data from PR25 RANS iPRSV.

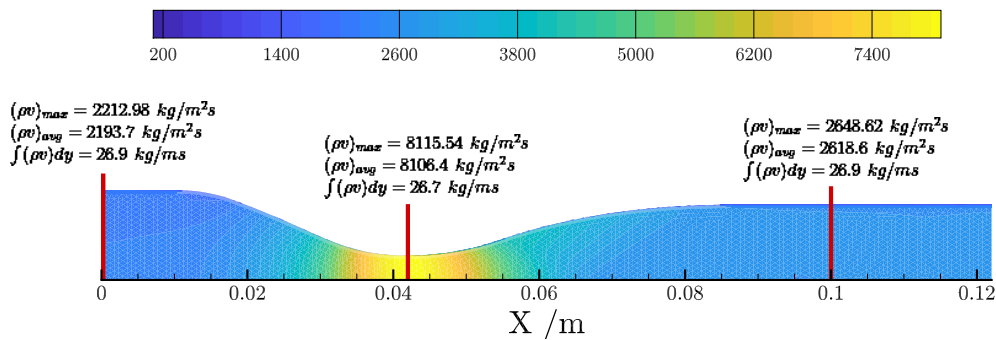


Figure A.1: X-momentum in the ORCHID nozzle for PR25. RANS simulation using the iPRSV Eos. centreline values are compared against the average and the integrated value for the inlet, throat, and outlet.

Mass flow 1D uses the centreline momentum values multiplied by the height and width of nozzle.

Mass flow integral uses the momentum integrated along the height from tecplot multiplied by the nozzle width.

Inlet height is 0.246m, throat height is 0.0066m, outlet height is 0.0206m. Width is 0.02 m

Method	Inlet	Throat	Outlet
Uniform flow	1.089 kg/s	1.07125 kg/s	1.09123 kg/s
Integral	1.076 kg/s	1.068 kg/s	1.076 kg/s

These values are deterministic and do not have any uncertainty quantified. The Euler Peng-Robinson calculated $\dot{m} = 1.03 \pm 0.02$ kg/s. The difference in the mass flows is negligible, but possibly the throat underestimates.

B

Ideal Specific Heat Uncertainty Quantification

The ideal isobaric specific heat is an uncertain parameter since it is calculated with an empirical thermodynamic model. Equation 2.24 is a polynomial which uses constants determined with experiments that have uncertainty associated with them. To assess the effect of specific heat η coefficient uncertainties on the $C_p^{ig} = f(T)$ polynomial, a sensitivity study was done calculating C_p using Eqn. 2.24. This was done using the stochastic collocation (SC) method and variance based decomposition (VBD). Figure B.1 shows the Sobol indices of the equation variables, and Tab. B.1 shows the differences in the results from the SC and VBD methods. Both methods are implemented in Dakota [1].

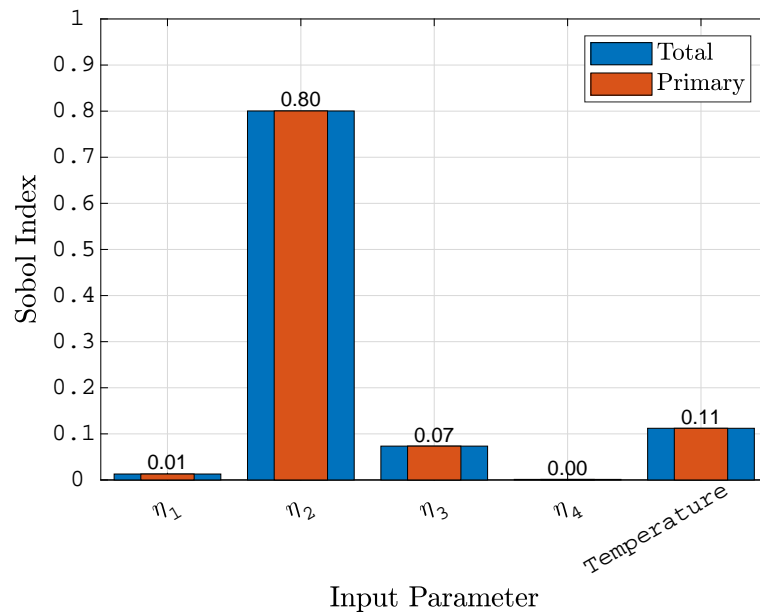


Figure B.1: image of the C_p^{ig} sensitivity to its coefficients. An example of the Sobol Index

It was found that the final coefficient of the C_p polynomial has negligible effects on the uncertainty of C_p . The final coefficient can be treated as deterministic in all cases, while η_1 and η_3 can be treated as deterministic when the specific heat calculation is used as a submodel.

Sobol indices calculated from the SC UQ have a negligible difference when compared to the converged VBD results. The VBD method was also computationally more expensive than SC; VBD needed thousands of samples, SC 3rd order took 351 samples.

Input	VBD	SC
η_1	0.0128	0.0129
η_2/K^{-1}	0.8007	0.8004
η_3/K^{-2}	0.0712	0.0734
η_4/K^{-3}	0.0012	0.0012
T	0.1109	0.1121

Table B.1: Comparison of the VBD and SC sobol index results

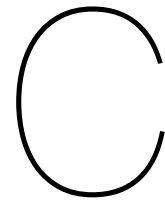
To find the value of the isobaric heat capacity statistical moments, mean and standard deviation, a traditional latin hypercube sampling (LHS) was done, in addition to an LHS and SC from Dakota. Table B.2 shows the results for each method.

Statistical Moment	LHS calculated	LHS dakota	SC dakota
<i>mean</i>	2.7083 e+3	2.7083 e+3	2.7083 e+3
<i>standard deviation</i>	45.9959	45.9959	45.9431

Table B.2: Comparison of LHS and SC uncertainty calculation results

Results from the SC UQ are identical to the converged LHS from both methods. The LHS UQ needed 5000 samples, while the SC 3rd order UQ took 351 samples. Since the results are the same the SC is the better method considering the computational cost.

The SC UQ implemented in Dakota is quick and reliable for uncertainty quantifications and sensitivity studies required.



Residuals

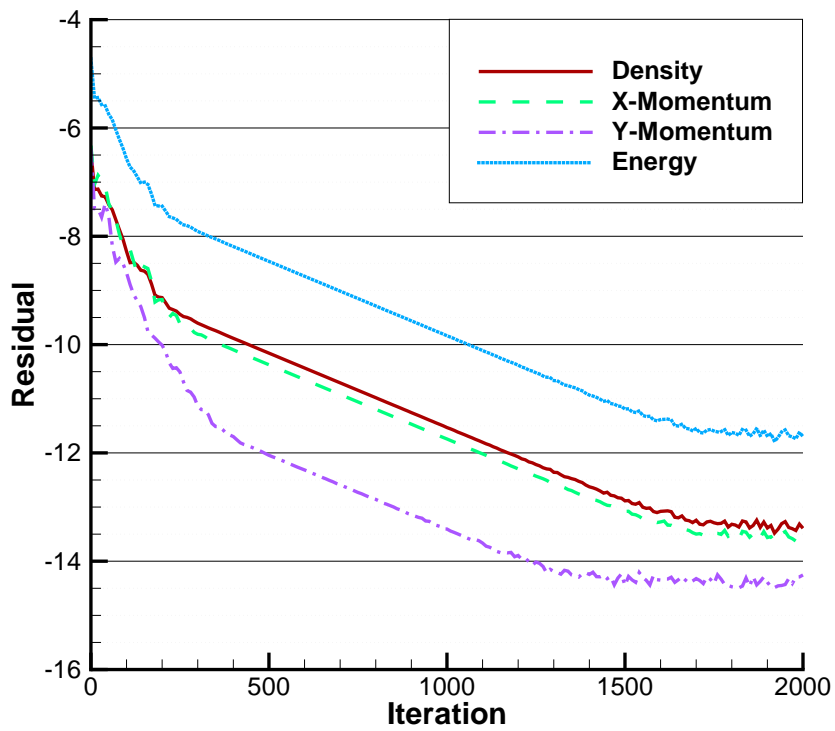


Figure C.1: Residuals for the convergence of a PR.025-NT.001 compressible Euler flow case in SU2 run using the Peng-Robinson Equation of State. The simulation starts from the first order converged solution and is run second order.

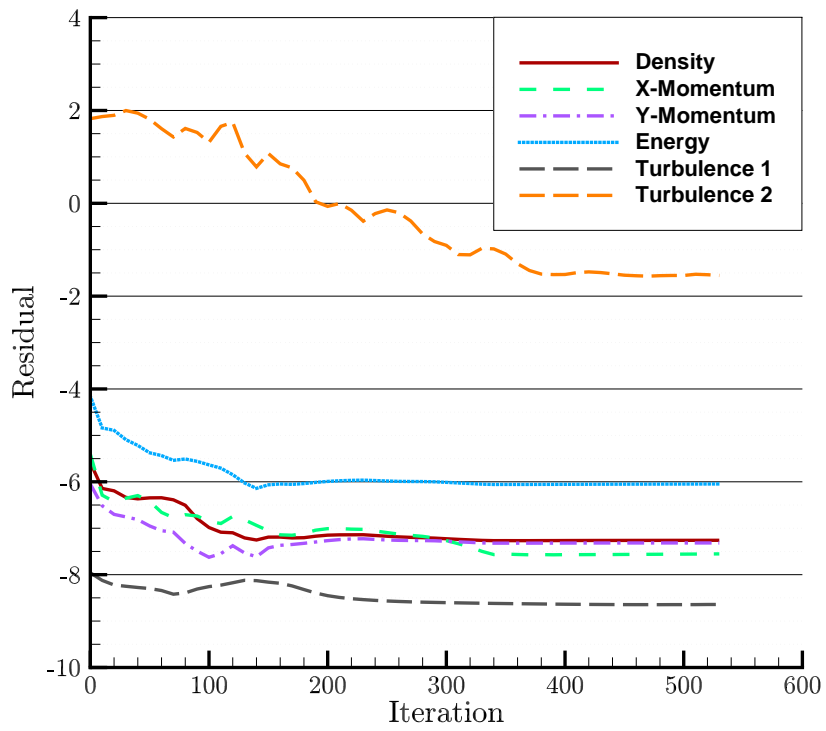
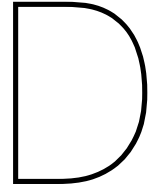


Figure C.2: Residuals for the convergence of a PR.027-NT.001 compressible RANS flow case in SU2 run using the iPRSV Equation of State. The simulation starts from the first order converged solution and is run second order.



Remaining Results

D.1. Uncertainty Quantification PR.025-NT.001

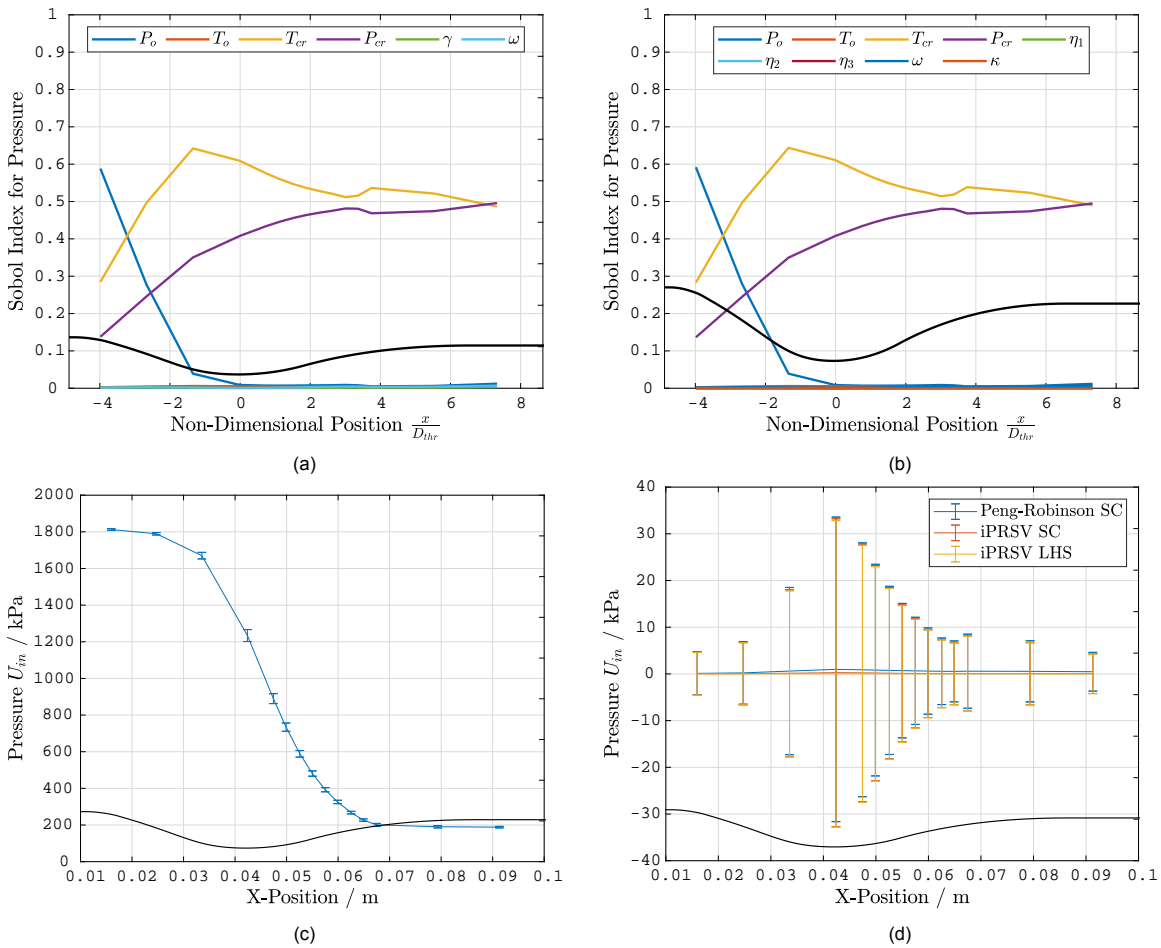


Figure D.1: PR.025-NT.001 Centreline: UQ Results for Pressure. **a)** Sobol Indices using Peng Robinson EoS. **b)** Sobol Indices using iPRSV EoS. **c)** Response with uncertainty bars using Peng Robinson EoS. **d)** Plot of U_{in} vs location. The reference value is the LHS mean.

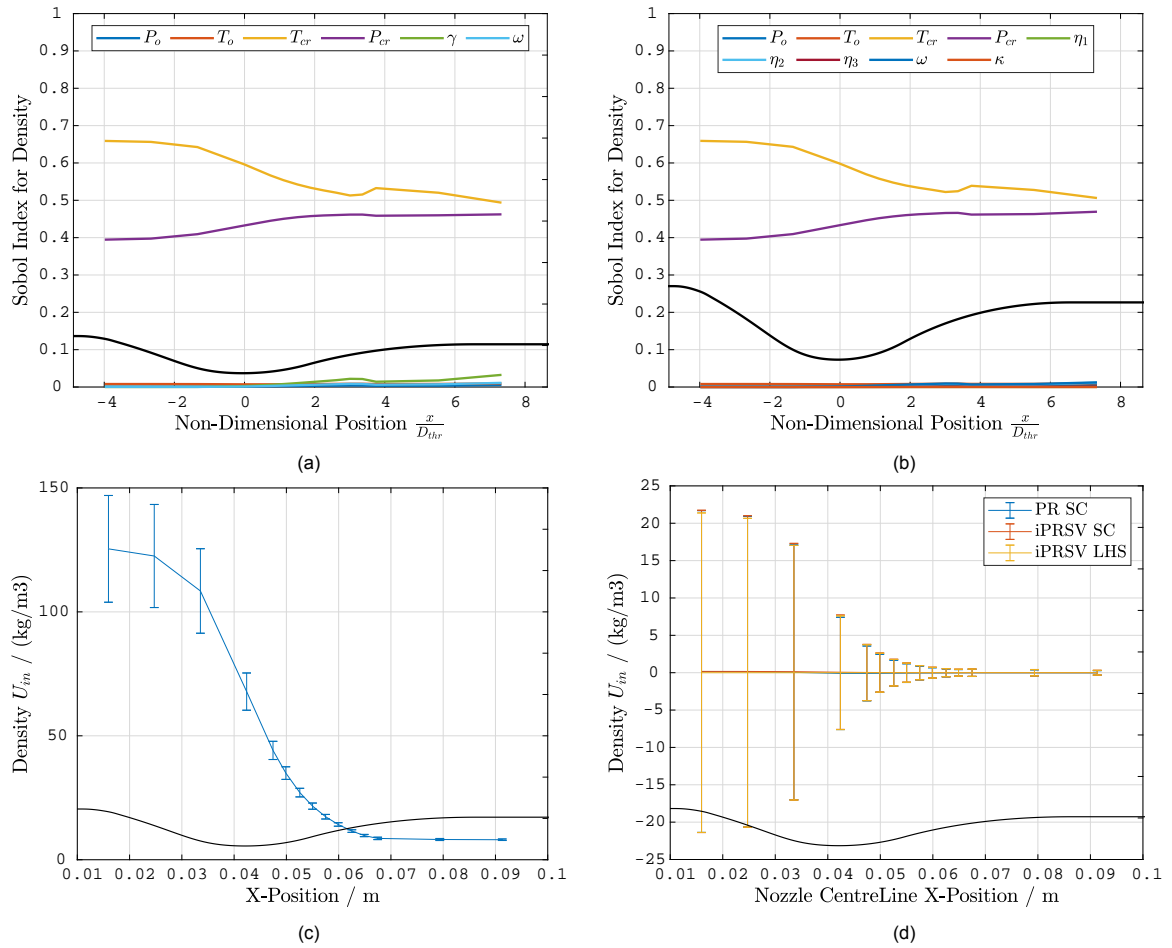


Figure D.2: PR.025-NT.001 Centreline: UQ Results for Density. **a)** Sobol Indices using Peng Robinson EoS. **b)** Sobol Indices using iPRSV EoS. **c)** Response with uncertainty bars using Peng Robinson EoS. **d)** Plot of U_{in} vs location. The reference value is the LHS mean.

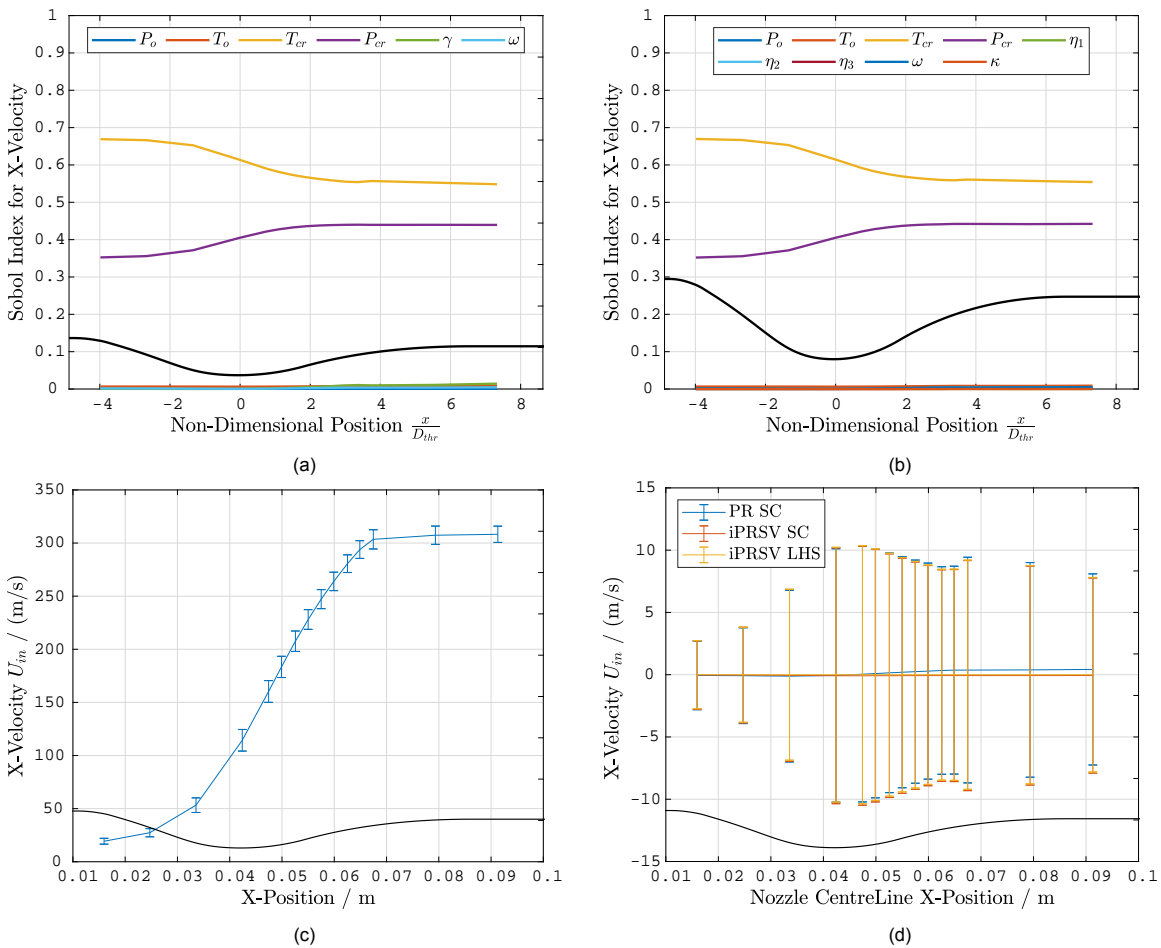


Figure D.3: PR.025-NT.001 Centreline: UQ Results for Velocity. **a)** Sobol Indices using Peng Robinson EoS. **b)** Sobol Indices using iPRSV EoS. **c)** Response with uncertainty bars using Peng Robinson EoS. **d)** Plot of U_{in} vs location. The reference value is the LHS mean.

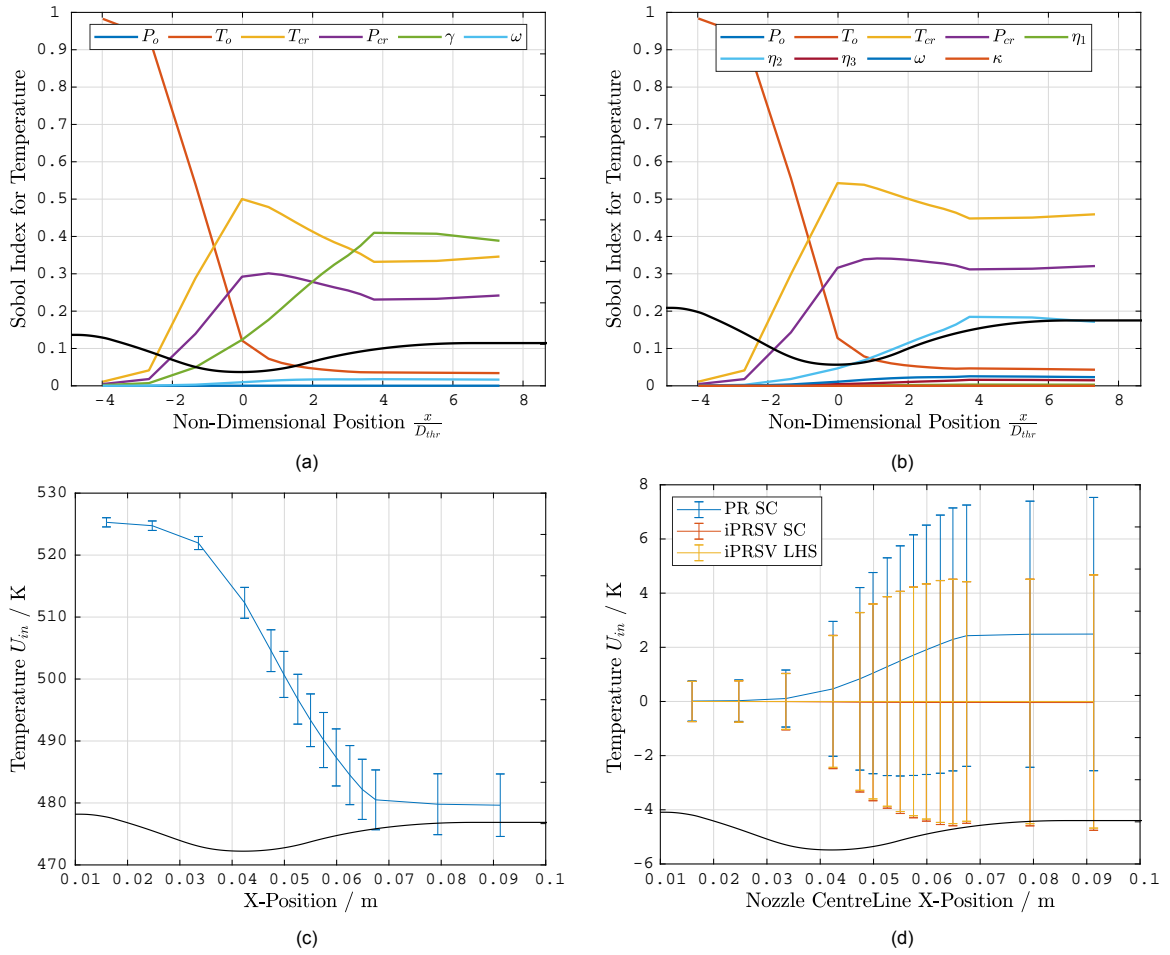


Figure D.4: PR.025-NT.001 Centreline: UQ Results for Temperature. **a)** Sobol Indices using Peng Robinson EoS. **b)** Sobol Indices using iPRSV EoS. **c)** Response with uncertainty bars using Peng Robinson EoS. **d)** Plot of U_{in} vs location. The reference value is the LHS mean.

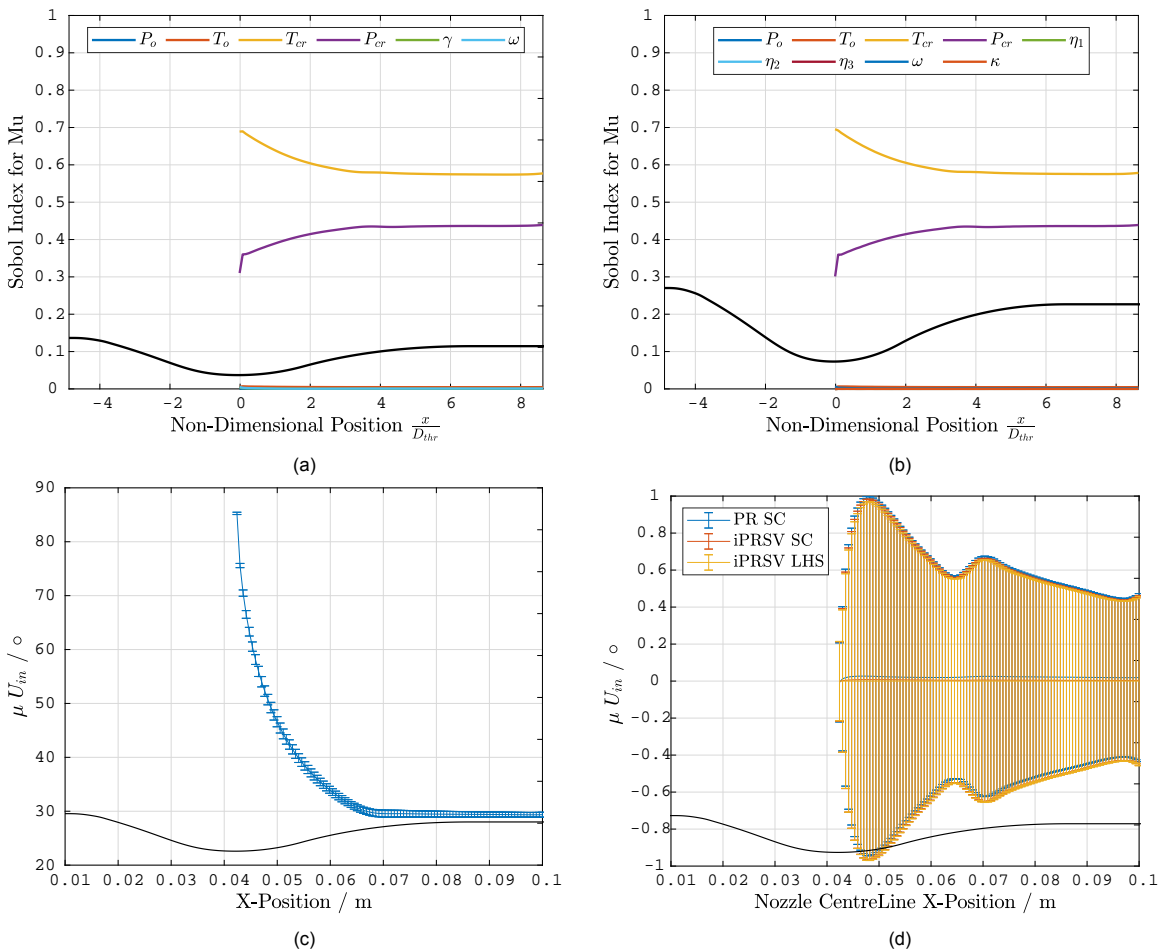


Figure D.5: PR.025-NT.001 Centreline: UQ Results for μ . **a)** Sobol Indices using Peng Robinson EoS. **b)** Sobol Indices using iPRSV EoS. **c)** Response with uncertainty bars using Peng Robinson EoS. **d)** Plot of U_{in} vs location. The reference value is the LHS mean.

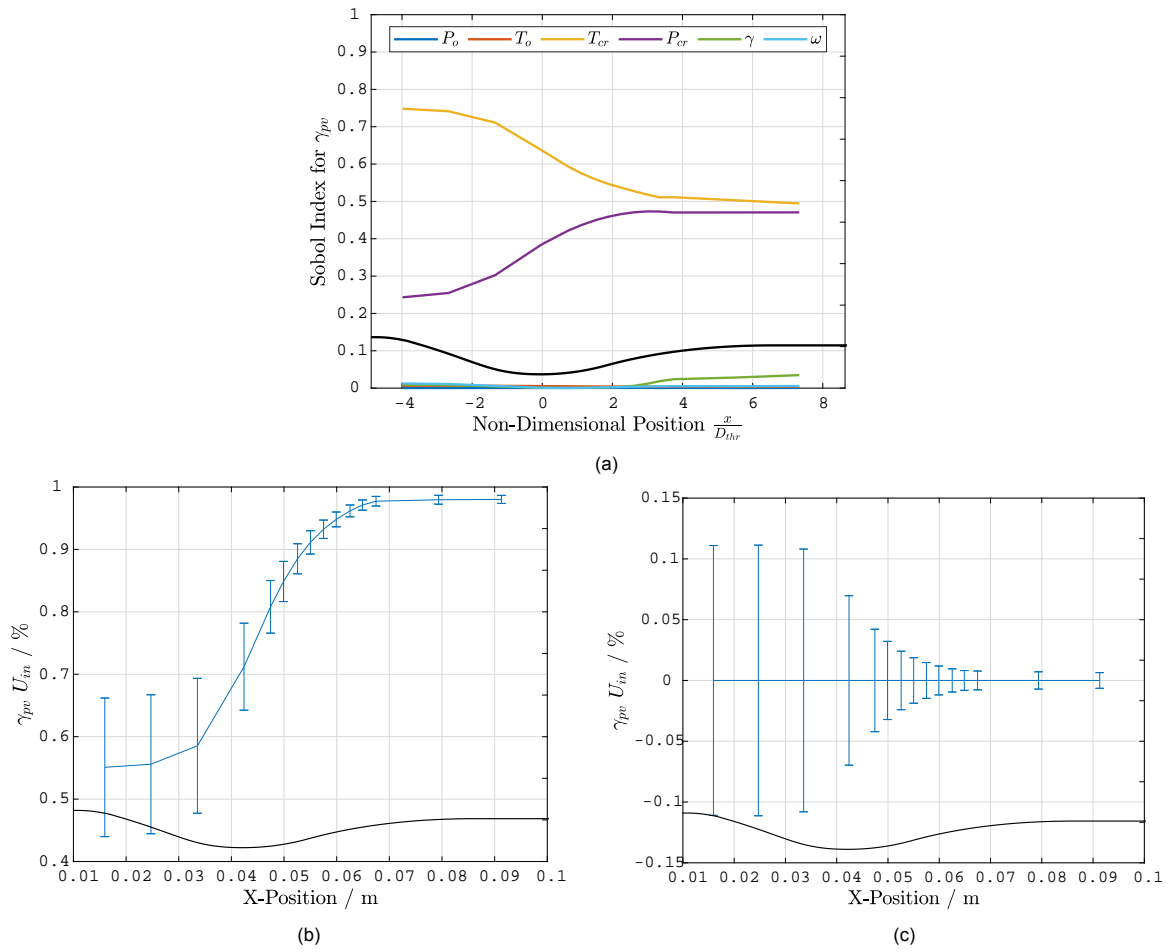


Figure D.6: PR.025-NT.001 Centreline: UQ Results for γ_{pv} . **a)** Sobol Indices using Peng Robinson EoS. **b)** Response with uncertainty bars using Peng Robinson EoS. **c)** Plot of U_{in} vs location.

D.2. Uncertainty Quantification PR.027-NT.001

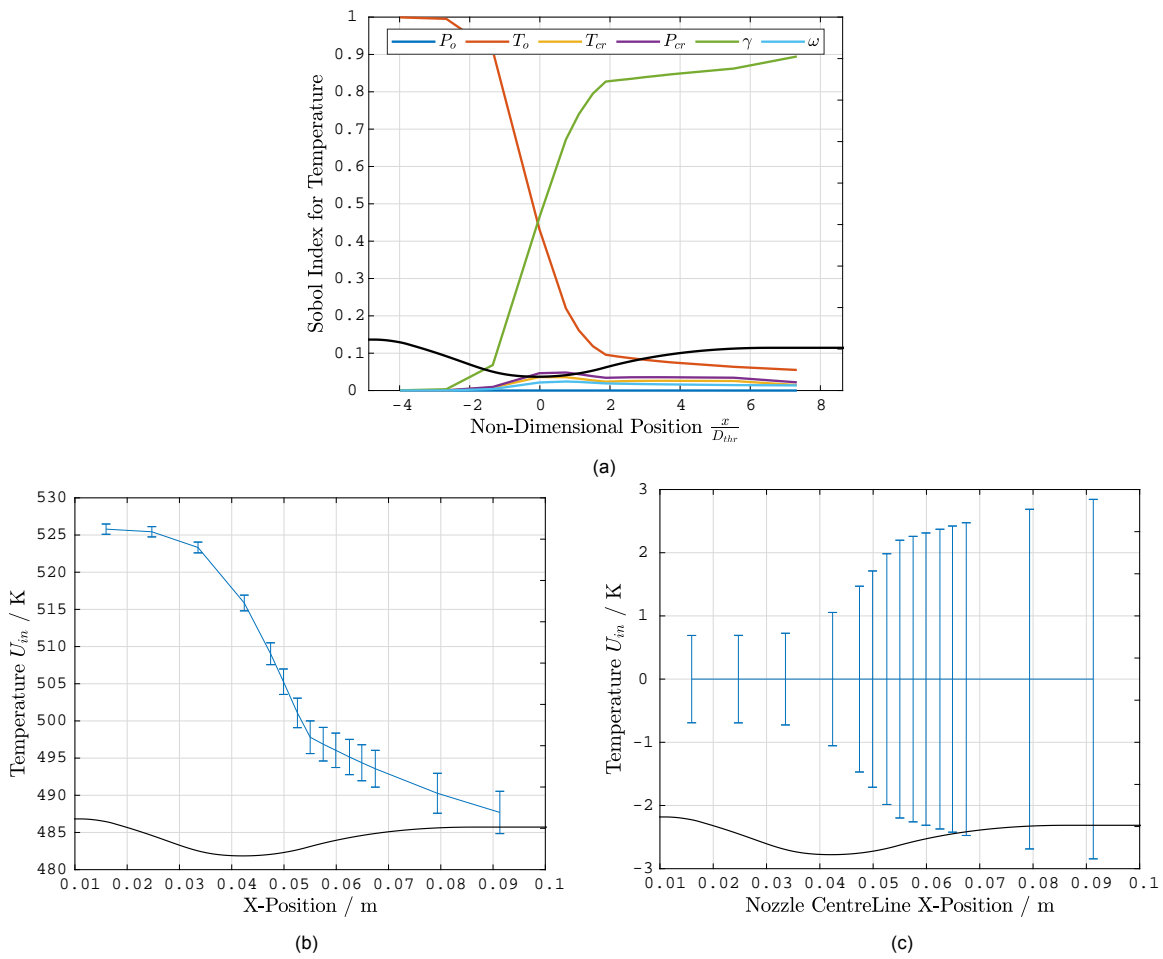


Figure D.7: PR.027-NT.001 Nozzle Profile: UQ Results for Temperature. **a)** Sobol Indices using Peng Robinson EoS. **b)** Response with uncertainty bars using Peng Robinson EoS. **c)** Plot of U_{in} vs location.

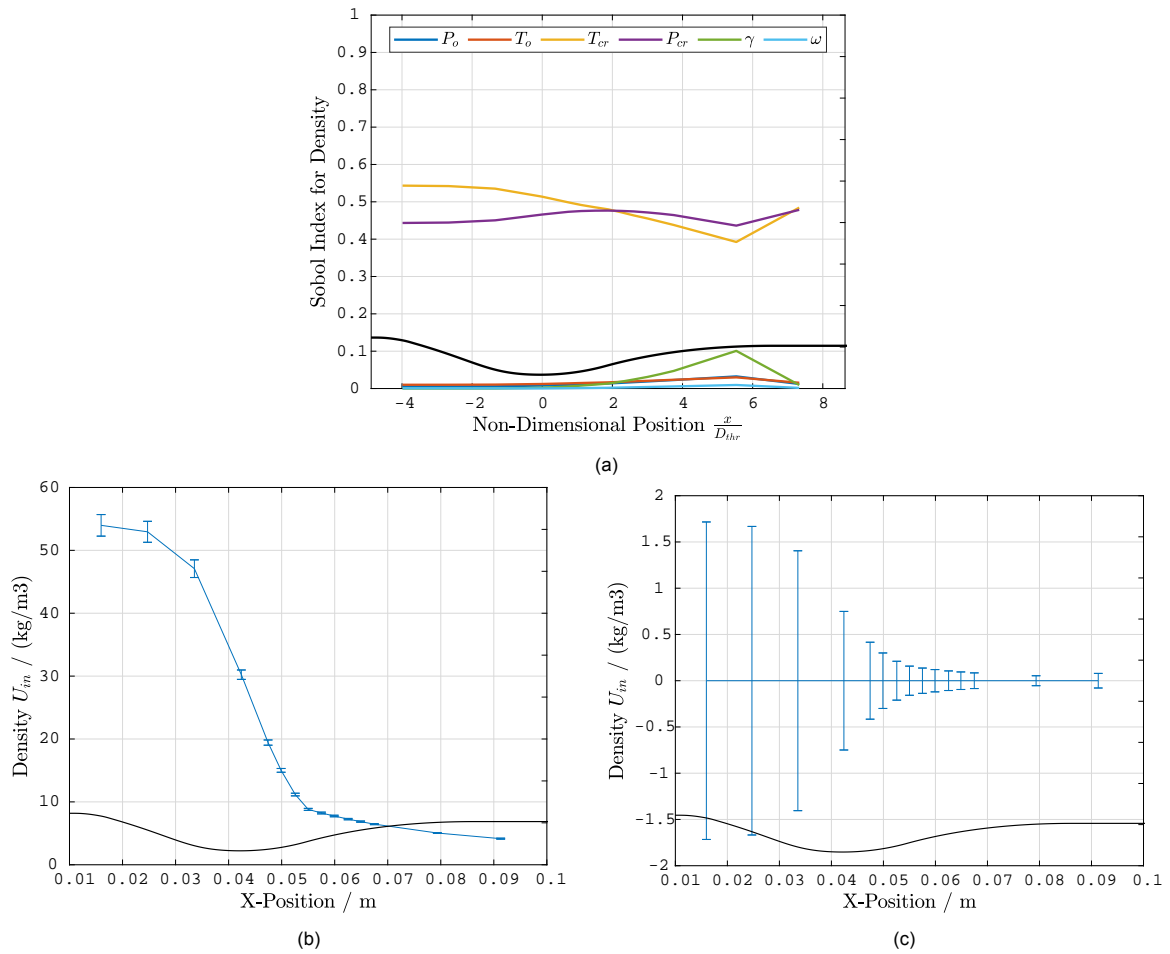


Figure D.8: PR.027-NT.001 Nozzle Profile: UQ Results for Density. **a)** Sobol Indices using Peng Robinson EoS. **b)** Response with uncertainty bars using Peng Robinson EoS. **c)** Plot of U_{in} vs location.

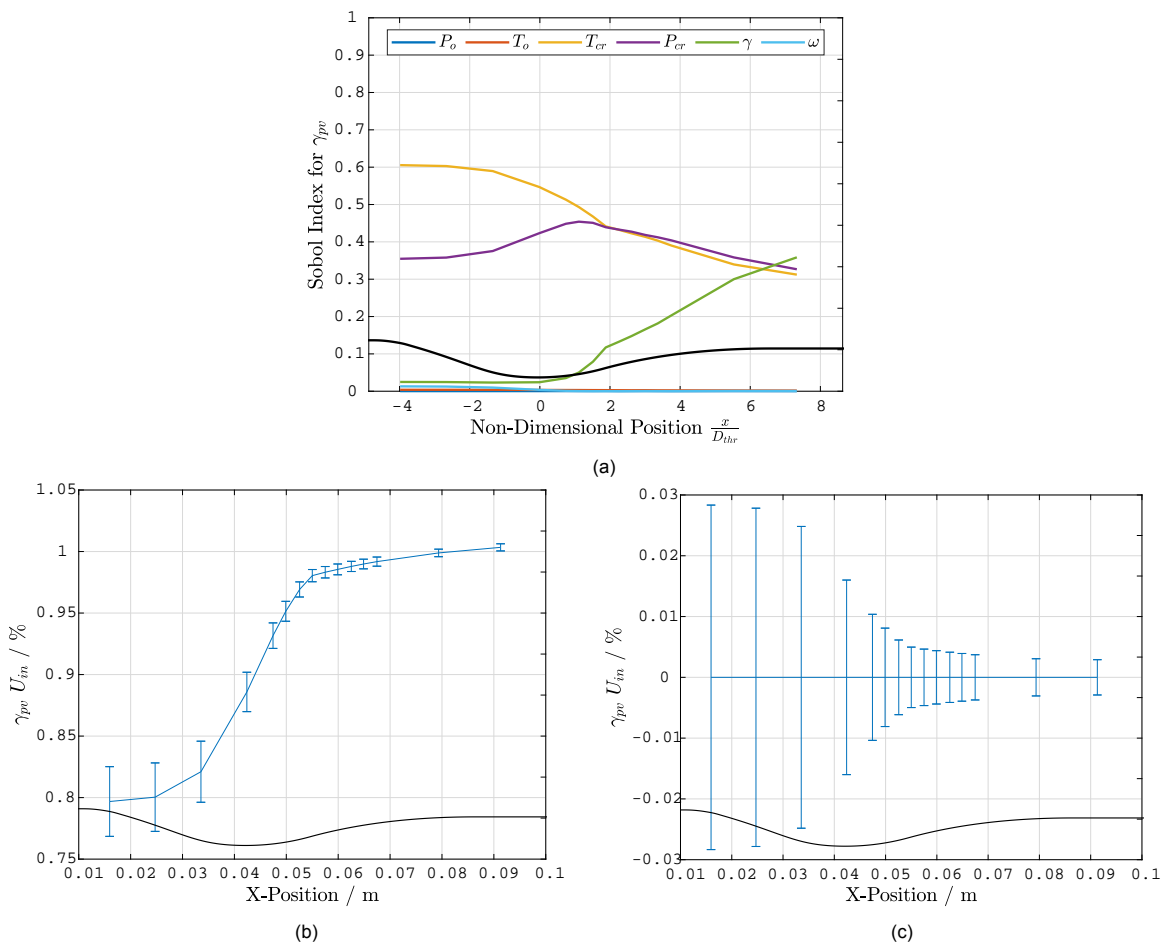


Figure D.9: PR.027-NT.001 Nozzle Profile: UQ Results for γ_{pv} . **a)** Sobol Indices using Peng Robinson EoS. **b)** Response with uncertainty bars using Peng Robinson EoS. **c)** Plot of U_{in} vs location.

D.3. Validation

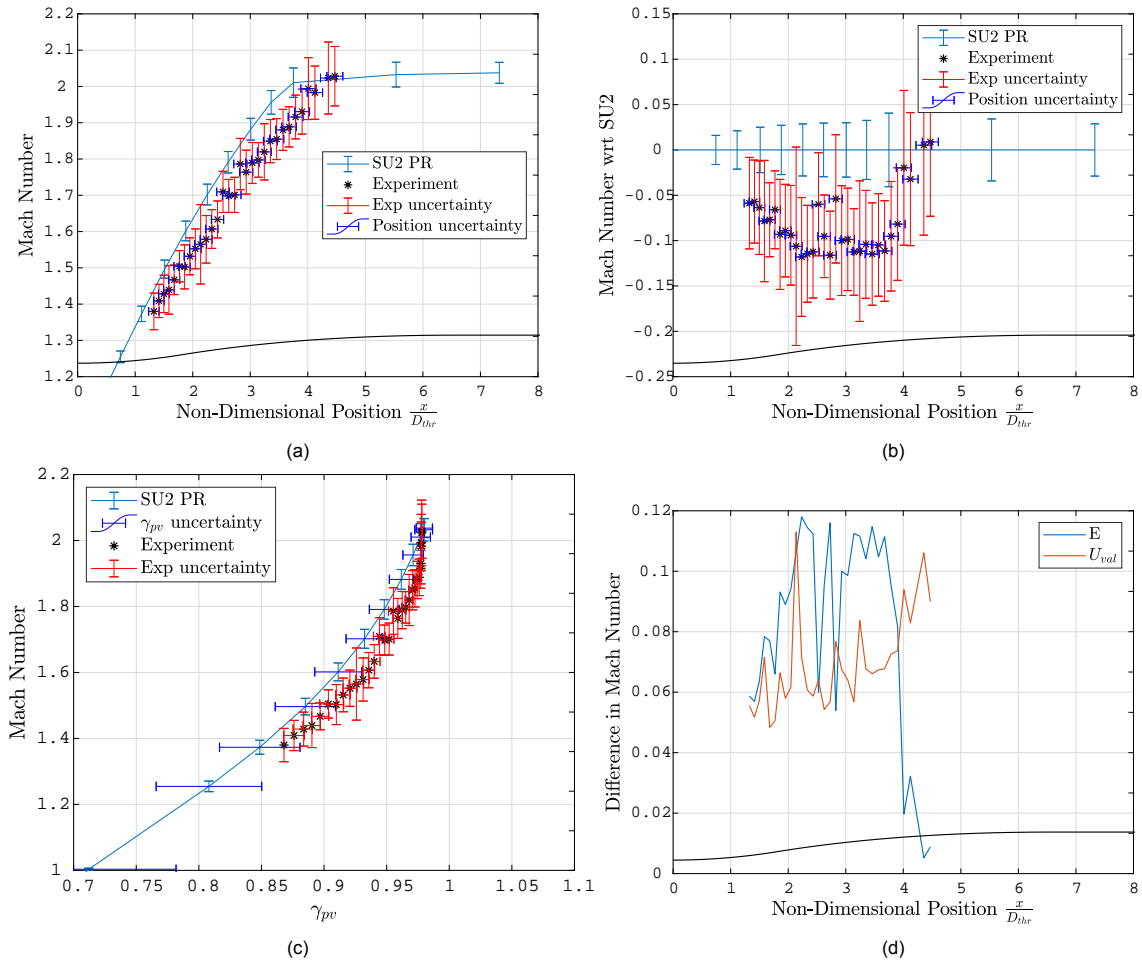


Figure D.10: Validation plots of Mach number for a converging-diverging nozzle modelled in SU2 using the compressible Euler equations and the Peng-Robinson EoS. The test case is described in Sec. 3.2 and the model definition summarised in Sec 3.3. The mean simulation results along the nozzle centreline are compared against the mean ORCHID PR.025-NT.002 schlieren data. **a)** Mach number as a function of nozzle position non-dimensionalised with respect to the throat height. **b)** Mach number with respect to the SU2 model mean simulation value as a function of nozzle location non-dimensionalised with respect to the throat height. This is a version of the real space metric. **c)** Mach number as a function of polytropic exponent γ_{pv} . **d)** ASME V&V 20 validation metric plot of Mach number as a function of nozzle position non-dimensionalised with respect to the throat height.

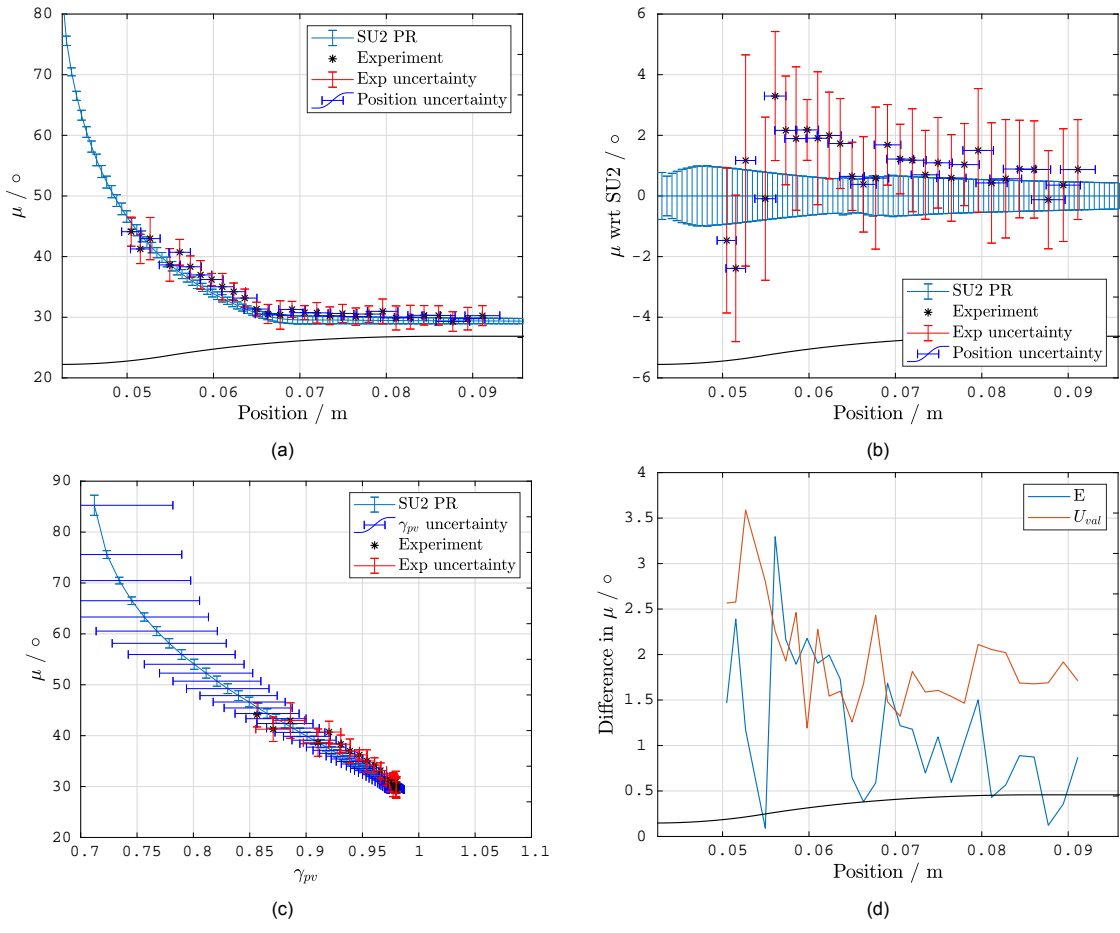


Figure D.11: PR.025-NT.001: Comparison of the measured μ angle along the centreline of the nozzle test section and the SU2 simulated value. **a)** Absolute Value of μ vs nozzle position. **b)** μ with respect to the SU2 model mean simulation value as a function of nozzle location non-dimensionalised with respect to the throat height. This is a version of the real space metric. **c)** Absolute Value of μ as a function of polytopic exponent γ_{pv} . **d)** ASME V&V 20 validation metric plot of μ as a function of nozzle position.

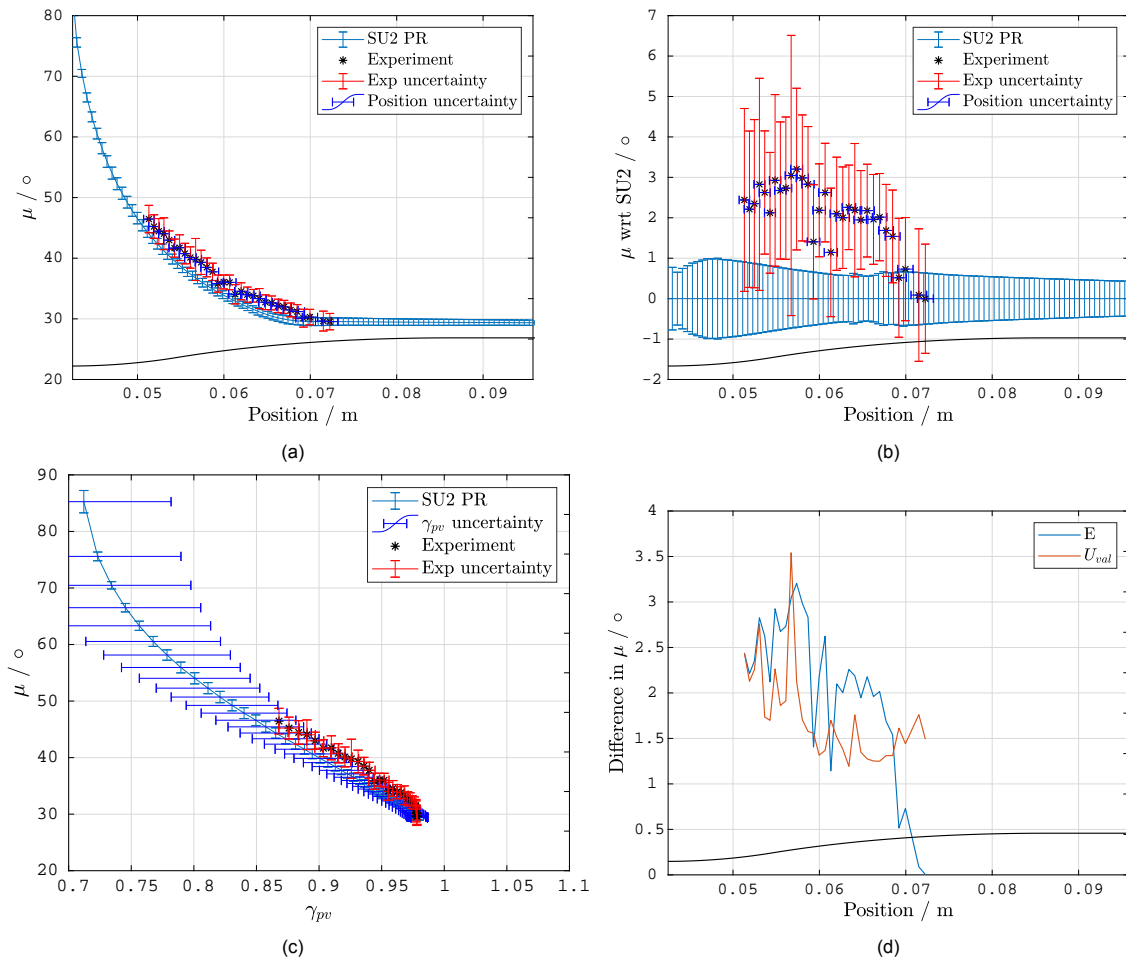
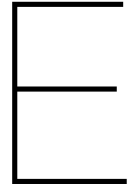


Figure D.12: PR.025-NT.002: Comparison of the measured μ angle along the centreline of the nozzle test section and the SU2 simulated value. **a)** Absolute Value of μ vs nozzle position. **b)** μ with respect to the SU2 model mean simulation value as a function of nozzle location non-dimensionalised with respect to the throat height. This is a version of the real space metric. **c)** Absolute Value of μ as a function of polytopic exponent γ_{pv} . **d)** ASME V&V 20 validation metric plot of μ as a function of nozzle position.



Detailed UQ Code Structure

The UQ was done with a third order polynomial chaos stochastic collocation method with Smolyak sparse grid sampling, done using Dakota version 6.11 [1] on a Linux Ubuntu 16.04 LTS operating system. Python 2.7 was used as the interface with additional MATLAB Shock wave calculation based on Euler relations as was done by Iyer [38] and Head [35]. The flow chart of the process is shown in Fig. 4.1. Before running the UQ the Dakota input file, SU2 configuration, Python scripts, and MATLAB scripts must be complete. The software listed in App. F must also be installed before running the code. The code for the thesis is found in a folder called "Bills2020_Thesis_Code" which includes a full list of the scripts. It is arranged in folders corresponding to thesis sections, and Readme files accompany each section. For access to the code please contact Adam Head. The connections between the scripts are highlighted in Figs. E.1, E.2, E.3, and E.4.

Note that there are hard coded library addresses are in some versions of the ORCHIDNozzle_UQ.py and the FPPython.py scripts. These need to be customised for the machine of interest. When running layers of python and operating systems there may be times when the references to the libraries break. The most robust way is thus to have the addresses hard coded for the UQ. However this makes it difficult to move between infrastructures.

Numerical Uncertainty Calculation Infrastructure

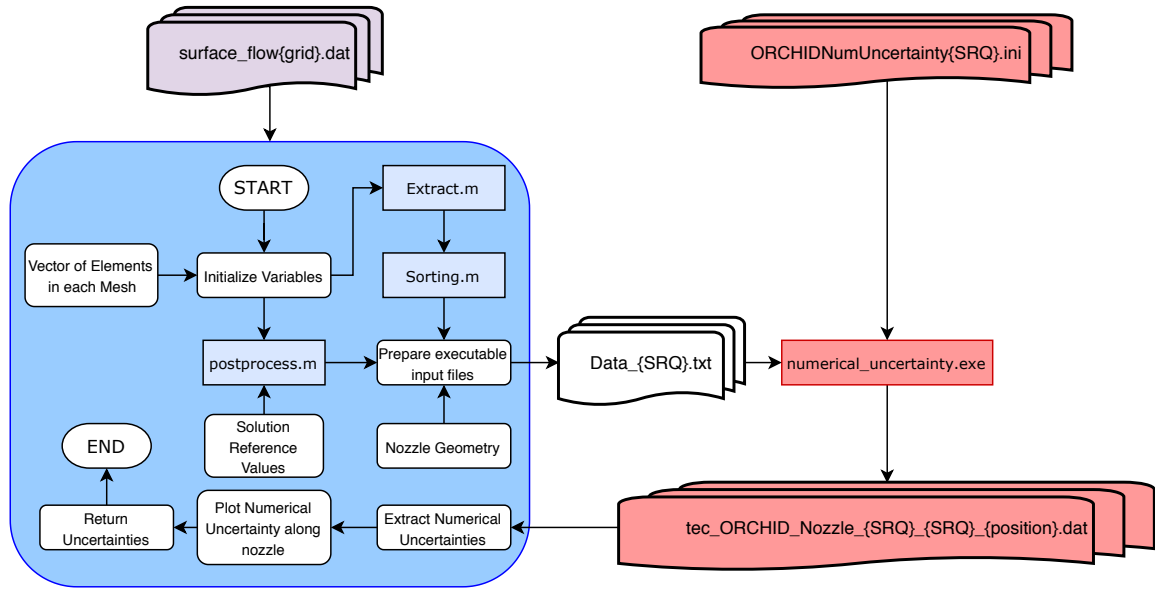


Figure E.1: Flow chart of 'NumericalUncertainty.m'. The numerical uncertainty calculations which integrates the SU2 solutions with the Richardson extrapolation. The executable code from Refresco is in red, while the MatLab scripts are in blue. The solutions from each grid must be complete before the code is used.

Forward UQ Infrastructure

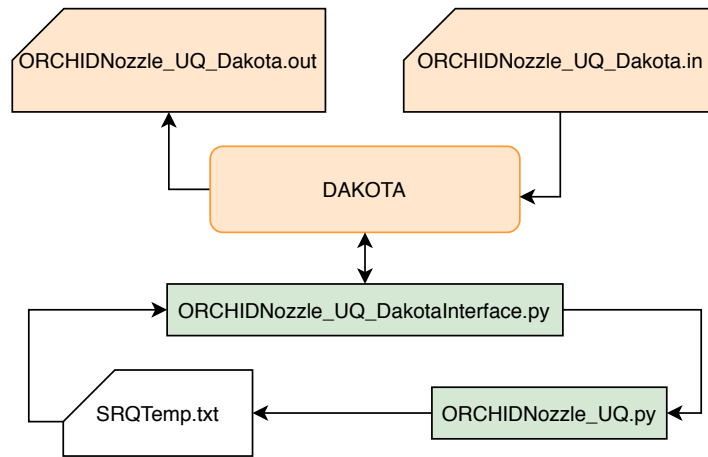


Figure E.2: Top level of the UQ infrastructure. The Dakota input file must be configured, then when Dakota is run the python scripts are called automatically. Dakota selects the inputs for the simulation and provides them to the ORCHID nozzle analysis.

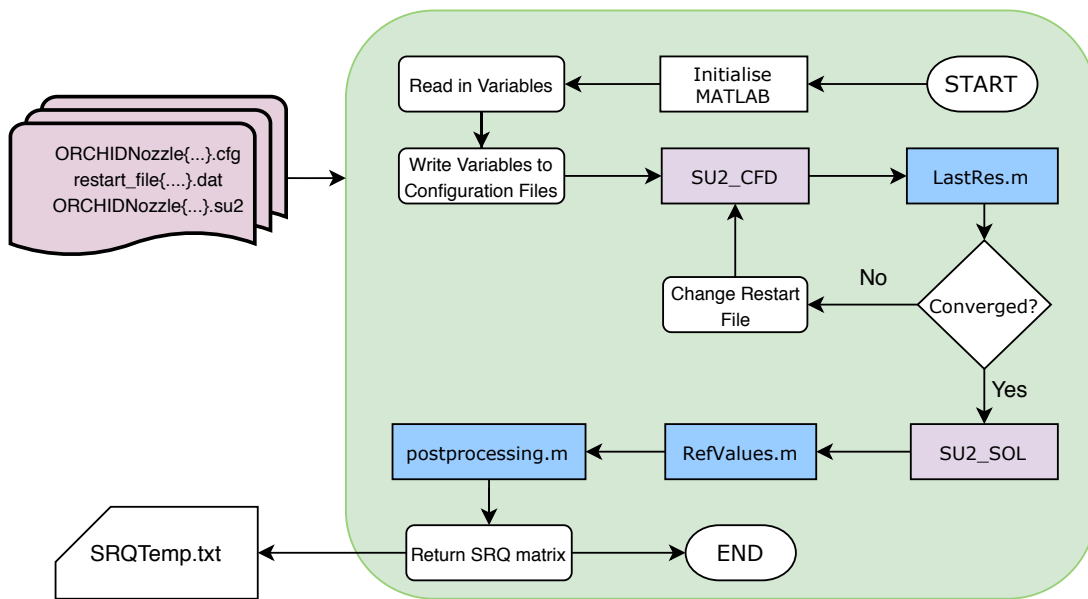


Figure E.3: Mid-level UQ infrastructure: 'ORCHIDNozzle_UQ.py'. The script is run on every evaluation of the SU2 solution. The Python script is called by Dakota to run SU2 and postprocess the results. A unique solution for the ORCHID nozzle simulation is produced for the set of input variables passed into the code by Dakota. The script can be run independently for a single run and analysis of the nozzle model.

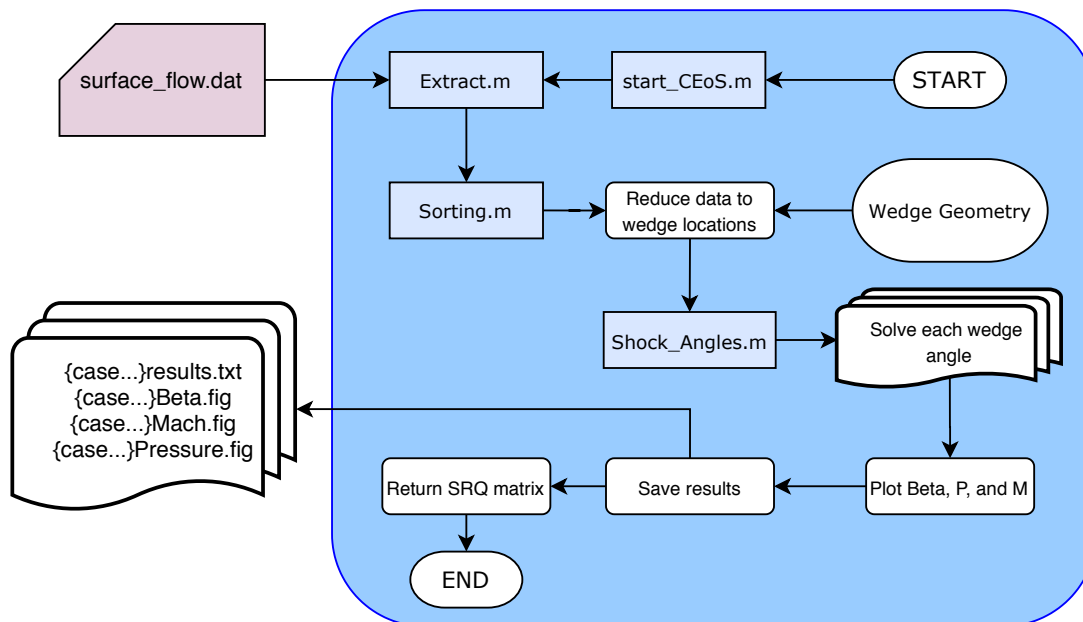


Figure E.4: Bottom level UQ infrastructure: 'postprocess.m'. The post-processing framework for shock solving and data storage of the SU2 solution. This code can be run independently to extract the SRQ of interest from an SU2 solution file and present them in a txt file and figures. Producing figures is not done on every loop of a UQ, but can be done for analysis of a single SU2 solution.

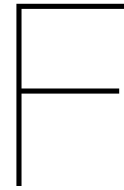
PR.025-NT.001 with iPRSV EoS UQ Input

There are nine uncertain variables, seven thermodynamic and two flow variables in the model created for PR.025-NT.001 with iPRSV EoS. The variables are listed in Tab. E.1. Uniform distributions are assumed since there is not enough experimental data to extrapolate a full normal distribution.

Parameter	Uncertainty	Assumed Distribution
$T_o / ^\circ\text{C}$	0.729	normal
P_o / Pa	3511	normal
$T_{cr} / ^\circ\text{C}$	3%	uniform
P_{cr} / Pa	5%	uniform
ω	15%	uniform
k_1	15%	uniform
η_1	3%	uniform
η_2	3%	uniform
η_3	3%	uniform

Table E.1: Input uncertainties used for the PR.025-NT.001 iPRSV UQ.

The boundary conditions, T_o and P_o , include the Type A and Type B uncertainties from the experiment. The back pressure is treated as deterministic due to the physics of a supersonic expansion. The potential uncertainty due to geometry is neglected due to machine tolerances being high, and precise measurements of the facility. The thermodynamic constant uncertainties are directly taken from the work of Colonna et al. [17], however the uncertainty of γ is not reported and had to be calculated from the C_p uncertainty by using Eqn. 3.6. Cinnella et al. [14] reports $\pm 3\%$ uncertainty of C_p over the temperature range of the ORCHID experiments, thus was used as a reference to estimate the η uncertainties. The acentric factor and κ_1 have no reported uncertainty except for Iyer [38] who reports 15% uncertainty with no effect on the system responses. However, since the model used in the thesis is different from the one reported here, the same 15% value is taken and treated as uncertain.



List of Equipment

Hardware

The final UQ studies were done on a machine with 20 physical dual core processors (2 x Intel(R) Xeon(R) CPU E5-2687W v3 @ 3.10 GHz) and 64 Gb of Ram.

Software

SU2 version 3.2.8 "eagle" is used to model the simulation of the nozzle test section of the ORCHID with MM working fluid. Once set with boundary conditions to match those of the ORCHID from the experiments this model can be analysed and compared against the experiments to evaluate the validity of SU2 for NICFD. The exact branch of SU2 used for the validation study is '*feature_fluidprop*' committed to GitHub on Feb 3, 2016.

In *feature_fluidprop* the EoS is provided either with internal implementations or a link to FluidProp coded by Colonna et al. [19]. FluidProp is a software developed by TUD which is now controlled by Asimptote for thermodynamic calculations. It has different thermodynamic equations of state internally coded, including iPRSV and the SW form for MM. Version 3.2.354 of the software is used for interfacing with SU2.

Dakota was custom built from source code enabling the Python add-in: see 'BuildDakotaCustom.cmake' in the supporting code folder "Bills2020_Thesis_Procedures". This folder also contains the installation procedure and method to run the validation codes.

Linux	Ubuntu 16.04.6 LTS
SU2	3.2.8 "eagle" <i>feature_fluidprop</i> (6.2.0 installed)
FluidProp	Linux 3.2.354
umg2	mcrv.exe; bgrid.exe; umg2d.exe; hybsd.exe
Tecplot	360ex2018r1
Dakota	6.11.0 src-UI
Refresco V&V	2018.1.0-x64 windows
Python	2.7
MATLAB	2018b
MATLAB	9.5
Simulink	9.2
Parallel Computing	6.13
Partial Differentiation Toolbox	3.1
Statistics and Machine Learning	11.4
Symbolic Math	8.2
Optimization Toolbox	8.2



Configuration Files

SU2 iPRSV Configuration for PR25

```
%%%%%%%%%%%%%%%%%%%%%%%%%%%%%%%%%%%%%%%%%%%%%%%%%%%%%%%%%%%%%%%%%%%%%%%%%  
%  
% SU2 configuration file %  
% Case description: ORCHID Nozzle PR.25: Siloxane MM Euler using StanMix iPRSV %  
% Author: Liam Bills %  
% Institution: Technical University of DELFT %  
% Date: 6 March 2020 %  
% File Version 3.2.8.3 "eagle" %  
%  
%%%%%%%%%%%%%%%%%%%%%%%%%%%%%%%%%%%%%%%%%%%%%%%%%%%%%%%%%%%%%%%%%%%%%%%%%  
  
% ----- DIRECT, ADJOINT, AND LINEARIZED PROBLEM DEFINITION -----%  
PHYSICAL_PROBLEM= EULER  
KIND_TURB_MODEL= NONE  
MATH_PROBLEM= DIRECT  
RESTART_SOL= YES  
REGIME_TYPE= COMPRESSIBLE  
SYSTEM_MEASUREMENTS= SI  
  
% ----- COMPRESSIBLE FREE-STREAM DEFINITION -----%  
MACH_NUMBER= 0.3  
AoA= 0.0  
INIT_OPTION= TD_CONDITIONS  
FREESTREAM_OPTION= TEMPERATURE_FS  
FREESTREAM_PRESSURE= 1000000  
FREESTREAM_TEMPERATURE= 515.85  
  
% ----- REFERENCE VALUE DEFINITION -----%  
REF_PRESSURE= 1000000  
REF_TEMPERATURE= 515.85  
REF_DENSITY= 48.9223  
  
% ---- IDEAL GAS, POLYTROPIC, VAN DER WAALS AND PENG ROBINSON CONSTANTS -----%  
FLUID_MODEL= FLUIDPROP  
FLUID_SUBLIBRARY= StanMix  
FLUID_N_COMPONENTS= 1  
FLUID_COMPONENTS= (MM)  
FLUID_MOLE_FRACS= ( 1.00)  
FLUID_SINGLE_PHASE_ONLY = YES  
  
% ----- THERMAL CONDUCTIVITY MODEL -----%  
CONDUCTIVITY_MODEL= CONSTANT_PRANDTL  
KT_CONSTANT= 0.0257  
  
% ----- BOUNDARY CONDITION DEFINITION -----%  
MARKER_EULER=( wall1 )
```

```

MARKER_SYM= ( symmetry )
MARKER_PLOTTING= ( symmetry, wall1 )
INLET_TYPE= TOTAL_CONDITIONS
MARKER_RIEMANN= ( inflow , TOTAL_CONDITIONS_PT, 1836000, 525.85 , 1.0 , 0.0 , 0.0 , ...
outflow , STATIC_PRESSURE, 206000, 0.0 , 0.0 , 0.0 , 0.0 )

% ----- COMMON PARAMETERS DEFINING THE NUMERICAL METHOD -----%
NUM_METHOD GRAD= WEIGHTED_LEAST_SQUARES
CFL_NUMBER= 40.0
CFL_ADAPT= NO
MAX_DELTA_TIME= 1E6
RK_ALPHA_COEFF= ( 0.66667 , 0.66667 , 1.000000 )

% ----- SLOPE LIMITER DEFINITION -----%
REF_ELEM_LENGTH= 0.1
LIMITER_COEFF= 0.3
LIMITER_ITER= 999999

% ----- LINEAR SOLVER DEFINITION -----%
LINEAR_SOLVER= FGMRES
LINEAR_SOLVER_PREC= LU_SGS
LINEAR_SOLVER_ERROR= 1E-4
LINEAR_SOLVER_ITER= 5

% ----- MULTIGRID PARAMETERS -----%
MGLEVEL= 0

% ----- FLOW NUMERICAL METHOD DEFINITION -----%
CONV_NUM_METHOD_FLOW= ROE
SPATIAL_ORDER_FLOW= 2ND_ORDER
SLOPE_LIMITER_FLOW= VENKATAKRISHNAN
ENTROPY_FIX_COEFF= 0.1
AD_COEFF_FLOW= ( 0.15 , 0.5 , 0.02 )
VISCOUS_LIMITER_FLOW= NO
TIME_DISCRE_FLOW= EULER_IMPLICIT
RELAXATION_FACTOR_FLOW= 1.0

% ----- HEAT NUMERICAL METHOD DEFINITION -----%
THERMAL_DIFFUSIVITY= 1.0

% ----- CONVERGENCE PARAMETERS -----%
EXT_ITER= 10000
CONV_CRITERIA= RESIDUAL
RESIDUAL_REDUCTION= 7
RESIDUAL_MINVAL= -16
STARTCONV_ITER= 10
CAUCHY_ELEMS= 100
CAUCHY_EPS= 1E-10
CAUCHY_FUNC_FLOW= DRAG
CAUCHY_FUNC_ADJFLOW= SENS_GEOMETRY

% ----- INPUT/OUTPUT INFORMATION -----%
MESH_FILENAME= ORCHIDNozzle10K.su2
MESH_FORMAT= SU2
MESH_OUT_FILENAME= mesh_out.su2
SOLUTION_FLOW_FILENAME= restart_flow.dat
OUTPUT_FORMAT= TECPLOT
CONV_FILENAME= history
BREAKDOWN_FILENAME= forces_breakdown.dat
RESTART_FLOW_FILENAME= restart_flow.dat
VOLUME_FLOW_FILENAME= flow
SURFACE_FLOW_FILENAME= surface_flow
WRT_SOL_FREQ= 1000
WRT_SOL_FREQ_DUALTIME= 1
WRT_CON_FREQ= 1
WRT_CON_FREQ_DUALTIME= 10
WRT_RESIDUALS= YES
WRT_LIMITERS= NO
WRT_SHARPEDES= NO
LOW_MEMORY_OUTPUT= NO
CONSOLE_OUTPUT_VERBOSITY= HIGH

```

SU2 Peng-Robinson Configuration for PR27

```

%%%%%%%%%%%%%%%%%%%%%%%%%%%%%%%%%%%%%%%%%%%%%%%%%%%%%%%%%%%%%%%%%%%%%%%%
%
% SU2 configuration file
% Case description: ORCHID Nozzle PR.27: Siloxane MM Euler using Peng Robinson
% Author: Liam Bills
% Institution: Technical University of DELFT
% Date: 6 March 2020
% File Version 3.2.8.3 "eagle"
%
%%%%%%%%%%%%%%%%%%%%%%%%%%%%%%%%%%%%%%%%%%%%%%%%%%%%%%%%%%%%%%%%%%%%%%%%

% ----- DIRECT, ADJOINT, AND LINEARIZED PROBLEM DEFINITION -----%
PHYSICAL_PROBLEM= EULER
KIND_TURB_MODEL= NONE
MATH_PROBLEM= DIRECT
RESTART_SOL= YES
REGIME_TYPE= COMPRESSIBLE
SYSTEM_MEASUREMENTS= SI

% ----- COMPRESSIBLE FREE-STREAM DEFINITION -----%
MACH_NUMBER= 0.3
AoA= 0.0
INIT_OPTION= TD_CONDITIONS
FREESTREAM_OPTION= TEMPERATURE_FS
FREESTREAM_PRESSURE= 600000
FREESTREAM_TEMPERATURE= 515.85

% ----- REFERENCE VALUE DEFINITION -----%
REF_PRESSURE= 600000
REF_TEMPERATURE= 515.85
REF_DENSITY= 26.0436

% ---- IDEAL GAS, POLYTROPIC, VAN DER WAALS AND PENG ROBINSON CONSTANTS -----%
FLUID_MODEL= PR_GAS
GAMMA_VALUE= 1.02605
GAS_CONSTANT= 51.2
CRITICAL_TEMPERATURE= 518.7
CRITICAL_PRESSURE= 1939000.0
ACENTRIC_FACTOR= 0.419

% ----- THERMAL CONDUCTIVITY MODEL -----%
CONDUCTIVITY_MODEL= CONSTANT_PRANDTL
KT_CONSTANT= 0.0257

% ----- BOUNDARY CONDITION DEFINITION -----%
MARKER_EULER=( wall1 )
MARKER_SYM= ( symmetry )
MARKER_PLOTTING= ( symmetry, wall1 )
INLET_TYPE= TOTAL_CONDITIONS
MARKER_RIEMANN= (inflow , TOTAL_CONDITIONS_PT, 1122000.0 , 526.02 , 1.0 , 0.0 , 0.0 , ...
outflow , STATIC_PRESSURE, 108000, 0.0 , 0.0 , 0.0 , 0.0)

% ----- COMMON PARAMETERS DEFINING THE NUMERICAL METHOD -----%
NUM_METHOD_GRAD= WEIGHTED_LEAST_SQUARES
CFL_NUMBER= 20
CFL_ADAPTE= NO
MAX_DELTA_TIME= 1E6
RK_ALPHA_COEFF= ( 0.66667 , 0.66667 , 1.000000 )

% ----- SLOPE LIMITER DEFINITION -----%
LIMITER_COEFF= 0.3
LIMITER_ITER= 999999

% ----- LINEAR SOLVER DEFINITION -----%
LINEAR_SOLVER= FGMRES
LINEAR_SOLVER_PREC= LU_SGS
LINEAR_SOLVER_ERROR= 1E-4

```

```
LINEAR_SOLVER_ITER= 5

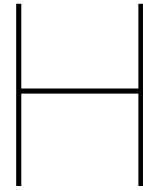
% ----- MULTIGRID PARAMETERS -----%
MGLEVEL= 0

% ----- FLOW NUMERICAL METHOD DEFINITION -----%
CONV_NUM_METHOD_FLOW= ROE
SPATIAL_ORDER_FLOW= 2ND_ORDER
SLOPE_LIMITER_FLOW= VENKATAKRISHNAN
ENTROPY_FIX_COEFF= 0.1
AD_COEFF_FLOW= ( 0.15, 0.5, 0.02 )
VISCOSUS_LIMITER_FLOW= NO
TIME_DISCRE_FLOW= EULER_IMPLICIT
RELAXATION_FACTOR_FLOW= 1.0

% ----- HEAT NUMERICAL METHOD DEFINITION -----%
THERMAL_DIFFUSIVITY= 1.0

% ----- CONVERGENCE PARAMETERS -----%
EXT_ITER= 5000
CONV_CRITERIA= RESIDUAL
RESIDUAL_REDUCTION= 7
RESIDUAL_MINVAL= -16
STARTCONV_ITER= 10
CAUCHY_ELEMS= 100
CAUCHY_EPS= 1E-10
CAUCHY_FUNC_FLOW= DRAG

% ----- INPUT/OUTPUT INFORMATION -----%
MESH_FILENAME= ORCHIDNozzle10K.su2
MESH_FORMAT= SU2
MESH_OUT_FILENAME= mesh_out.su2
SOLUTION_FLOW_FILENAME= restart_flow.dat
OUTPUT_FORMAT= TECPLOT
CONV_FILENAME= history
BREAKDOWN_FILENAME= forces_breakdown.dat
RESTART_FLOW_FILENAME= restart_flow.dat
VOLUME_FLOW_FILENAME= flow
SURFACE_FLOW_FILENAME= surface_flow
WRT_SOL_FREQ= 100
WRT_SOL_FREQ_DUALTIME= 1
WRT_CON_FREQ= 10
WRT_CON_FREQ_DUALTIME= 10
WRT_RESIDUALS= YES
WRT_LIMITERS= NO
WRT_SHARPEDGES= NO
LOW_MEMORY_OUTPUT= NO
CONSOLE_OUTPUT_VERBOSITY= HIGH
```



Tips for Converging NICFD SU2 Simulations

NICFD simulations are occasionally challenging due to the complex thermodynamic relations. Some tips for ensuring a solution converges are listed below.

- Use Non-Dimensional solution with respect to the free-stream. This reduced truncation errors.
- Initialise the free-stream with average values instead of the boundary conditions. Large gradients are difficult to numerically resolve.
- The reference values which are used to dimensionalise the results are given in the preamble of SU2 upon starting the solver. Confirm these values are as expected.
- Use the 2nd order limited with van albada if non-polytropic simulations are desired.
- There is a strange occurrence for certain combinations of inputs where the SU2 run stops before it should. This was fixed by playing with the output frequency of the convergence history.
- Simulations with StanMix iPRSV for some cases cannot always be started. If there is problems at the beginning of the simulation use a restart file, for example from a RefProp solution. StanMix iPRSV has a limited range and can cause the solution to diverge if the initial guess of temperature and pressure are outside this range.
- **RANS simulations:** For the nozzle flow the boundary layer needs to be made thicker, however to capture the fully developed boundary layer by the outlet of the nozzle the thickness is very large. For UMG2 this means the body mesh needs to be very coarse, otherwise the hybridisation gives an error. A solution may be to reduce the nozzle outlet length, or use a different mesh generator.
- **RANS simulations:** The hypothesised reason that the the RANS does not converge beyond two orders of magnitude is that the boundary layer grows beyond the boundary layers created in the mesh. But this only occurs at the outlet section.

Bibliography

- [1] B. M. Adams, M. S. Eldred, G. Geraci, R.W. Hooper, J. D. Jakeman, K.A. Maupin, Monschke J.A., A.A. Rushdi, J. A. Stephens, L. P. Swiler, T. M. Wildey, W.J. Bohnhoff, K.A. Dalbey, M.S. Ebeida, J.P. Eddy, P.D. Hough, Khalil M., K.T. Hu, E.M. Ridgeway, D.M. Vigil, and J.G. Winokur. Dakota, A Multilevel Parallel Object-Oriented Framework for Design Optimization, Parameter Estimation, Uncertainty Quantification, and Sensitivity Analysis: Version 6.10 User's Manual. Technical Report SAND2014-4633, Sandia National Laboratories, 2019. URL <http://dakota.sandia.gov>.
- [2] Fouad A. Aly and Lloyd L. Lee. Self-consistent equations for calculating the ideal gas heat capacity, enthalpy, and entropy. *Fluid Phase Equilibria*, 6(3):169 – 179, 1981. ISSN 0378-3812. doi: [https://doi.org/10.1016/0378-3812\(81\)85002-9](https://doi.org/10.1016/0378-3812(81)85002-9).
- [3] American Institute of Aeronautics and Astronautics (AIAA). *Guide for the Verification and Validation of Computational Fluid Dynamics Simulations*. AIAA G-077-1998, 1998. ISBN 978-1-56347-285-5. Pg.
- [4] American Society of Mechanical Engineers (ASME). Standard for Verification and Validation in Computational Fluid Dynamics and Heat Transfer. Technical Report V&V20-2009, ASME, 2009. Pg.
- [5] American Society of Mechanical Engineers (ASME). Test Uncertainty. Technical Report PTC 19.1, ASME, 2013.
- [6] N. Anand. Supersonic turbine design using method of characteristics. Master's thesis, Delft University of Technology, 2016.
- [7] J.D. Anderson. *Modern Compressible Flow: With Historical Perspective*. Aeronautical and Aerospace Engineering Series. McGraw-Hill Education, 2003. ISBN 9780072424430.
- [8] J.D. Anderson. *Fundamentals of Aerodynamics*. McGraw-Hill Education, 2010. ISBN 9780073398105.
- [9] F. Beltrame. Accuracy assessment of the su2 flow solver for non-ideal organic vapor supersonic expansions using experimental data. Master's thesis, Politecnico di Torino, 2020.
- [10] Klaus Brun, Peter Friedman, and Richard Dennis, editors. *Fundamentals and Applications of Supercritical Carbon Dioxide (sCO₂) Based Power Cycles*. Woodhead Publishing, 2017. ISBN 978-0-08-100804-1. doi: <https://doi.org/10.1016/B978-0-08-100804-1.00010-4>.
- [11] Ting Horng Chung, Lloyd L. Lee, and Kenneth E. Starling. Applications of kinetic gas theories and multiparameter correlation for prediction of dilute gas viscosity and thermal conductivity. *Industrial & Engineering Chemistry Fundamentals*, 23(1):8–13, 1984. doi: 10.1021/i100013a002.
- [12] Ting Horng Chung, Mohammad Ajlan, Lloyd L. Lee, and Kenneth E. Starling. Generalized multiparameter correlation for nonpolar and polar fluid transport properties. *Industrial & Engineering Chemistry Research*, 27(4):671–679, 1988. doi: 10.1021/ie00076a024.
- [13] P. Cinnella, P.M. Congedo, L. Parussini, and V. Pediroda. Quantification of uncertainties in compressible flows with complex thermodynamic behavior. In *Proceedings of 19th AIAA Computational Fluid Dynamics*, San Antonio, Texas, June 22-25 2009. AIAA.
- [14] P. Cinnella, P.M. Congedo, V. Pediroda, and L. Parussini. Sensitivity analysis of dense gas flow simulations to thermodynamic uncertainties. *Physics of Fluids*, 23, 2011.
- [15] H. W. Coleman and W. G. Steele. *Experimentation, Validation, and Uncertainty Analysis for Engineers*. John Wiley & Sons, Inc., third edition, 2009. pg.

- [16] H. W. Coleman and F. Stern. Uncertainties and CFD Code Validation. *Journal of Fluids Engineering*, 119(4):795 – 803, December 1997. (Also “Discussion and Authors’ Closure,” Vol. 120, Sept. 1998, pp. 635–636.). Pg.
- [17] P. Colonna, N. R. Nannan, A. Guardone, and E. W. Lemmon. Multiparameter equations of state for selected siloxanes. *Fluid Phase Equilibria*, 244(2):193–211, 2006.
- [18] P. Colonna, N. R. Nannan, and A. Guardone. Multiparameter equations of state for siloxanes: $[(\text{CH}_3)_3\text{-Si-O}_{1/2}]_2\text{-[O-Si-(CH}_3)_2]_{i=1,\dots,3}$ and $[\text{O-Si-(CH}_3)_2]_6$. *Fluid Phase Equilibria*, 263(2): 115–130, 2008.
- [19] P. Colonna, T. P. van der Stelt, and A. Guardone. FluidProp (version 3.0): A program for the estimation of thermophysical properties of fluids, 2012.
- [20] P. M. Congedo. *Contributions to the reliability of numerical simulations in fluid mechanics. Application to the flow simulation of thermodynamically complex gases*. PhD thesis, University of Bordeaux, 2013.
- [21] D. Dijkshoorn. Simulation of two dimensional steady state boundary layer effects applied to non-ideal gas flows. Master’s thesis, Delft University of Technology, 2020.
- [22] L. Eça and M. Hoekstra. A procedure for the estimation of the numerical uncertainty of CFD calculations based on grid refinement studies. *Journal of Computational Physics*, 262:104 – 130, 2014. ISSN 0021-9991. Pg.
- [23] L. Eça, G. Vaz, and M. Hoekstra. Code Verification, Solution Verification and Validation in RANS Solvers. In *ASME 2010 29th International Conference on Ocean, Offshore and Arctic Engineering*, pages 597–605, 2010. pg.
- [24] L. Eça, G. Vaz, A. Koop, F. Pereira, and H. Abreu. Validation: What, why and how. In *Proceedings of ASME 35rd International Conference on Ocean, Offshore and Arctic Engineering*, Busan, South Korea, June 19-25 2016. ASME.
- [25] T.D. Economon, F. Palacios, S.R. Copeland, T.W. Lukaczyk, and J.J. Alonso. Su2: An open-source suite for multiphysics simulation and design. *AIAA Journal*, 54:828–846, 2016.
- [26] D.R. Eklund, V.J. Romero, J.A. Pearce, Keim N.S., and U.B. (Ed) Mehta. Simulation credibility: Advances in verification, validation, and uncertainty quantification. Technical Report TP-2016-219422 & GL-2016-0001, NASA & JANNAF, 2016.
- [27] G.H.J. Florussen, H.A.M. Spaan, and T.M. Spaan-Burke. Assessing the accuracy of five axis machines by comparing machine measurement data with test work piece deviations. *Procedia Manufacturing*, 6:25 – 32, 2016. ISSN 2351-9789. doi: <https://doi.org/10.1016/j.promfg.2016.11.004>. URL <http://www.sciencedirect.com/science/article/pii/S2351978916301408>. 16th Machining Innovations Conference for Aerospace Industry - MIC 2016.
- [28] A. Ghidoni, E. Pelizzari, S. Rebay, and V. Selmin. 3d anisotropic unstructured grid generation. *International Journal for Numerical Methods in Fluids*, 51(9–10):1097–1115, 2006. doi: 10.1002/flid.1151. URL <https://onlinelibrary.wiley.com/doi/abs/10.1002/flid.1151>.
- [29] G. Gori, M. A. Zocca, G. Cammi, A. Spinelli, and A. Guardone. Experimental assessment of the open-source su2 suite for orc applications. *Energy Procedia*, 129:256–263, 2017. ISSN 1876-6102.
- [30] G. Gori, M. A. Zocca, G. Cammi, Spinelli, P. M. Congedo, and A. Guardone. Accuracy assessment of the non-ideal computational fluid dynamics model for siloxane mdm from the open-source su2 suite. *European Journal of Mechanics / B Fluids*, 79:109–120, 2020. ISSN 0997-7546.
- [31] E.M. Greitzer, C.S. Tan, and M.B. Graf. *Internal Flow: Concepts and Applications*. Cambridge Engine Technology Series. Cambridge University Press, 2007. ISBN 9781139451116.

- [32] B. Grossman. Fundamental concepts of real gasdynamics. Technical report, Virginia Tech, January 2000.
- [33] A. Head, C. De Servi, E. Casati, M. Pini, and P. Colonna. Preliminary design of the ORCHID: A facility for studying non-ideal compressible fluid dynamics and testing ORC expanders. *ASME Turbo Expo*, GT2016-56103:14, 2016. pg.
- [34] A. J. Head. *Novel Experiments for the Investigation of Non-Ideal Compressible Fluid Dynamics: The ORCHID and First Results of Optical Measurements*. PhD thesis, Delft University of Technology, 2020.
- [35] A. J. Head, S. Iyer, C. de Servi, and M. Pini. Towards the validation of a CFD solver for non-ideal compressible flows. *Energy Procedia*, 129(Supplement C):240 – 247, 2017. ISSN 1876-6102. 4th International Seminar on ORC Power Systems September 13-15th 2017. Pg.
- [36] Richard G. Hills. Model Validation: Model Parameter and Measurement Uncertainty. *Journal of Heat Transfer*, 128(4):339–351, 10 2005. ISSN 0022-1481. doi: 10.1115/1.2164849. URL <https://doi.org/10.1115/1.2164849>.
- [37] IEC. Uncertainty of measurement — Part 3: Guide to the expression of uncertainty in measurement (GUM:1995). Standard, International Organization for Standardization (ISO), Geneva, CH, 2008.
- [38] S. Iyer. Influence of thermodynamic property perturbations on nozzle design and non-ideal compressible flow phenomena. Master’s thesis, Delft University of Technology, 2015.
- [39] MARIN. Refresco V&V tools, 2019. URL <https://www.refresco.org/verification-validation/utilitiesvv-tools/>.
- [40] X. Merle and P. Cinnella. Bayesian quantification of thermodynamic uncertainties in dense gas flows. *Reliability Engineering and System Safety*, 2014.
- [41] F. Montomoli, M. Massini, S. Salvadori, M. Carnevale, and R. Ahlfeld. *Uncertainty Quantification in Computational Fluid Dynamics and Aircraft Engines*. Springer International Publishing AG, second edition, 2019.
- [42] N.R. Nannan and P. Colonna. Improvement on multiparameter equations of state for dimethylsiloxanes by adopting more accurate ideal-gas isobaric heat capacities: Supplementary to p. colonna, n.r. nannan, a. guardone, e.w. lemmon, fluid phase equilib. 244, 193 (2006). *Fluid Phase Equilibria*, 280(1):151 – 152, 2009. ISSN 0378-3812. doi: <https://doi.org/10.1016/j.fluid.2009.02.009>.
- [43] P. Nederstigt. Real gas thermodynamics and the isentropic behavior of substances. Master’s thesis, Delft University of Technology, 2017.
- [44] NIST. Nist reference fluid thermodynamic and transport properties database (refprop), 2019. URL <https://www.nist.gov/srd/refprop>.
- [45] W. L. Oberkampf and C. J. Roy. *Verification and Validation in Scientific Computing*. Cambridge University Press, 2010. pg.
- [46] Ding-yu Peng and Donald Robinson. New two-constant equation of state. *Industrial & Engineering Chemistry Fundamentals*, 15, 02 1976. doi: 10.1021/i160057a011.
- [47] M. Pini, S. Vitale, P. Colonna, G. Gori, A. Guardone, T. Economon, J.J. Alonso, and F. Palacios. Su2: the open-source software for non-ideal compressible flows. *Journal of Physics: Conference Series*, 821, 2017.
- [48] Kenneth S. Pitzer, David Z. Lippmann, R. F. Curl, Charles M. Huggins, and Donald E. Petersen. The volumetric and thermodynamic properties of fluids. ii. compressibility factor, vapor pressure and entropy of vaporization1. *Journal of the American Chemical Society*, 77(13):3433–3440, 1955. doi: 10.1021/ja01618a002. URL <https://doi.org/10.1021/ja01618a002>.

- [49] M. Poerner and A. Rimpel. 10 - waste heat recovery. In Klaus Brun, Peter Friedman, and Richard Dennis, editors, *Fundamentals and Applications of Supercritical Carbon Dioxide (sCO₂) Based Power Cycles*, pages 255 – 267. Woodhead Publishing, 2017. ISBN 978-0-08-100804-1. doi: <https://doi.org/10.1016/B978-0-08-100804-1.00010-4>. URL <http://www.sciencedirect.com/science/article/pii/B9780081008041000104>.
- [50] W.C. Reynolds and P. Colonna. *Thermodynamics: Fundamentals and Engineering Applications*. Cambridge University Press, 2018. ISBN 9781108546737.
- [51] P. J. Roache. *Verification and Validation in Computational Science and Engineering*. Hermosa Publishers, Albuquerque, 1998.
- [52] P. J. Roache. *Fundamentals of Verification and Validation*. Hermosa Publishers, Socorro, 2009.
- [53] V. Romero. Comparison of a pragmatic and versatile "real space" model validation framework against several other frameworks. In *Proceedings of ASME 2011 VV Symposium*, SAND2011-7613C, Las Vegas, NV, USA, October 13-15 2011. Sandia National Laboratories.
- [54] V. Romero. The real space model validation approach as a (unifying?) extended hybrid of the asme vv10 and vv20 approaches. In *Proceedings of ASME 2015 VV Symposium*, Las Vegas, NV, USA, May 13-15 2015. ASME.
- [55] C. Roy and W. Oberkampf. A complete framework for verification, validation, and uncertainty quantification in scientific computing (invited). In *Aerospace Sciences Meetings*, page 124. AIAA, January 2010. Pg.
- [56] G.S. Settles. *Schlieren and Shadowgraph Techniques: Visualizing Phenomena in Transparent Media*. Experimental Fluid Mechanics. Springer Berlin Heidelberg, 2012. ISBN 9783642566400.
- [57] Giorgio Soave. Equilibrium constants from a modified redlich-kwong equation of state. *Chemical Engineering Science*, 27(6):1197 – 1203, 1972. ISSN 0009-2509. doi: [https://doi.org/10.1016/0009-2509\(72\)80096-4](https://doi.org/10.1016/0009-2509(72)80096-4).
- [58] A. Spinelli, V. Dossena, P. Gaetani, C. Osnaghi, and D. Colombo. Design of a Test Rig for Organic Vapours. In *Proceedings of ASME Turbo Expo 2010*, Glasgow, UK, June 14-18 2010. ASME.
- [59] A. Spinelli, M. Pini, V. Dossena, P. Gaetani, and F. Casella. Design, Simulation, and Construction of a Test Rig for Organic Vapors. *J. Eng. Gas Turb. Power - T. ASME*, 135(4):10, March 2013.
- [60] A. Spinelli, F. Cozzi, V. Dossena, P. Gaetani, M. Zocca, and A. Guardone. Experimental investigation of a non-ideal expansion flow of siloxane vapor MDM. In *ASME Turbo Expo 2016*, 2016.
- [61] A. Spinelli, G. Cammi, C. C. Conti, S. Gallarini, M. Zocca, F. Cozzi, P. Gaetani, V. Dossena, and A. Guardone. Experimental observation and thermodynamic modeling of non-ideal expanding flows of siloxane MDM vapor for ORC applications. *Energy*, 168:285–294, 2019. ISSN 0360-5442.
- [62] Roman Stryjek and Juan Vera. Prsv - an improved peng-robinson equation of state for pure compounds and mixtures. *The Canadian Journal of Chemical Engineering*, 64:323 – 333, 04 1986. doi: 10.1002/cjce.5450640224.
- [63] Philip A. Thompson. A fundamental derivative in gasdynamics. *The Physics of Fluids*, 14(9): 1843–1849, 1971. doi: 10.1063/1.1693693.
- [64] Francesco Tosto, Claudio Lettieri, Matteo Pini, and Piero Colonna. One-dimensional compressible flows of dense vapours. *Manuscript in Preparation*, TBD(TBD):TBD, 2020. doi: TBD.
- [65] T.P. van der Stelt, N.R. Nannan, and Colonna P. The iprsv equation of state. *Fluid Phase Equilibria*, 330:24–35, 2012.
- [66] S. Vitale, T. A. Albring, M. Pini, N.R. Gauger, and P. Colonna. Fully turbulent discrete adjoint solver for non-ideal compressible flow applications. *Journal of the Global Power and Propulsion Society*, 1:252–270, 2017.

-
- [67] F.M. White. *Fluid Mechanics*. McGraw-Hill series in mechanical engineering. McGraw Hill, 7th edition, 2011. ISBN 9780073529349.